Loma Linda University
TheScholarsRepository@LLU: Digital Archive of Research, Scholarship & Creative Works

Loma Linda University Electronic Theses, Dissertations & Projects

9-2017

The Role of VEGF and Smooth Muscle Phenotype in Hypoxic Remodeling of Ovine Carotid and Cerebral Arteries

Margaret C. Hubbell

Follow this and additional works at: http://scholarsrepository.llu.edu/etd

 Part of the Medical Biochemistry Commons

Recommended Citation
Hubbell, Margaret C., "The Role of VEGF and Smooth Muscle Phenotype in Hypoxic Remodeling of Ovine Carotid and Cerebral Arteries" (2017). *Loma Linda University Electronic Theses, Dissertations & Projects*. 464.
http://scholarsrepository.llu.edu/etd/464

This Dissertation is brought to you for free and open access by TheScholarsRepository@LLU: Digital Archive of Research, Scholarship & Creative Works. It has been accepted for inclusion in Loma Linda University Electronic Theses, Dissertations & Projects by an authorized administrator of TheScholarsRepository@LLU: Digital Archive of Research, Scholarship & Creative Works. For more information, please contact scholarsrepository@llu.edu.

LOMA LINDA UNIVERSITY
School of Medicine
in conjunction with the
Faculty of Graduate Studies

The Role of VEGF and Smooth Muscle Phenotype in Hypoxic Remodeling of Ovine Carotid and Cerebral Arteries

by

Margaret C. Hubbell

A Dissertation submitted in partial satisfaction of
the requirements for the degree
Doctor of Philosophy in Biochemistry

September 2017

© 2017

Margaret C. Hubbell
All Rights Reserved

Each person whose signature appears below certifies that this dissertation in his/her opinion is adequate, in scope and quality, as a dissertation for the degree Doctor of Philosophy.

_____, Chairperson
William J Pearce, Professor of Physiology

_____
Penelope Duerksen-Hughes, Professor of Biochemistry

_____
Omid Khorram, Associate Professor of Obstetrics and Gynecology, University of California, Los Angeles

_____
Wolff Kirsch, Professor of Biochemistry

_____
Lubo Zhang, Professor of Pharmacology

ACKNOWLEDGEMENTS

First of all, I want to thank God for life and the amazing opportunities that He has made available to me for these past several years. His blessings are abundant and His guidance was with me every step of the way.

I would like to express my sincere gratitude to Dr. William J. Pearce who has been my mentor and my guide through the difficult but rewarding experience of graduate school. Thank you for your amazing support and the endless sharing of ideas and scientific wisdom during my graduate experience.

To my family, especially my mom, Dr Sheila Horsley and my dad, Dr Carl Hubbell who have pioneered the way, and my numerous siblings, Gwen, Ellen, Bryce, Claire, Miles, Alex, and Hugh, thank you for your love and support. You have been an inspiration.

To my friends and lab partners, especially Tanya, Dahlim, James, Ric, Yemi, Jinjutha, Naomi, Lara, Desi, Adam, Dane, and others who have shared methods, ideas, lab specimens, food, enthusiasm and so much more, thank you! A special thank you to my dear friend Alane Bristow who has been a pillar of support and a second pair of hands for all night rounds of IHC, and to Dr's Ric and Donna Thorpe who have shared their enthusiasm, wisdom and welcoming abode so many times, thank you!

CONTENT

FIGURES

Figures Page

TABLES

Tables Page

ABBREVIATIONS

8pCPT	8-(p-chlorophenylthio)-guanosine 3’,5’-cyclic monophosphate
8-pCPT-cGMP	8-(4-chlorophenylthio)-guanosine-3’,5’cyclic monophosphate
AA	Alpha-actin
AEBSF	4-(2-Aminoethyl) benzenesulfonyl fluoride hydrochloride
AH	Hypoxic adults
AN	Normoxic adults
BQ-123	Selective ET¬A endothelin receptor antagonist
BQ-788	Selective ET¬B endothelin receptor antagonist
BSA	Bovine serum albumin
Ca2+	Calcium
CaCl2	Calcium chloride
cGMP	Cyclic guanosine monophosphate
CNS	Central nervous system
CO2	Carbon Dioxide
DAPI	4',6-diamidino-2-phenylindole
DMEM	Dulbecco’s Modified Eagle’s Medium
ECM	Extracellular Matrix
EDTA	Ethylenediamine tetraacetic acid
EGTA	ethylene glycol tetraacetic acid
EM	Electron microscopy
eNOS	Endothelial nitrous oxide synthase
EPO	Erythropoietin

ERK	Extracellular signal-regulated kinase
ET	Endothelin
ET-1	Endothelin 1
ET-A	Endothelin receptor type A
ET-B	Endothelin receptor type B
FBS	Fetal bovine serum
FGF	Fibroblast growth factor
FH	Hypoxic fetuses
Flk-1	Fetal liver kinase, VEGF receptor 2 (mouse)
Flt-1	FMS-like tyrosine kinase 1, VEGF receptor 1
FMS	Fibromyalgia syndrome
FN	Normoxic fetuses
HEPES	4-(2-hydroxyethyl)-1-piperazineethanesulfonic acid
HIF	Hypoxia Inducible Factor
HIF-1	Hypoxia Inducible Factor 1
HIF-1a	Hypoxia Inducible Factor 1-alpha
HIF-1b	Hypoxia Inducible Factor 1-beta
IGF-2	Insulin like Growth Factor II
JNK	c-Jun N-terminal kinase
K+	Potassium
KCl	Potassium chloride
KDR	VEGF Receptor 2 (human), Kinase insert domain receptor (mouse)
LL	Lower left

L-NAME	L-NG-Nitroarginine Methyl Ester
LR	Lower right
MCA	Middle cerebral arteries
MgSO4	Magnesium sulfate
MHC	Myosin Heavy Chain
miRNA	micro RNA (ribonucleic acid)
MLC20	Myosin Light Chain 20
MLCK	Myosin Light Chain Kinase
N2	Nitrogen
Na2HCO3	Sodium bicarbonate
NaCl	Sodium chloride
NaHCO3,	Sodium carbonate
NM-MHC	Non-muscle Myosin Heavy Chain Isoform
NO	Nitric Oxide
O2	Oxygen
OC	Organ Culture
p38	Protein 38
PBS	Phosphate Buffered Saline
PDGF	Platelet-derived growth factor
PDGF-B	Platelet-derived growth factor subunit B
PI3K	Phosphatidylinositol-4,5-bisphosphate 3-kinase
PKG	Protein Kinase G
SDS-PAGE	sodium dodecyl sulphate-polyacrylamide gel electrophoresis

SEM	Standard error of measurement
SM1	Smooth Muscle type 1 Myosin Heavy Chain Isoform
SM2	Smooth Muscle type 2 Myosin Heavy Chain Isoform
SMC	Smooth muscle cell
SMemb	Smooth Muscle embryonic
SM-MHC	Smooth Muscle Myosin Heavy Chain Isoform
SM-αA	Smooth Muscle-alpha Actin
Superscript A	Age
Superscript H	Hypoxia
Superscript I	VEGFR Inhibitor-treatment
Superscript V	VEGF-treatment
TBS	Tris-buffered saline
UL	Upper left
UR	Upper right
VEGF	Vascular Endothelial Growth Factor
VEGF-A165	Vascular endothelial growth factor 165 kDa
VEGFR1/2	VEGF Receptors 1 and 2
VSM	Vascular smooth muscle
VSMC	Vascular Smooth Muscle Cell

ABSTRACT OF THE DISSERTATION

The Role of VEGF
and Smooth Muscle Phenotype in Hypoxic Remodeling of
Ovine Carotid and Cerebral Arteries

by

Margaret C. Hubbell

Doctor of Philosophy, Graduate Program in Biochemistry
Loma Linda University, September 2017
Dr. William J. Pearce, Chairperson

Arteries are a dynamic tissue with multiple cell types that incorporate systemic and local factors to maintain homeostasis. Hypoxia stimulates capillary angiogenesis to effectively match metabolic demand with perfusion. With chronic hypoxia, vascular remodeling of even large vessels can occur. This predisposes to pathologic states as seen with atherosclerosis, hypoxic brain injury, myocardial ischemia, diabetes, and developmental anomalies. With this remodeling comes changes in vessel structure including medial thickness and organization of contractile proteins as well as changes in myogenic tone. All of these factors culminate in changes in status or behavior of the vascular smooth muscle within the vessel wall, likely secondary to changes in smooth muscle phenotype. This investigation examines the hypothesis that hypoxia induces vascular remodeling through transformation of vascular smooth muscle cell phenotype mediated by VEGF action directly on smooth muscle and indirectly through the endothelium. This was performed with harvested middle cerebral and common carotid arteries from fetal and adult sheep after exposure to a hypoxic setting (3280m for 110 days) or normoxic setting (sea level). These arteries were then subjected to endothelial

denudation or left intact and then underwent structural and functional contractility assays, immunoblotting, and immunohistochemistry either immediately after harvest or following *in vitro* treatment with organ culture. Hypoxia and VEGF in organ culture had similar effects on contractile function and reorganization of contractile proteins including mature and immature myosin heavy chains (MHC) isoforms, Smooth muscle-MHC and Non-muscle MHC respectively with Smooth muscle-alpha Actin (SM-AA). The endothelium appeared to be a significant component of VEGF alterations to contractile function and MHC:SM-AA re-organization and this was mediated in part through VEGF stimulation of the NO pathway. Hypoxic acclimatization was found to not only alter acute responses to contractile stimulants but to alter reactivity to future insults with VEGF. In conclusion, hypoxic vascular remodeling significantly alters vascular SMC function and phenotype through VEGF and endothelial regulation.

CHAPTER ONE

INTRODUCTION

Arteries are dynamic tissues with multiple cellular players contributing to vascular growth, structure, and contractility to maintain homeostasis. Although arteries were originally thought to act as static conduit vessels, the last decade has provided a new wave of studies that demonstrate the responsive remodeling of small and even large arteries under physiological and pathological conditions (13, 28, 33). A key aspect of this new paradigm is the role of the Vascular Smooth Muscle cell (VSMC) phenotype present within the artery wall (28). The VSMC phenotype regulates the vessel structure, the functional response to contractile stimulus, and in part the regulation of new blood vessel development (13, 28) (37). At least four stable phenotypes have been recognized: migratory, proliferative, synthetic, and contractile with the last two contributing largely to the contractile infrastructure and force-apparatus of the artery (29, 33). Synthetic VSMCs synthesize and organize elastin and collagen, the principle components of the extra-cellular matrix (ECM) that passively defines the majority of vascular tone (37). Similarly, fully differentiated contractile VSMCs actively constrict the vessel through Actin-Myosin cross bridge cycling and subsequent cell shortening. Smooth Muscle-alpha Actin (SM-AA) and SM-Myosin Heavy Chain (SM-MHC) are key components for force-production and are established VSMC markers (13, 33). MHC isoforms SM-embryonic (SMemb or NM-MHC), SM1 and SM2 were recently found to have unique contractile characteristics (11). Additionally, expression of these isoforms is developmentally regulated and may prove to be distinctive determinants of both phenotype and contractility (8). Each phenotype plays a different role in physiologic processes including blood pressure

regulation and angiogenesis as well as contributing to pathological processes as seen in tumorigenesis, macular degeneration, atherosclerotic lesion formation, and hypoxic remodeling, which can be particularly important during embryonic development (1, 7).

In the developing fetus, hypoxia can occur as a consequence of placental insufficiency or maternal anemia and is a leading cause of premature birth (14). For neonates born pre-35 weeks of gestation, nearly 50% experience cerebral hemorrhaging due to compromised vascular development that can result in extensive neurological damage (10, 35) (22). Hypoxia drives whole artery remodeling, augments the endothelium, thickens the medial smooth muscle and adventitia, and acts on even the non-cellular factors including the composition of the ECM (30, 31). However, the cellular mechanisms mediating these hypoxic effects are incompletely understood.

Central to the hypoxic response is the activation of the Hypoxia Inducible Factor (HIF) family of transcription factors that upregulate genes for numerous adaptive proteins (17). HIF-1a plays a fundamental role by upregulating the potent pro-angiogenic factor Vascular Endothelial Growth Factor (VEGF) (6). VEGF is thought to act primarily on endothelial cells but has recently been found to act on other vascular cells as well, namely VSMCs (2, 18). VEGF binds to VEGF Receptors 1 and 2 (VEGFR1/2) that in turn activate ERK and PI3K to upregulate other pro-angiogenic genes (7, 36).

During angiogenesis the endothelium releases vasotrophic factors that act on smooth muscle and initiate hypoxic vascular remodeling. VEGF may induce these intermediate vasotrophic factors from the endothelium or act directly on the smooth muscle itself. Two prominent vasotrophic factors from the endothelium that act on VSMCs are Endothelin (ET) and nitric oxide (NO) (19). Both compounds can act

immediately on contraction as well as stimulate long term changes in smooth muscle gene expression and phenotype (3, 4).

Background and Significance

Vascular adaptability is essential to cardiovascular homeostasis and acute local hypoxia is an important physiological stress that induces these vascular adaptations. However, recurring or chronic hypoxia results in various pathologies during development as well as later in life (27). Chronic prenatal fetal hypoxia is one such case that can occur with placental insufficiency and maternal hypertension or diabetes, affecting several areas of development including alveolar maturation in the lungs and cerebrovascular development (16, 30). Generally chronic hypoxia stimulates the fetal cardiovascular system to redirect cardiac output to favor the developing brain and heart. However, systemic changes in vascular function and structure occur that are collectively known as hypoxic vascular remodeling.

Hypoxic vascular remodeling was first established as a fundamental fetal response to chronic hypoxia in the 1970s and has since been characterized extensively. Structural changes with hypoxia include thickening of the medial and adventitial wall, changes in ECM content, and a decreased contractile response as seen in both the pulmonary and cerebral circulation (24, 30). However, hypoxic remodeling has been found to vary with artery size, artery type, maturation and smooth muscle phenotype (33, 37). This may in large part be due to the inherent heterogeneity of the smooth muscle that synthesizes the ECM and drives the contractile response (28). While four functional phenotypic states (synthetic, proliferative, migratory, and contractile) have been identified, a continuum of

intermediate states exist (4, 33). This broad spectrum of phenotypes results from the differing sources of smooth muscle progenitor cells (mesoderm, neuroectoderm, epicardium, endothelium) (27) and the ability of VSMCs to undergo dramatic phenotypic modulation at all levels of maturity (13). Both result in a milieu of smooth muscle phenotypes present in a single vessel each of which differ in their response to a single stimulus such as hypoxia (37). It is because of this innate versatility of smooth muscle that hypoxic vascular remodeling can occur, enabling the vessel to adapt to chronic changes respective of local conditions (33). To better understand the remodeling process, the initial and final phenotypic state of the smooth muscle must be determined and which vasotrophic factors may have carried out this process must be identified.

Hypoxia Inducible Factor (HIF) and its Primary Angiogenic Target VEGF

In response to systemic hypoxia, the total oxygen-transporting capacity increases with the production of new erythrocytes following erythropoietin (EPO) synthesis in the liver and kidney (7). However, tissues can also respond locally to hypoxia by recruiting new microvessels to increase local blood perfusion. The formation of additional blood vessels is stimulated through the HIF family of transcription factors, and activation of target pro-angiogenic genes. HIF-1 is central to the hypoxic response pathway. It is a heterodimer of oxygen sensing HIF-1a and constitutively expressed HIF-1b that is activated under hypoxic conditions (36). Upon activation, HIF-1 binds and activates transcription of several pro-angiogenic genes including glycolytic enzymes, Insulin like Growth Factor II (IGF-2), endothelial Nitric Oxide Synthase (eNOS), and glucose transporters. Another target of HIF-1 and principle initiator of angiogenesis is VEGF

(17). VEGF is secreted from hypoxic tissue in a gradient-like fashion to induce vessel budding by activating the endothelial cells of nearby microvessels. Arterial endothelium is also responsive to VEGF and is an established source of vasotrophic factors for VSMCs (21).

Two prominent trophic factors released from the endothelium are endothelin (ET) and nitric oxide (NO). ET-1 is a potent vasoconstrictor and contributes to cardiovascular disease, in part by stimulating VSMC proliferation and subsequent vascular hyperplasia as seen with atherosclerosis (19). VSMCs bear both G protein-coupled receptors ET-A (predominantly) and ET-B with downstream activation of phospholipase C, ERK and Ca^{2+}release from the endoplasmic reticulum to stimulate contraction, migration, and other phenotype-dependent responses (20). In contrast, NO is a well-known vasodilator that also modulates smooth muscle toward the contractile, non-proliferative, non-migratory phenotype at physiological levels (4). Low or absent levels of NO are associated with active remodeling of the vessel, increased synthesis of ECM proteins, and accelerated formation of atherosclerotic lesions and hyperplasia (34). Under hypoxia, NO production is required for vascular remodeling to occur (34). Downstream of NO are several signaling pathways to accomplish this, including ERK, p38, and JNK that inhibit proliferative genes and cGMP-dependent protein kinase (PKG) to activate contractile genes (4, 21). Interestingly, VEGF has previously been found to upregulate NO in at least damaged endothelial cells, making NO a promising vasotrophic target downstream of hypoxia and VEGF.

Given that vasotrophic factors (such as PDGF, FGF, ET, NO, and VEGF) are upregulated with hypoxia, and that hypoxic vascular remodeling changes each

component of the vessel wall (especially the adventitia and ECM), changes in smooth muscle phenotype may accompany or even direct this remodeling process. VEGF is central to hypoxic remodeling, activates the endothelium as well as the release of vasotrophic factors, and has been shown to stimulate non-endothelial cells including sympathetic neurons, macrophages, fibroblasts and recently smooth muscle cells (23, 28). Therefore, hypoxic vascular remodeling may occur through either direct action of VEGF on smooth muscle or through indirect action of VEGF on endothelium to modulate smooth muscle phenotype with subsequent ECM degradation/synthesis and changes in contractile characteristics. This was examined with this dissertation and is expounded upon in the following chapters. Synthetic and contractile markers of phenotype have been identified for smooth muscle, although few are expressed uniquely in a certain phenotype which prompted the quadrant analysis utilized in the studies discussed in subsequent chapters (13, 28). High SM-AA expression is distinct to VSMCs. SM-MHC are established contractile protein markers that recent studies have identified three main MHC isoforms for: SMemb, SM1, and SM2. Each MHC isoform has unique functional characteristics: SM2 is prevalent in fully mature contractile VSMCs while SM1 is 34 residues longer, more prevalent in semi-mature VSMCs early in development and was shown to be more sensitive to ligand-induced than stretch-induced contraction in SM2 knockout mice (15, 32). SMemb, also known as non-muscle MHC (NM-MHC), is highly expressed in embryonic vessels and is quickly upregulated during the transition to synthetic phenotype (12, 33). We provided a unique integration of these four markers to characterize phenotype-dependent actions of smooth muscle during hypoxic vascular remodeling. Of note, it has also recently come to light that the antibodies available for

SM1 in large mammals including ovine, bovine and human is not selective for SM1 alone and instead identifies both MHC isoforms SM1 and SM2. Therefore, myosin heavy chains were categorized into mature contractile SM-MHC (SM1 and SM2) and NM-MHC (SMemb) in all studies described below.

Significance

From a basic science perspective, the significance of the proposed work is represented in the unique hypoxia-organ culture model and a new technical approach to identify the role of vasotrophic factors and smooth muscle phenotype in hypoxic vascular remodeling. Previous work has been limited to molecular perturbations in non-physiological cell culture with functional assessment only possible in freshly dissected arteries. Here, we propose to couple chronic hypoxia in vivo to organ culture of large and small arteries in the presence of hypoxia-induced vasotrophic factors. This enables a mechanistic investigation of both age-dependent and artery type-dependent changes in the vasculature as well as exposure of the artery to specific vasotrophic factors (namely VEGF) while maintaining smooth muscle phenotype and physiologic cell-to-cell interactions. New isoforms of established smooth muscle markers were quantified in parallel high-resolution measurements for abundance and co-localization with functional partners (namely SM-AA). These molecular findings were coupled with robust functional endpoints of stress-strain relations to elucidate the functional role of these contractile proteins in maintaining vascular tone. Both of these techniques are unprecedented in fetal cerebral and carotid arteries and were repeated in adult arteries for developmental comparison. In light of this, the proposed work uniquely relates functional and molecular

analysis of novel phenotypic contributors to hypoxic vascular remodeling in both the fetal and adult vasculature.

From a clinical perspective, this is of principle importance in the cerebrovasculature of neonates exposed to chronic hypoxia in utero as well as in the development of various pathologies that occur in adulthood including atherosclerotic lesion formation and hypertension. In the fetus, even brief periods of hypoxia can cause neuronal death and subsequent pediatric strokes, intracranial hemorrhage, and other patterns of cerebral damage resulting in significant neurological impairment and economic cost. Much of this is due to alterations of the vasculature that stem from changes in smooth muscle behavior and may be reversible if the mechanisms of action are elucidated. Similarly, in the adult, if phenotypic pressures toward VSMC proliferation and synthesis could be identified, pharmaceuticals could be developed to reverse or inhibit atherosclerotic lesion formation. Current therapies are already available for angiogenic factors such as VEGF that are known to contribute to hypoxic vascular remodeling. How such factors regulate hypoxic changes in smooth muscle phenotype and the functional and structural consequences of these changes remain highly uncertain. A better understanding of how the fetal and adult vasculature is altered by sustained hypoxia is needed to identify and optimize therapeutic strategies for these patients and is the objective of this dissertation.

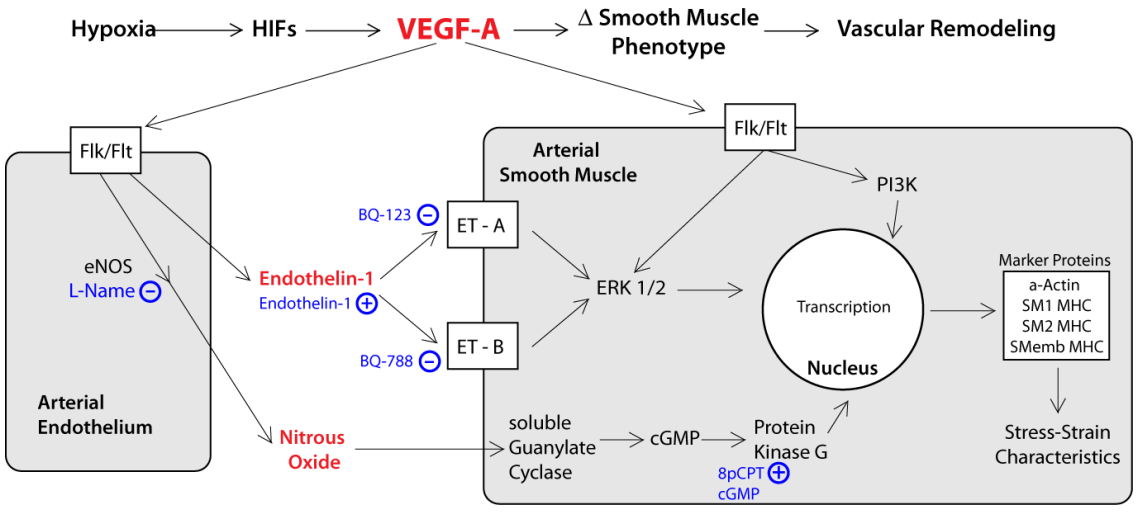

Figure 1. Hypoxic Vascular Remodeling.
Hypoxia stabilizes transcription factor HIF, that then upregulates VEGF. VEGF stimulates the endothelium to release vasotrophic factors. These factors, specifically endothelin-1 and NO, stimulate phenotypic changes in the smooth muscle. VEGF may also act directly on the smooth muscle, altering its phenotypic state. Said phenotypic modulations result in structural and functional changes of the vessel including degradation/synthesis of the ECM and changes in stress-strain relations.

Hypoxia Modulates vascular function and SMC Phenotype

As described above, hypoxia stimulates changes in vascular structure and the contractile response of smooth muscle. Contractile function is regulated by both intercellular and intracellular reactions. Intercellular actions include endothelium secretion of contractants and relaxants to the smooth muscle as well as smooth muscle active dispersion of force to the ECM. Intracellular regulation acts on cell-anchor components and force-producing components of the actin-myosin cross-linking. Many studies have focused on structural changes of the whole artery with hypoxia as well as intracellular signaling pathways. Yet little is known of the long term effects of hypoxia on the expression and working interactions of contractile proteins specifically. These proteins combine to form a force-producing apparatus that can be activated through multiple stimuli and pathways. To separate out signaling pathways that initiate contraction, both stretch-induced (myogenic) stress and potassium-induced (active) stress were studied in conjunction with expression of contractile proteins. Both myogenic and active stress are thought to culminate in Ca^{++} activation of Myosin Light Chain Kinase (MLCK), phosphorylation of MLC_{20} and cross-bridge formation and movement along SM-AA. The uncoupling of these two forms of contraction under hypoxia suggest changes upstream of the contractile apparatus or in the components/response of the contractile apparatus itself. This could include changes in receptor coupling, Ca^{++} influx, or at the cross-bridge formation between actin and myosin via changes in the MHC isoform. Previous work has considered changes in Ca^{++} influx and sensitivity **(25) (26)**. However, these were incomplete in their explanation.

Shifts in smooth muscle phenotype and contractile markers are relevant to force production and a budding area of focus. There are 3 smooth muscle MHC isoforms: synthetic SMemb and the two contractile SM1 (immature) and SM2 (mature). To explore whether the type of MHC associated with SM-AA changed with hypoxia and development, MHC isoform abundance and co-localization with SM-AA were determined in ovine carotid arteries from non-pregnant adult sheep exposed to normoxic or hypoxic conditions.

VEGF Modulates Trophic Influences of Arterial Endothelium

During angiogenesis, VEGF acts on the microvascular endothelium (6). Recent evidence suggests VEGF also acts on arterial endothelium and may stimulate smooth muscle differentiation through the endothelial release of vasotrophic factors (21). To determine if hypoxia with VEGF might act through this mechanism in ovine arteries, we examined the effects of *in vivo* chronic hypoxia and organ culture with VEGF. For organ culture, matched segments from a single artery, half of which are endothelium-denuded and the other half endothelium-intact, were treated with vasotrophic factors or respective pathway inhibitors.

Experimental Background

The central hypothesis investigated in this dissertation was that hypoxia induces vascular remodeling through transformation of vascular smooth muscle cell phenotype mediated by VEGF action directly on smooth muscle and indirectly through the endothelium. This hypothesis was explored through two separate corollaries: Hypoxic

changes in SMC phenotype and vascular remodeling occur through Aim 1) Direct action of VEGF on smooth muscle as modeled in endothelium-denuded ovine carotid arteries; Aim 2) Direct action of VEGF on smooth muscle and indirect action of VEGF through the endothelium as modeled in endothelium-denuded and endothelium-intact ovine middle cerebral arteries. (Figure 10). To test these corollaries, arteries from normoxic fetal and adult sheep were placed in organ culture in the presence and absence of physiological levels of VEGF (3ng/mL) and other vasotrophic factors to investigate which hypoxic effects can be reproduced.

Previous studies have demonstrated the dynamic nature of VSMCs when removed from arterial context (as seen with single cell culture, in co-cultures with endothelial cells, and in Matrigel^{TM} cultures with synthetic ECM) (37) (38). Likewise, the presence of other growth factors including angiotensin-2, fibroblast growth factor, and transforming growth factor-b, significantly alters the VSMC phenotype (9) (32) (15). Given the variable growth factor content of Fetal Bovine Serum (FBS), and to identify the extent VEGF alone plays a role in hypoxic vascular remodeling, whole artery rings were cultured in minimal essential medium without FBS. All arteries designated for organ culture will undergo an initial 24hr serum-starvation period without VEGF as previously shown, to align VSMC cell cycle and to clear the culture of autocrine and paracrine factors (5). This would then be followed by 24 hour culture with and without VEGF followed by allocation of tissue towards three respective assays: (1) Measurements of MHC isoform abundance using calibrated Western blotting, (2) Measurements of MHC isoform co-localization with SM-αActin, and (3) functional contractility measurements of active and passive stress-strain relations.

Hypothesis of Dissertation

To identify these endothelial and non-endothelial mitogenic actions of VEGF, this dissertation investigates the main hypothesis that **hypoxia induces vascular remodeling through transformation of vascular smooth muscle cell phenotype mediated by VEGF.** This hypothesis gives rise to two specific corollaries: 1) chronic hypoxia stimulates phenotypic transformation and vascular remodeling through ***direct*** actions of VEGF on arterial smooth muscle; and 2) chronic hypoxia stimulates phenotypic transformation and vascular remodeling ***indirectly*** through VEGF-induced release of Endothelin and NO from the endothelium. The following chapters address these corollaries:

Chapter 2: Measure the effects of chronic hypoxia and VEGF on the organization and function of contractile proteins as indicated by medial thickness, artery stiffness, active stress-strain relations, and MHC markers of smooth muscle phenotype in **endothelium-denuded ovine carotid arteries**.

Chapter 3: Measure the effects of chronic hypoxia and VEGF on the organization and function of contractile proteins in the presence or absence of NO, the eNOS inhibitor L-NAME, and/or Protein Kinase G (PKG) activator 8-pCPT-cGMP, as indicated by medial thickness, artery stiffness, active stress-strain relations, and MHC markers of smooth muscle phenotype in **endothelium intact and denuded ovine middle cerebral arteries**.

Chapter 4: Measure the change in response to VEGF in **chronic hypoxia** arteries on the organization and function of contractile proteins as indicated by medial thickness, artery stiffness, active stress-strain relations, and MHC markers of smooth muscle phenotype in **endothelium-denuded ovine carotid arteries**.

Chapter 5: Measure the effects of chronic hypoxia and VEGF on the organization and function of contractile proteins in the presence or absence of ET, ET receptor inhibitors BQ-123 and BQ-788 as indicated by medial thickness, artery stiffness, active stress-strain relations, and MHC markers of smooth muscle phenotype in **endothelium intact and denuded ovine middle cerebral arteries**.

To define the effects of hypoxia, arteries were studied from animals maintained at sea level and after acclimatization to an altitude of 3280m for 110 days. To identify developmental and maturational differences in mechanisms mediating hypoxic vascular remodeling, these experiments were carried out in arteries from term fetal lambs and non-pregnant, nulliparous young ewes. To assess the role of VEGF, arteries were organ cultured in either the presence or absence of media containing low physiological concentrations (3-30 ng/ml) of VEGF. Smooth muscle phenotype was evaluated by the extent of SM-AA co-localized with either the immature (SMemb aka Non-Muscle) or the the mature Smooth Muscle isoforms (SM1 and SM2) of Myosin Heavy Chain (MHC) isoforms of myosin heavy chain (MHC). Together, these measures offer an original perspective of the age-dependent mechanisms through which hypoxia mediates vascular remodeling.

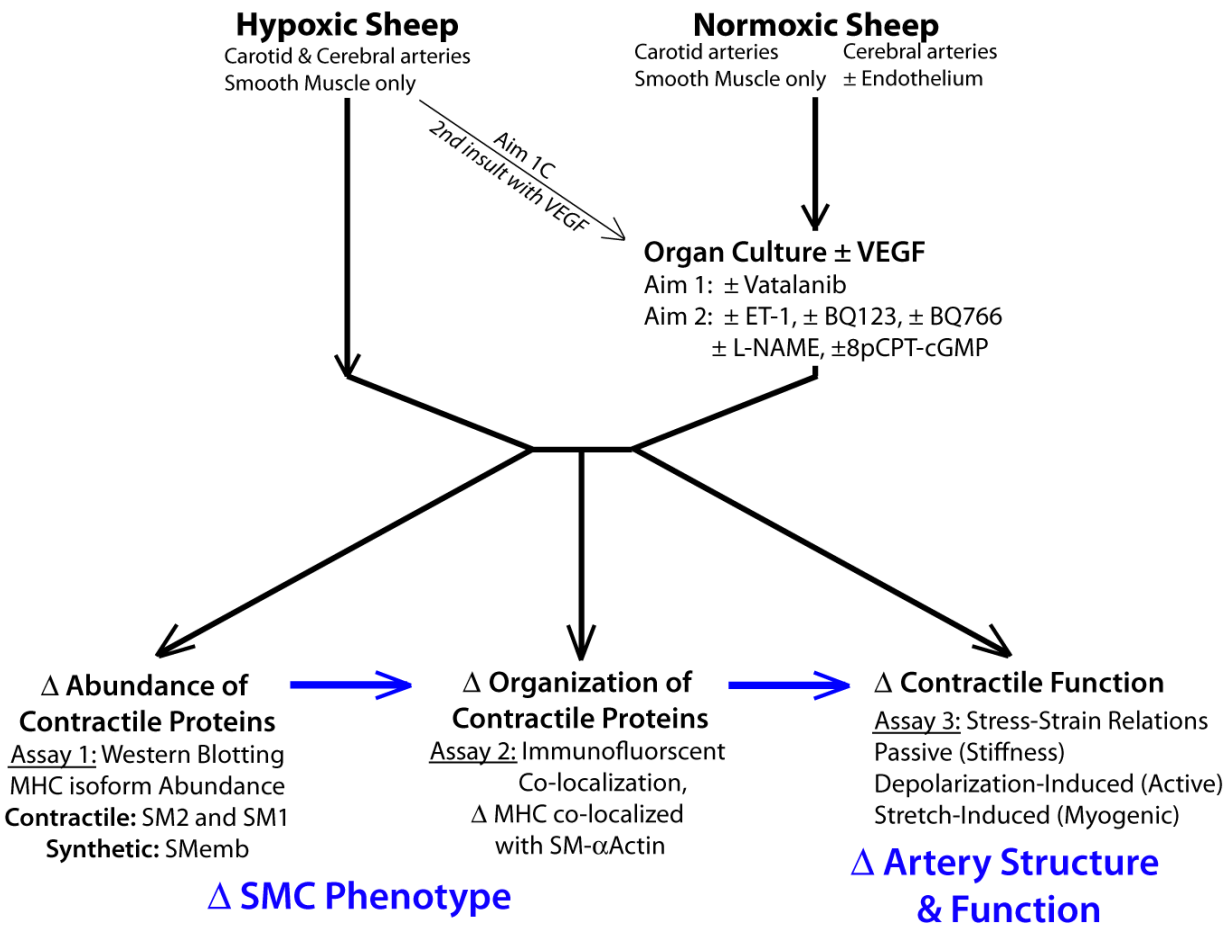

Figure 2. Main experimental paradigm.
Hypoxic alterations to SMC phenotype as well as artery structure and function were determined in ovine fetal and adult, middle cerebral and carotid arteries using 3 different assays: changes in contractile protein abundance (Immunoblotting), changes in the organization of contractile proteins (Confocal Immunofluorescent), and changes in contractile function (stress-strain relations). To determine the role of VEGF and the endothelium in this process, matching artery segments were organ cultured with or without VEGF, intact endothelium, and/or vasotrophic factors.

References

1. **Aikawa M, Yamaguchi H, Yazaki Y, and Nagai R**. Smooth muscle phenotypes in developing and atherosclerotic human arteries demonstrated by myosin expression. *J Atheroscler Thromb* 2: 14-23, 1995.

2. **Ball SG, Shuttleworth CA, and Kielty CM**. Vascular endothelial growth factor can signal through platelet-derived growth factor receptors. *J Cell Biol* 177: 489-500, 2007.

3. **Bouallegue A, Daou GB, and Srivastava AK**. Endothelin-1-induced signaling pathways in vascular smooth muscle cells. *Curr Vasc Pharmacol* 5: 45-52, 2007.

4. **Bundy RE, Marczin N, Birks EF, Chester AH, and Yacoub MH**. Transplant atherosclerosis: role of phenotypic modulation of vascular smooth muscle by nitric oxide. *Gen Pharmacol* 34: 73-84, 2000.

5. **Butler SM, Abrassart JM, Hubbell MC, Adeoye O, Semotiuk A, Williams JM, Mata-Greenwood E, Khorram O, and Pearce WJ**. Contributions of VEGF to age-dependent transmural gradients in contractile protein expression in ovine carotid arteries. *Am J Physiol Cell Physiol* 301: C653-666, 2011.

6. **Byrne AM, Bouchier-Hayes DJ, and Harmey JH**. Angiogenic and cell survival functions of vascular endothelial growth factor (VEGF). *J Cell Mol Med* 9: 777-794, 2005.

7. **Carmeliet P**. Angiogenesis in health and disease. *Nat Med* 9: 653-660, 2003.

8. **Chi M, Zhou Y, Vedamoorthyrao S, Babu GJ, and Periasamy M**. Ablation of smooth muscle myosin heavy chain SM2 increases smooth muscle contraction and results in postnatal death in mice. *Proc Natl Acad Sci U S A* 105: 18614-18618, 2008.

9. **de Cavanagh EM, Ferder M, Inserra F, and Ferder L**. Angiotensin II, mitochondria, cytoskeletal, and extracellular matrix connections: an integrating viewpoint. *Am J Physiol Heart Circ Physiol* 296: H550-558, 2009.

10. **Del Balzo F, Spalice A, Ruggieri M, Greco F, Properzi E, and Iannetti P**. Stroke in children: inherited and acquired factors and age-related variations in the presentation of 48 paediatric patients. *Acta Paediatr* 98: 1130-1136, 2009.

11. **Eddinger TJ, and Meer DP**. Myosin II isoforms in smooth muscle: heterogeneity and function. *Am J Physiol Cell Physiol* 293: C493-508, 2007.

12. **Ferreira LS, Gerecht S, Shieh HF, Watson N, Rupnick MA, Dallabrida SM, Vunjak-Novakovic G, and Langer R**. Vascular progenitor cells isolated from human embryonic stem cells give rise to endothelial and smooth muscle like cells and form vascular networks in vivo. *Circ Res* 101: 286-294, 2007.

13. **Fukuda D, and Aikawa M**. Intimal smooth muscle cells: the context-dependent origin. *Circulation* 122: 2005-2008, 2010.

14. **Gilbert JS, Nijland MJ, and Knoblich P**. Placental ischemia and cardiovascular dysfunction in preeclampsia and beyond: making the connections. *Expert Rev Cardiovasc Ther* 6: 1367-1377, 2008.

15. **Goumans MJ, Liu Z, and ten Dijke P**. TGF-beta signaling in vascular biology and dysfunction. *Cell Res* 19: 116-127, 2009.

16. **Groenman FA, Rutter M, Wang J, Caniggia I, Tibboel D, and Post M**. Effect of chemical stabilizers of hypoxia-inducible factors on early lung development. *Am J Physiol Lung Cell Mol Physiol* 293: L557-567, 2007.

17. **Hoeben A, Landuyt B, Highley MS, Wildiers H, Van Oosterom AT, and De Bruijn EA**. Vascular endothelial growth factor and angiogenesis. *Pharmacol Rev* 56: 549-580, 2004.

18. **Ishida A, Murray J, Saito Y, Kanthou C, Benzakour O, Shibuya M, and Wijelath ES**. Expression of vascular endothelial growth factor receptors in smooth muscle cells. *J Cell Physiol* 188: 359-368, 2001.

19. **Ivey ME, Osman N, and Little PJ**. Endothelin-1 signalling in vascular smooth muscle: pathways controlling cellular functions associated with atherosclerosis. *Atherosclerosis* 199: 237-247, 2008.

20. **Kida T, Chuma H, Murata T, Yamawaki H, Matsumoto S, Hori M, and Ozaki H**. Chronic treatment with PDGF-BB and endothelin-1 synergistically induces vascular hyperplasia and loss of contractility in organ-cultured rat tail artery. *Atherosclerosis* 214: 288-294, 2011.

21. **Li D, Zhang C, Song F, Lubenec I, Tian Y, and Song QH**. VEGF regulates FGF-2 and TGF-beta1 expression in injury endothelial cells and mediates smooth muscle cells proliferation and migration. *Microvasc Res* 77: 134-142, 2009.

22. **Limperopoulos C**. Disorders of the fetal circulation and the fetal brain. *Clin Perinatol* 36: 561-577, 2009.

23. **Marko SB, and Damon DH**. VEGF promotes vascular sympathetic innervation. *Am J Physiol Heart Circ Physiol* 294: H2646-2652, 2008.

24. **Mura M, dos Santos CC, Stewart D, and Liu M**. Vascular endothelial growth factor and related molecules in acute lung injury. *J Appl Physiol* 97: 1605-1617, 2004.

25. **Nauli SM, Ally A, Zhang L, Gerthoffer WT, and Pearce WJ**. Maturation attenuates the effects of cGMP on contraction, [Ca2+]i and Ca2+ sensitivity in ovine basilar arteries. *Gen Pharmacol* 35: 107-118, 2000.

26. **Nauli SM, Williams JM, Gerthoffer WT, and Pearce WJ**. Chronic hypoxia modulates relations among calcium, myosin light chain phosphorylation, and force differently in fetal and adult ovine basilar arteries. *J Appl Physiol* 99: 120-127, 2005.

27. **Orlandi A, and Bennett M**. Progenitor cell-derived smooth muscle cells in vascular disease. *Biochemical pharmacology* 79: 1706-1713, 2010.

28. **Owens GK**. Molecular control of vascular smooth muscle cell differentiation and phenotypic plasticity. *Novartis Found Symp* 283: 174-191; discussion 191-173, 238-141, 2007.

29. **Owens GK, Kumar MS, and Wamhoff BR**. Molecular regulation of vascular smooth muscle cell differentiation in development and disease. *Physiol Rev* 84: 767-801, 2004.

30. **Pearce W**. Hypoxic regulation of the fetal cerebral circulation. *J Appl Physiol* 100: 731-738, 2006.

31. **Petersen W, Pufe T, Zantop T, Tillmann B, and Mentlein R**. Hypoxia and PDGF have a synergistic effect that increases the expression of the angiogenetic peptide vascular endothelial growth factor in Achilles tendon fibroblasts. *Arch Orthop Trauma Surg* 123: 485-488, 2003.

32. **Presta M, Dell'Era P, Mitola S, Moroni E, Ronca R, and Rusnati M**. Fibroblast growth factor/fibroblast growth factor receptor system in angiogenesis. *Cytokine Growth Factor Rev* 16: 159-178, 2005.

33. **Rensen SS, Doevendans PA, and van Eys GJ**. Regulation and characteristics of vascular smooth muscle cell phenotypic diversity. *Netherlands heart journal : monthly journal of the Netherlands Society of Cardiology and the Netherlands Heart Foundation* 15: 100-108, 2007.

34. **Rudic RD, Shesely EG, Maeda N, Smithies O, Segal SS, and Sessa WC**. Direct evidence for the importance of endothelium-derived nitric oxide in vascular remodeling. *J Clin Invest* 101: 731-736, 1998.

35. **Sarkar S, Bhagat I, Dechert R, Schumacher RE, and Donn SM**. Severe intraventricular hemorrhage in preterm infants: comparison of risk factors and short-term neonatal morbidities between grade 3 and grade 4 intraventricular hemorrhage. *Am J Perinatol* 26: 419-424, 2009.

36. **Semenza GL**. Vasculogenesis, angiogenesis, and arteriogenesis: mechanisms of blood vessel formation and remodeling. *J Cell Biochem* 102: 840-847, 2007.

37. **Wagenseil JE, and Mecham RP**. Vascular extracellular matrix and arterial mechanics. *Physiol Rev* 89: 957-989, 2009.

38. **Williams B**. Mechanical influences on vascular smooth muscle cell function. *J Hypertens* 16: 1921-1929, 1998.

CHAPTER TWO

CHRONIC HYPOXIA AND VEGF DIFFERENTIALLY MODULATE ABUNDANCE AND ORGANIZATION OF MYOSIN HEAVY CHAIN ISOFORMS IN FETAL AND ADULT OVINE ARTERIES

Margaret C. Hubbell[1], Andrew J. Semotiuk[1], Richard B. Thorpe[1], Olayemi O. Adeoye[1], Stacy M. Butler[1], James M. Williams[1], Omid Khorram[2], and William J. Pearce[1]

Running Title: Hypoxia and VEGF Alter Vascular Myosin Isoform Profiles

The work presented in this chapter has been published:

Hubbell MC, Semotiuk AJ, Thorpe RB, et al. Chronic hypoxia and VEGF differentially modulate abundance and organization of myosin heavy chain isoforms in fetal and adult ovine arteries. *American Journal of Physiology - Cell Physiology*. 2012;303(10):C1090-C1103. doi:10.1152/ajpcell.00408.2011. PMID: 22992677

[1]Divisions of Physiology, Pharmacology, and Biochemistry, Center for Perinatal Biology, Loma Linda University School of Medicine, Loma Linda, CA 92350

[2]Department of Obstetrics and Gynecology Harbor/UCLA Medical Center, Box 489, 1000 W. Carson St., Torrance, California 90502

Address correspondence to: William J. Pearce, Ph.D., Center for Perinatal Biology, Loma Linda University School of Medicine, Loma Linda, CA 92350; Phone: 909-558-4325; FAX: 909-558-4029; E-Mail: wpearce@llu.edu

Abstract

Chronic hypoxia increases Vascular Endothelial Growth Factor (VEGF) and thereby promotes angiogenesis. The present study explores the hypothesis that hypoxic increases in VEGF also remodel artery wall structure and contractility through phenotypic transformation of smooth muscle. Pregnant and non-pregnant ewes were maintained at sea level (normoxia) or 3,820m (hypoxia) for the final 110 days of gestation. Common carotid arteries harvested from term fetal lambs and non-pregnant adults were denuded of endothelium and studied in vitro. Stretch-dependent contractile stresses were 32% and 77% of normoxic values in hypoxic fetal and adult arteries. Hypoxic hypo-contractility was coupled with increased abundance of Non-Muscle Myosin Heavy Chain (NM-MHC) in fetal (+37%) and adult (+119%) arteries. Conversely, hypoxia decreased Smooth Muscle MHC (SM-MHC) abundance by 40% in fetal arteries but increased it 123% in adult arteries. Hypoxia decreased colocalization of NM-MHC with Smooth Muscle-Alpha Actin (SM-AA) in fetal arteries and decreased colocalization of SM-MHC with SM-AA in adult arteries. Organ culture with physiological concentrations (3 ng/ml) of VEGF-A_{165} similarly depressed stretch-dependent stresses to 37% and 49% of control fetal and adult values. The VEGF receptor antagonist vatalanib ablated VEGF's effects in adult but not fetal arteries, suggesting age-dependent VEGF receptor signaling. VEGF replicated hypoxic decreases in colocalization of NM-MHC with SM-AA in fetal arteries and decreases in colocalization of SM-MHC with SM-AA in adult arteries. These results suggest that hypoxic increases in VEGF not only promote angiogenesis, but may also help mediate hypoxic arterial

remodeling through age-dependent changes in smooth muscle phenotype and contractility.

Key Words

Confocal Colocalization, Non-Muscle Myosin Heavy Chain, Organ Culture, Smooth Muscle Phenotype, VEGF Receptors

Introduction

Vascular remodeling is a highly dynamic process that continuously matches tissue perfusion to changing metabolic demands (59). Patterns of vascular remodeling vary greatly in relation to vessel type, size, age, and anatomical location (31, 60) and are particularly important during periods of rapid growth, such as those occurring in a mother and fetus during pregnancy and following birth (31, 46). Vascular remodeling is also a driving influence of many pathophysiological processes, particularly those induced by chronic hypoxia (23, 68), ischemia (41), hypertension (66), and atherosclerosis (50).

Remodeling alters the shape and size of arterial smooth muscle cells (18, 59) with corresponding changes in contractility and vascular reactivity (31, 33, 38). These changes in structure and function are presumably coupled with transformations of smooth muscle phenotype, which can be identified by characteristic changes in key contractile proteins (31, 49). In turn, changing abundance of smooth muscle-Alpha Actin (SM-AA) (44, 45) together with other contractile proteins, such as myosin heavy chain (MHC) isoforms (49, 50) reliably and dynamically reveal corresponding changes in smooth muscle phenotype during both physiological (31), and pathophysiological (23, 59, 66) vascular remodeling.

The exact mechanisms that drive vascular remodeling and phenotypic transformation of smooth muscle remain poorly understood but appear to include the actions of a broad variety of growth factors including fibroblast growth factor (48), platelet-derived growth factor (21), transforming growth factor-β (6), and vascular endothelial growth factor (28, 44). Some vasotrophic factors originate from local metabolically active parenchymal cells and act primarily at the serosal surface of blood vessels (1), whereas others such as endothelin and NO (10, 15), emanate from the

vascular endothelium and act more prominently at the luminal surface. Others are released into both the interstitium and the bloodstream and thereby coordinate widely distributed effects on vascular structure and function. An excellent example in this latter category is Vascular Endothelial Growth Factor (VEGF). Long recognized as a key mediator of angiogenesis (16), VEGF also can exert trophic effects on non-endothelial cell types including pericytes (61), CNS neurons (32), astrocytes (22), Schwann cells (58), sympathetic neurons (39), skeletal muscle (9) and smooth muscle (11, 26, 43). Equally important, the synthesis and release of VEGF are strongly stimulated by hypoxia via multiple pathways (20, 62). Together, these characteristics give VEGF the potential to broadly influence vascular remodeling and phenotypic transformation of smooth muscle, particularly in response to chronic hypoxia.

The present study explores the hypothesis that VEGF may contribute to age-dependent hypoxic remodeling of artery structure and function through changes in contractile protein abundance and organization secondary to changes in smooth muscle phenotype. In the context of this study, artery "structure" was assessed through measurements of medial layer thickness, unstressed diameter, and the transmural distribution and intracellular organization of smooth muscle contractile proteins. In turn, intracellular organization and smooth muscle phenotype were defined by the patterns of colocalization of Non-Muscle and Smooth Muscle Myosin Heavy Chain with Smooth Muscle-□Actin (49, 50). The experimental design focused first on the effects of chronic hypoxia on artery structure, contractile protein organization, and function using established methods for immunoblotting, confocal microscopy, and measurements of in vitro contractility (11, 14). The same endpoints also helped define the structural and functional effects of organ

culture with VEGF in a second tier of experiments. These experiments employed VEGF at 3 ng/ml, a low physiologically relevant concentration (19, 64) that minimized non-specific activation of non-VEGF receptors (4). To minimize influences attributable to the release of parenchymal metabolites, we performed all measurements in carotid arteries. Comparisons between arteries harvested from sheep maintained at sea level, and those maintained at high altitude (3820 m) for 110 days served to define the effects of chronic hypoxia, as previously described (47). Because vascular remodeling manifests very differently in mature and immature arteries (12), the experimental design also included comparisons between arteries harvested from non-pregnant adult sheep and term fetal lambs. Together, these approaches enabled a unique perspective of the role of VEGF in age-dependent hypoxic vascular remodeling.

Materials and Methods

All procedures used in these studies were approved by the Animal Research Committee of Loma Linda University, adhered to the policies and practices set forth by the National Institutes of Health Guide for the Care and Use of Laboratory Animals, and have been previously described in detail (11, 67).

Tissue Harvest and Preparation

Common carotid arteries were harvested using sterile techniques from fetal (139-142 days gestation) and young non-pregnant adult sheep (18-24 month old) that had been maintained at either sea level (Normoxic) or at 3820 m for 110 days (Hypoxic). Hypoxic acclimatization occurred during the final 110 days of gestation for pregnant ewes. For

tissue harvest, pregnant ewes were anesthetized with 30 mg/kg pentobarbital, intubated, and then placed on 1.5%-2.0% halothane. The fetus was then exteriorized through a midline vertical laparotomy and sacrificed by rapid removal of the heart and exsanguination. Adult animals were sacrificed by intravenous administration of 100 mg/kg IV pentobarbital. Harvested arteries were placed in sterile HEPES buffer solution containing in mM: 122 NaCl, 25.0 HEPES, 11.1 dextrose, 5.15 KCl, 2.40 $MgSO_4$, 1.6 $CaCl_2$ and 0.050 EDTA. Following gentle removal of extracellular and loose connective tissue the arteries were mechanically denuded of endothelium, as previously described (67). The denuded carotid segments were cut into segments 2 to 3 mm in length, then distributed to the various protocols.

Organ Culture

As described previously (11), artery segments designated for organ culture were maintained in untreated 12-well plates with DMEM (Sigma Aldrich, St. Louis, #M56469C) supplemented with: Na_2HCO_3 (3.7 g/L), 0.5% amino acid solution (Sigma Aldrich, St. Louis, #M5550), 1% non-essential amino acid solution (Sigma Aldrich, St. Louis, #M7145), 4 mM glutamine (Sigma Aldrich, St. Louis, #G7513), 2% antibiotic-antimycotic solution (Gibco, Carlsbad, #15240-096), and Gentamycin at 70 µg/ml (Gibco, Carlsbad, #15750-060). Cultures were maintained in a humidified incubator with 5% CO_2 in room air at 37 ºC.

Matched artery segments were cultured in supplemented DMEM without FBS for the initial 24 hours and for an additional 24 hours in media containing either DMEM (Control), 3 ng/ml VEGF-A_{165} (VEGF), or 3 ng/ml VEGF-A_{165} plus the selective VEGF

receptor inhibitor vatalanib at 240 nM (35) (VEGF+Vat). Preliminary dose-finding studies at vatalanib concentrations between 120–1200 nM were performed to identify the optimal concentration for inhibition of VEGF effects, which was 240 nM. The concentration of VEGF used (3 ng/ml) was chosen to mimic serum levels measured in pregnant sheep (64) and to minimize nonspecific binding of VEGF to other receptors (4). Following organ culture, arteries were allocated for analysis via fluorescent immunohistochemistry, Western blots, or contractility studies. Matched fresh uncultured artery segments were studied in parallel for all cultured treatments and subsequent assays.

Contractility Studies

Artery segments designated for contractility measurement were wire-mounted in vitro between an isometric force transducer and a micrometer slide used to set artery diameters. Mounted segments were first equilibrated for 30 min in calcium-replete Na^+-Krebs buffer containing (in mM) 122 NaCl, 25.6 $NaHCO_3$, 5.17 KCl, 2.56 dextrose, 2.49 $MgSO_4$, 1.60 $CaCl_2$, 0.114 ascorbic acid, and 0.027 EGTA. Buffer pH was maintained at ≈7.4 with continuous bubbling of 95% O_2, 5% CO_2 at normal ovine core temperature of 38 ^{O}C. After initial equilibration, the unstressed artery diameter (D_0) of each segment was measured at a passive tension of 0.03 g. Working diameters (D) were calculated for each artery based on its D_0 at strain ratios of D/D_0 = 1.5, 1.8, 2.1, 2.4, 2.7, 3.0, and 3.3. Contractile stresses in dynes/cm^2 were recorded at each of these strain values, in increasing order under resting conditions to determine spontaneous myogenic stress, followed by contraction in a high potassium buffer containing (in mM) 122 KCl, 11.1 Dextrose, 5.16 NaCl, 2.50 $MgSO_4$, 2.15 $NaHCO_3$, 1.60 ml $CaCl_2$, 0.114 Ascorbic Acid,

and 0.027 EDTA. After K^+-induced contractions had stabilized, arteries were returned to Na^+-Krebs buffer, allowed to relax, then stretched to and equilibrated at the next highest stretch ratio. Once the K^+-induced contraction had been measured at the maximum D/D_0 ratio of 3.3, the arteries were frozen in liquid nitrogen to rupture the cells, and then incubated in a calcium free Na^+-Krebs buffer containing 3 mM EGTA to further inhibit smooth muscle cell derived-force through Ca^{2+} sequestration. The level of passive stress produced at each strain ratio used was then recorded at each descending stretch ratio. Myogenic stresses were calculated as the spontaneous stresses measured under resting conditions at each strain ratio (D/D_0) minus the passive stresses measured after freezing in liquid N_2 at the same strain ratio. The potassium-induced stresses were calculated as the maximum stresses measured during exposure to high potassium at each strain ratio (D/D_0) minus the spontaneous stresses measured under resting conditions at the same strain ratio. Arterial stiffness was determined using the relations between strain and passive stress, using curve-fitting with a monotonic exponential model to determine the coefficient of stiffness. All methods used to quantify contractility have been previously described in detail (11).

Fluorescent Immunohistochemistry

Matched artery segments were fixed in 4% neutral buffered EM-grade formaldehyde (Electron Microscopy Sciences, Hatfield, #15713S) for 48 h at 4^OC. Segments were dehydrated and embedded in paraffin, sectioned at 5 µm, and mounted on slides. Sections were deparaffinized in Histo-Clear (National Diagnostic, Atlanta, #HS-200), rehydrated in decreasing concentrations of alcohol, and then microwaved in a

citrate buffer (pH 6.03) to retrieve antigenicity. Permeabilization and blocking was done with 0.1% Triton X-100 (Sigma Aldrich, St. Louis, #T-8787) and 1% Bovine Serum Albumin (Santa Cruz Biotechnology, Santa Cruz, #SC-2323) in PBS. To detect for changes in phenotype, artery sections were probed with antibodies to reveal expression of Non-Muscle Myosin Heavy Chain (NM-MHC), which is a marker for incompletely differentiated, partially contractile smooth muscle, and Smooth Muscle Myosin Heavy Chain (SM-MHC), a marker for differentiated, contractile smooth muscle (49, 50). Although the amino terminus of MHC can include a 7 amino acid insert in phasic smooth muscle (the MHC-B family), arterial MHC consistently lacks this insert (the MHC-A family) (17), and thus these studies assumed that all MHC detected was of the MHC-A family of smooth muscle myosin isoforms.

Arterial sections were exposed to primary antibodies overnight with polyclonal rabbit anti-human Non-Muscle Myosin Heavy Chain (NM-MHC; CoVance, Princeton, PPR-445P) at 1:500 or polyclonal rabbit anti-bovine Smooth Muscle Myosin Heavy Chain (SM-MHC; Abcam, Cambridge, ab53219) at 1:500. The following day, slides were washed for two 10-minute cycles in PBS and incubated using the appropriate secondary antibody with DyLight 488 Conjugated (Pierce Chemical, Rockford, #35502) for two hours at room temperature. The secondary antibody was a goat anti-rabbit-488 (Thermo Scientific, Rockford, #35552 Lot LI150311). To minimize photobleaching of the fluorescent dyes, slides were stored in the dark. Following two 10-minute cycles in PBS, tissue slides were coverslipped using SlowFade Gold anti-fade reagent with DAPI (Invitrogen, Carlsbad, S36939) then stored until imaged. All images were captured using

a Zeiss AXIO Imager A1 fluorescence microscope and Spot software (Diagnostic Instruments, Inc. Ver 4.6.4.5).

Transmural Morphometry

As previously described in detail (11), artery sections processed for fluorescent immunohistochemistry were analyzed using standard morphometric procedures to quantify the distribution of contractile proteins across the artery wall. For this analysis, six individual line-intensity scans were recorded along radial lines extending from the basal lamina to the adventitial-medial junction using Image Pro Plus (Media Cybernetics, Version 6.0). The radial scan lines mapped fluorescent intensity versus distance from the lumen and were equally distributed at 60-degree increments around the lumen. Distance measurements were normalized to medial thickness with a value of "0" assigned to the region just inside the basal lamina and a value of "100" assigned to the region just inside the adventitial-medial junction. Following published procedures (11), separately determined calibration curves were used to convert fluorescent intensities into relative fluorophore concentrations, and thereby linearize estimates of signal intensities and corresponding regional antigen concentration. These estimates were averaged as a function of relative distance from the lumen for all line scans from the same section. The "Inner", "Middle", and "Outer" regions were averaged across values from 5-20%, 45-60%, and 80-95% of the normalized distance from the lumen respectively. The innermost 5% and outermost 5% of the medial layer were excluded to avoid autofluorescent contamination from the basal elastic lamina and adventitial elastin and collagen, respectively. These lines determined the relative distribution of each marker across the

artery wall. The absolute abundance of each marker in the whole artery wall was determined by semi-quantitative Western blot. For each marker, the area beneath the distance-concentration curves were normalized to 100%, then multiplied by the Western blot values to calculate relative local abundance values that could be compared between regions and experimental groups.

Confocal Microscopy

Matched artery segments were collected, prepared and cut into 5 μm sections, deparaffinized, sectioned, and immunostained as described for Transmural Morphometry, with the exception that all sections were stained with primary monoclonal mouse anti-sheep antibodies against SM-AA (Sigma-Aldrich, A5228, 1:200) and a second primary antibody against one of the MHC isoforms. Because in arterial smooth muscle the □ isoform of actin is the main isoform involved in smooth muscle contraction (45), all colocalization of MHC was quantified relative to the abundance of □ actin. Because only alpha actin is involved in smooth muscle contraction, changes in the other actin isoforms that can also be expressed in smooth muscle (45) should have little if any influence on smooth muscle contractility. The antibodies used to detect the MHC isoforms were as described in the Fluorescent Immunohistochemistry section. Following incubation with the primary antibodies, sections were washed in PBS, equilibrated in darkness for 2 h at room temperature with two secondary antibodies labeled with Dylight-488 to detect SM-AA and Dylight-649 to detect MHC, as indicated for Fluorescent Immunohistochemistry. Following secondary staining, sections were cover-slipped using Slowfade Gold Antifade Reagent (S36936, Invitrogen), and then examined

with an Olympus FV1000 confocal microscope at an optical section thickness of 0.7 μm, a lateral resolution of 200 nm, and a numerical aperture of 18.

Antigen colocalization in confocal images was analyzed using FlouView software (version 2.1c), which provided multiple indices of co-localization including the Manders Colocalization Index 1 (actin signal in the denominator) that quantifies the portion of pixels that fluoresce for both MHC and SM-AA relative to the total number of pixels positive for SM-AA. Positive pixels were defined as having a fluorescent intensity equal to or greater than 5% of the maximum fluorescence intensity in the section. To eliminate cells with a small but significant above-threshold abundance of SM-AA characteristic of incompletely differentiated smooth muscle cells and some non-smooth muscle cell types (55), a second index of colocalization was developed. This second index, which we termed %Upper Right (%UR), was calculated to select for differentiated contractile smooth muscle as identified by high SM-AA abundance levels. This index counted only pixels that fluoresced at or above the mean intensity threshold for SM-AA, which in essence was equivalent to recalculating the Colocalization Index 1 with an SM-AA threshold of 50% of maximum intensity. This method of analysis was derived from a flow-cytometry quadrant analysis, and thus was referred to as the percentage in the upper right quadrant of the scatterplot of SM-AA intensities against MHC intensities. From a general perspective, Colocalization Index 1 and %UR were both proportional to the fraction of actin-positive pixels that were also positive for MHC. Interestingly, the results obtained for both Colocalization Index 1 and %UR varied somewhat in absolute values, but were qualitatively similar.

Immunoblotting

Artery segments were homogenized via glass on glass in 8 M Urea, 500 mM NaCl, 23 mM Glycine, 20 mM Tris, 10 mM EGTA, and 10% Glycerol at pH 8.6 with the addition of a protease inhibitor cocktail at 5 µl per ml of buffer (Sigma-Aldrich, Saint Louis, #M1745) that included (final concentrations): 52 mM AEBSF, 2 mM Bestatin, 1 mM Leupeptin, 750 µM Pepstatin A, 700 µM E-64, and 40 µM Aprotinin. Centrifugation of the homogenate at 5,000 G for 20 minutes yielded a supernatant in which protein concentration was determined using the Bio-Rad Bradford assay. Optimal masses of total soluble protein in the extracted supernatant were loaded after which the proteins were separated by SDS-PAGE alongside pooled reference standards prepared from adult ovine common carotid arteries used to calibrate sample abundances on each gel. Separated proteins were transferred to nitrocellulose at 350 mA for 90 minutes in Towbin's buffer (192 mM Glycine, 25 mM Tris, Methanol-10% for MHC and 20% for SM-AA) with beta-mercaptoethanol added to the upper buffer reservoir. Membranes were blocked with 5% milk in Tris-buffered saline at pH 7.5 (M-TBS) for 1 hour at room temperature using continuous shaking. All subsequent washes and incubations were done in M-TBS with 0.1% Tween-20. Membranes were incubated with the same primary antibodies listed above at the following concentrations: anti-SM-AA 1:3000, anti-NM-MHC 1:1000 and anti-SM-MHC 1:20,000 for 3 hours. For visualization, membranes were incubated for 90 minutes with a secondary antibody conjugated to DyLight 800 (Pierce Chemical, Rockford, #46422) and imaged on a LI-COR Bioscience's Odyssey system. All protein abundances were expressed as the equivalent mass of standard relative to the mass of protein loaded in each lane.

Data Analysis and Statistics

Contractile stresses were calculated as ratios of force per cross-sectional area, where force was calculated as contractile tension in grams times the acceleration due to gravity. Cross-sectional area (wall thickness x segment length) was corrected for changes with stretch as described previously (30, 46). Stress values were normalized within each artery segment by calculating the percent of the maximum force produced by the artery exerted at each stretch ratio. Percent maximum values were converted back into absolute units of stress by multiplying by the average maximum stress calculated across all segments within the same experimental group.

Immunofluorescence intensity values were recorded as a function of relative radial distance from the lumen to the adventitia, then normalized within each segment to yield an area beneath the intensity-distance curve of unity, as previously described in detail (11). Fluorescence intensity values were calibrated against relative marker abundance measured with Westerns, which in turn were calibrated for each marker against a standard curve pooled from adult common carotids. For confocal colocalization, all values were calculated among SM-AA positive pixels and determined the fractions of those pixels also positive for each of the MHC isoforms. The total colocalization values were obtained by adding the individual colocalization index values for each of the MHC isoforms, and the group error was calculated as a pooled variance. All statistical comparisons were done using Behrens-Fisher comparison at the $P<0.05$ level with each animal contributing equally to each treatment group.

Results

A total of 174 endothelium-denuded carotid artery segments were harvested from 8 normoxic fetuses (FN), 7 hypoxic fetuses (FH), 11 normoxic adults (AN), and 8 hypoxic adults (AH). When duplicate segments from a single animal were used in the same protocol, the resulting values were averaged and the resulting average was treated as a single observation. Throughout the text, "n" denotes the number of animals used in each experiment, not the number of segments. Statistical significance was defined at $P < 0.05$ for all assays, with all values given as means ± SEM.

Chronic Hypoxia Altered Age-Dependent Contractile Function of Large Arteries

Normoxic values of medial wall thicknesses and unstressed diameters were significantly less in fetal than in adult arteries, and these values were not significantly different than age-matched hypoxic values (**Table 1**). Maximum stretch-dependent stresses were significantly greater in fetal than in adult arteries, and were significantly less in hypoxic than in normoxic arteries from both age groups (**Figure 1**). Conversely, maximum K+-induced stresses were significantly greater in adult than in fetal arteries and were decreased only modestly by hypoxia in both age groups.

Chronic Hypoxia Altered Age-Dependent MHC Abundance and Distribution

Relative abundances of the embryonic isoform of MHC (NM-MHC) were significantly greater in fetal than adult arteries and were similarly increased by hypoxia in both age groups. Normoxic fetal values averaged 1,350% of normoxic adult values, and

hypoxic fetal values averaged 850% of hypoxic adult values (**Figure 2**). In hypoxic arteries, NM-MHC abundance values averaged 137% and 216% of normoxic values in fetal and adult arteries, respectively. In normoxic fetal arteries, the regional abundance of NM-MHC (in μg / μg standard) was significantly greater in the inner medial region (7.87 ± 0.67) than in either the middle medial (4.82 ± 0.33) or outer medial (4.75 ± 0.42) regions (**Figure 2**). A similar pattern was observed across the inner medial (9.90 ± 1.11), middle medial (6.94 ± 0.74) and outer medial (7.03 ± 0.76) regions of hypoxic fetal arteries. In adult arteries, NM-MHC abundance values did not vary significantly among regions in either normoxic or hypoxic arteries.

Table 1. Effects of Hypoxia and VEGF on Artery Structure and Function

		Medial Thickness (μm)	Unstressed Diameter (μm)	Stretch-Dependent Maximum Stress (dynes/cm^2)	K+-Induced Maximum Stress (dynes/cm^2)
Fetal	**Normoxic**	203±18 ^{A}	2,900±290 ^{A}	19,730±6,460 ^{A,H}	6,370±1,890 ^{A}
	Hypoxic	221±21 ^{A}	3,230±250 ^{A}	6,280±1,220 ^{A,H}	5,240±1,170 ^{A}
Adult	**Normoxic**	543±25 ^{A}	4,020±310 ^{A}	8,600±1,730 ^{A,H}	31,220±3,530 ^{A}
	Hypoxic	591±30 ^{A}	3,760±220 ^{A}	6,660±1,730 ^{A,H}	28,640±4,460 ^{A}
Fetal	**Control**	207±10 ^{A}	3,149±210 ^{A}	17,510±4995 ^{A,V}	6,037±636 ^{A,I}
	VEGF	211±14 ^{A}	3,339±296 ^{A}	6,541±2506 ^{A,V}	7,264±887 ^{A}
	VEGF+Vat	231±10 ^{A}	2,498±91 ^{A}	7,279±1285 ^{A}	9,995±1,945 ^{A,I}
Adult	**Control**	469±21 ^{A}	4,742±204 ^{A}	30,756±7685 ^{A,V}	8,167±1,773 ^{V}
	VEGF	501±26 ^{A}	4,645±270 ^{A}	15,192±3737 ^{A,V,I}	4,479±1,260 ^{V,I}
	VEGF+Vat	478±22 ^{A}	4,754±206 ^{A}	25,475±7876 ^{A,V}	6,990±1,197 ^{V}

Medial thicknesses were measured in unfixed specimens using phase contrast light microscopy. Unstressed diameters were measured in arteries mounted in vitro for contractility. Stretch-dependent maximum (myogenic) stresses and maximum active stresses induced by exposure to isotonic Krebs buffer containing 122 mM K^+ were averaged across arteries independent of the strain at which the maximum was observed. Note that the average of the maximum potassium-induced stresses (above) was greater than the maximum of the average potassium-induced stresses plotted against stretch-ratio in Figure 4. This difference implies that the stretch ratios at which maximum contractility was observed varied markedly among different segments. All normoxic and hypoxic values were obtained in freshly dissected arteries, whereas Control, VEGF, and VEGF+Vatalanib values were obtained in arteries organ cultured 48h. Indicated are means ± SEM for arteries from 8 normoxic fetuses, 4 hypoxic fetuses, 11 normoxic adults, and 8 hypoxic adults. The Control, VEGF, and VEGF+Vat means were calculated from 6 normoxic fetal lambs and 11 normoxic adult sheep. Superscript A, H, V, and I denote significant differences ($P<0.05$) due to Age, Hypoxia, VEGF-treatment, and VEGFR Inhibitor-treatment.

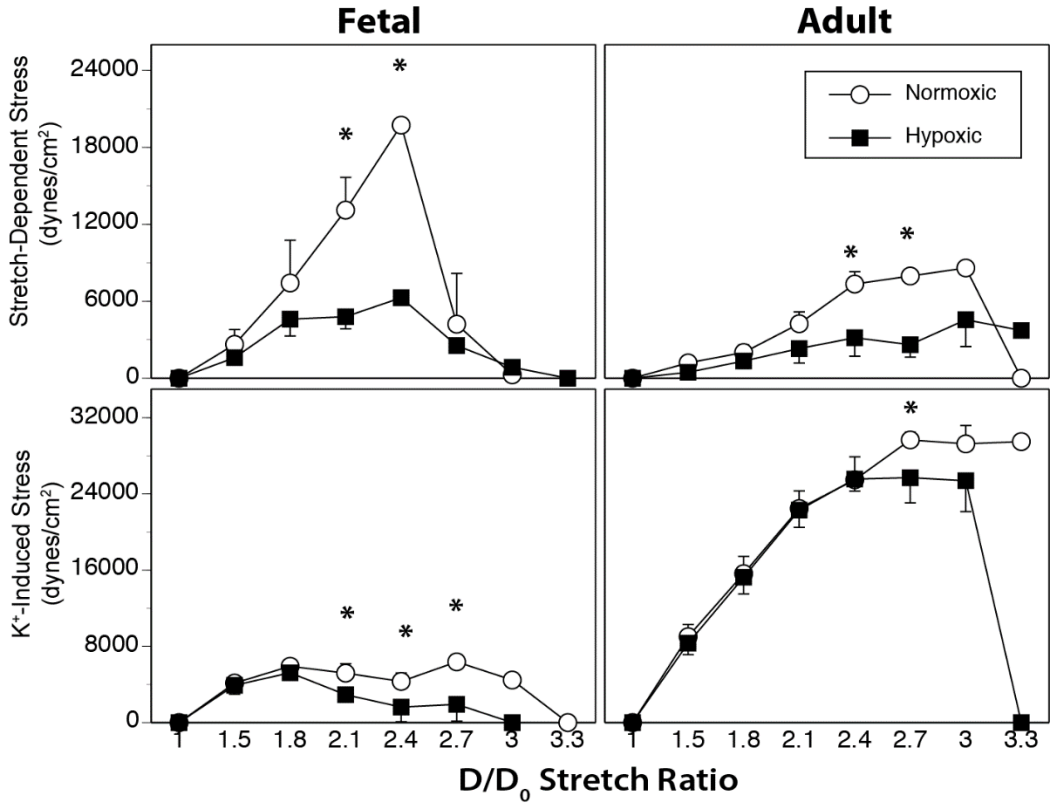

Figure 1. Chronic Hypoxia Decreases Myogenic Contractility.
Endothelium-denuded common carotid arteries harvested from fetal and adult sheep maintained at 3820 m for 110 days (Hypoxic) or at sea level (Normoxic) were used to determine stretch-induced myogenic stresses at different strains applied in increments of unstressed diameter (D/D_0). Myogenic stresses were calculated as the spontaneous stresses measured under resting conditions at each strain ratio (D/D_0) minus the passive stresses measured after freezing in liquid N_2 at the same strain ratio. Active potassium-induced stresses were induced by exposure to isotonic Krebs buffer containing 122 mM K^+. The potassium-induced stresses were calculated as the maximum stresses measured during exposure to high potassium at each strain ratio (D/D_0) minus the spontaneous stresses measured under resting conditions at the same strain ratio. Note that spontaneous myogenic stresses were greater in fetal than adult arteries (upper panels), whereas active potassium-induced stresses were less in fetal than adult arteries (lower panels). Error bars indicate SEM for arteries from 8 normoxic fetuses, 4 hypoxic fetuses, 11 normoxic adults, and 8 hypoxic adults. The * denotes significant differences between normoxic and hypoxic values at $P<0.05$.

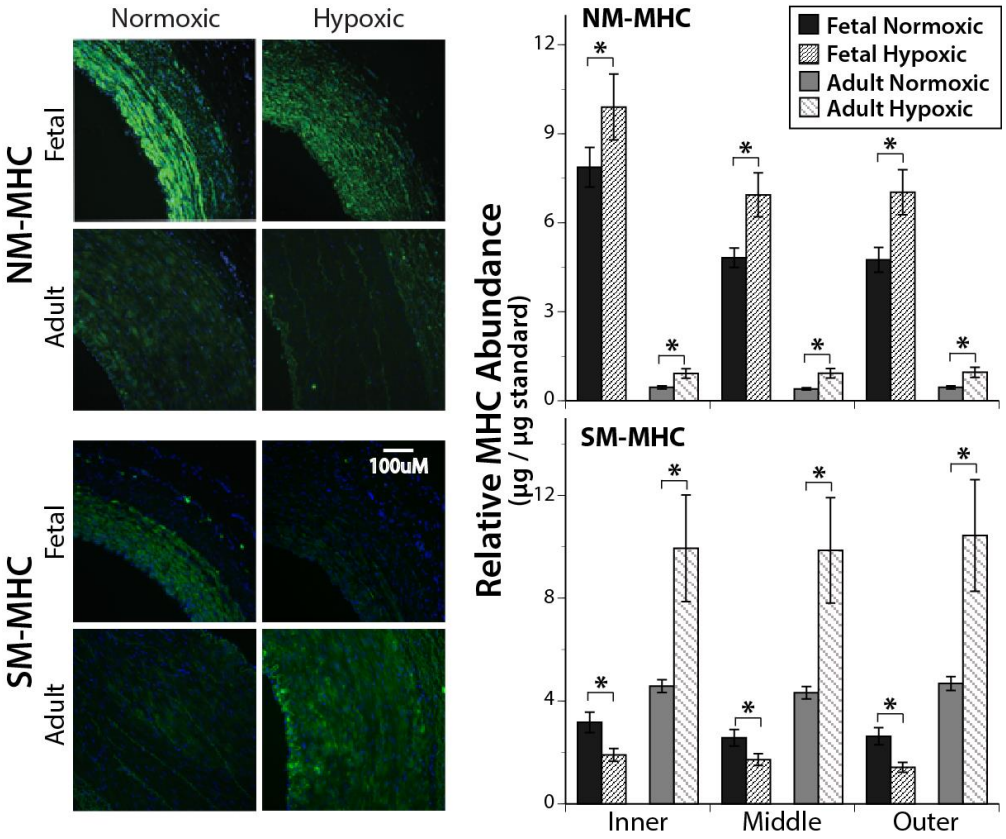

Figure 2. Chronic Hypoxia Alters Myosin Heavy Chain Abundance and Distribution. Coronal sections of endothelium-denuded carotid arteries from normoxic (N) and hypoxic (H) fetal and adult sheep were immunostained for Non-Muscle Myosin Heavy Chain (NM-MHC) or Smooth Muscle Myosin Heavy Chain (SM-MHC). Cell nuclei were stained with DAPI (blue). In the left panel are representative matched sections from a single animal for NM-MHC and SM-MHC. Whole artery abundance of each MHC was quantified via immunoblot and MHC distribution between the luminal and adventitial margins of the medial layer was determined by line scans of the images. Regions within the artery wall were defined as Inner (area just inside basal elastic lamina), Middle (area midway between basal elastic lamina and adventitial-medial border), and Outer (medial area immediately adjacent to the adventitial-medial border). Each individual MHC isoform differed significantly between normoxic and hypoxic arteries as denoted by asterisks on the figure ($P<0.05$). MHC abundances varied significantly ($P<0.05$) among the different intramural regions only in fetal arteries. Vertical error bars represent standard errors for $n\geq5$ for all groups.

For SM-MHC, relative abundance was significantly less in fetal than in adult arteries; fetal values averaged only 62% of adult values in normoxic arteries, and only 17% of adult values in hypoxic arteries. Hypoxia significantly decreased SM-MHC abundance to 60% of normoxic values in fetal arteries but increased it to 223% of normoxic values in adult arteries. Distribution was homogenous among all artery wall regions in all four treatment-age groups (**Figure 2**).

Hypoxia Altered Colocalization of MHC Isoforms and SM -Alpha Actin

Consistent with the abundance results, colocalization of NM-MHC with SM-AA in normoxic fetal arteries averaged 1,820% of colocalization in normoxic adult arteries (**Figure 3**), and in hypoxic fetal arteries averaged 880% of colocalization in hypoxic adult arteries; maturation markedly decreased NM-MHC colocalization. Hypoxia depressed NM-MHC colocalization to 52% of normoxic values in fetal arteries ($P<0.05$), but was without effect in adult arteries (**Figure 3**).

Although SM-MHC abundance was significantly less in fetal than adult arteries (**Figure 2**), colocalization of SM-MHC with SM-AA was greater in fetal than adult arteries. SM-MHC and SM-AA colocalization also was not affected by chronic hypoxia in fetal arteries, but was decreased by hypoxia in adult arteries. Colocalization values in normoxic fetal arteries were 220% of values in normoxic adult arteries, and in hypoxic fetal arteries colocalization averaged 390% of hypoxic adult arteries (**Figure 3**).

Effects of VEGF and VEGF Receptor Antagonism on Age-Dependent Contractility

To assess the potential role of VEGF in hypoxic vascular remodeling, the effects of VEGF on vascular contractility were determined in a separate series of arteries cultured in the presence and absence of the VEGF receptor antagonist vatalanib (**Figure 4**) (35). Medial wall thicknesses and unstressed diameters were significantly less in fetal than adult arteries in each treatment group and did not vary with treatment in either age group (**Table 1**).

Maximum stretch-dependent stresses averaged less in fetal than adult arteries in all three treatment groups (**Table 1**). In fetal arteries, maximum stretch-dependent stresses in VEGF-treated and VEGF+vatalanib treated arteries were only 37% and 42% of control values, respectively ($P<0.05$) and did not differ from one another. In adult arteries, maximum stretch-dependent stresses in VEGF-treated arteries were 49% of control whereas these values in the VEGF+vatalanib groups were 83% of control; vatalanib prevented the effects of VEGF such that stretch-dependent stresses in the VEGF+vatalanib group were similar to the control group.

Maximum K^+-induced stresses in fetal and adult arteries were similar in the control group, but in the VEGF and VEGF+vatalanib groups, fetal values were significantly greater than adult values (**Table 1**). In fetal arteries, stresses in VEGF and VEGF+vatalanib treatment groups were 120% (NS) and 166% ($P<0.05$) of control values, respectively, and did not differ from one another. In adult arteries, average stresses in the VEGF and VEGF+vatalanib groups were 55% ($P<0.05$) and 86% (NS) of control values; in adult arteries vatalanib prevented the effects of VEGF such that stretch-

dependent stresses in the VEGF+vatalanib group were significantly greater than in the VEGF group and were similar to the control group.

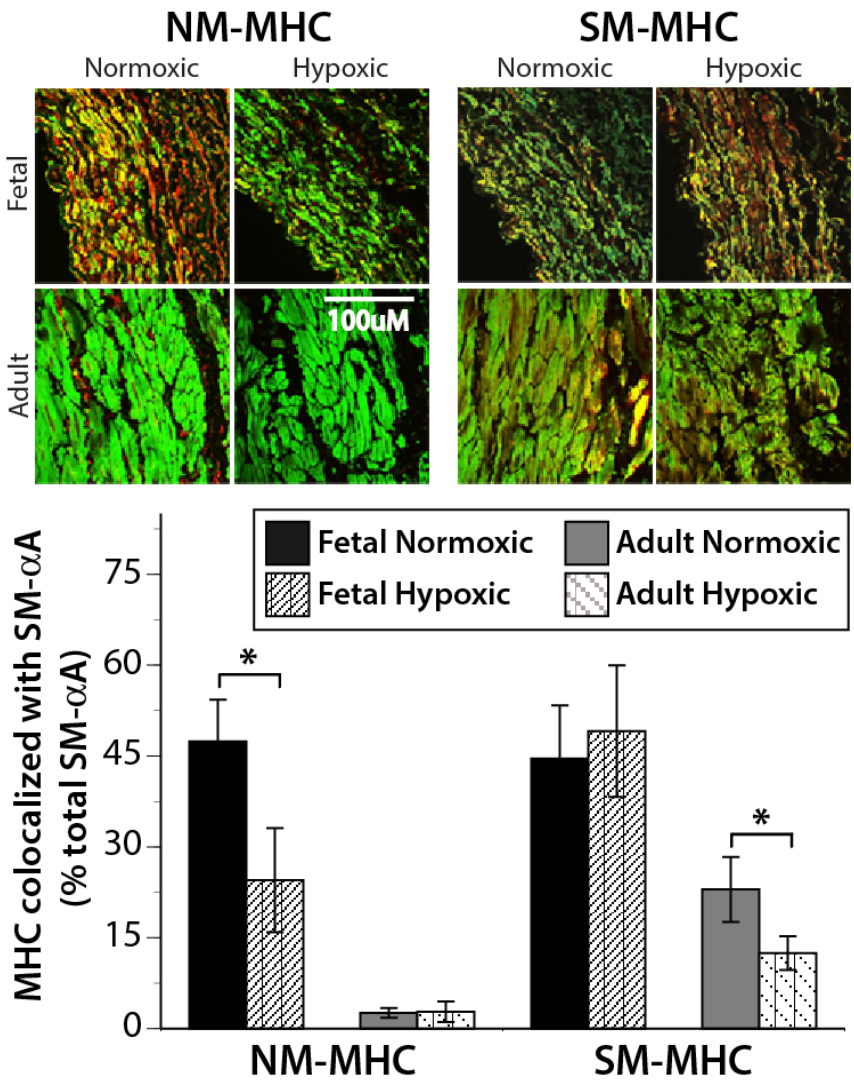

Figure 3. Hypoxia and Age Modulate Colocalization of Myosin Heavy Chain Isoforms with Smooth Muscle-Alpha Actin.

Coronal sections of endothelium-denuded carotid arteries from normoxic and hypoxic fetal and adult sheep were immunostained for myosin heavy chain isoforms NM-MHC or SM-MHC (red) and Smooth Muscle-Alpha Actin (SM-AA, green). Colocalizations of SM-AA with myosin heavy chain isoforms are displayed in the merged images (yellow). Colocalization of NM-MHC with SM-AA was significantly greater in fetal than in adult arteries and was also less in hypoxic than in normoxic fetal but not adult arteries. Colocalization of SM-MHC with SM-AA was significantly greater in fetal than in adult arteries and was also less in hypoxic than normoxic adult but not fetal arteries . Asterisks (*) indicate significant effects of hypoxia at $P<0.05$ for $N\geq 4$ in each group. Error bars indicate standard errors.

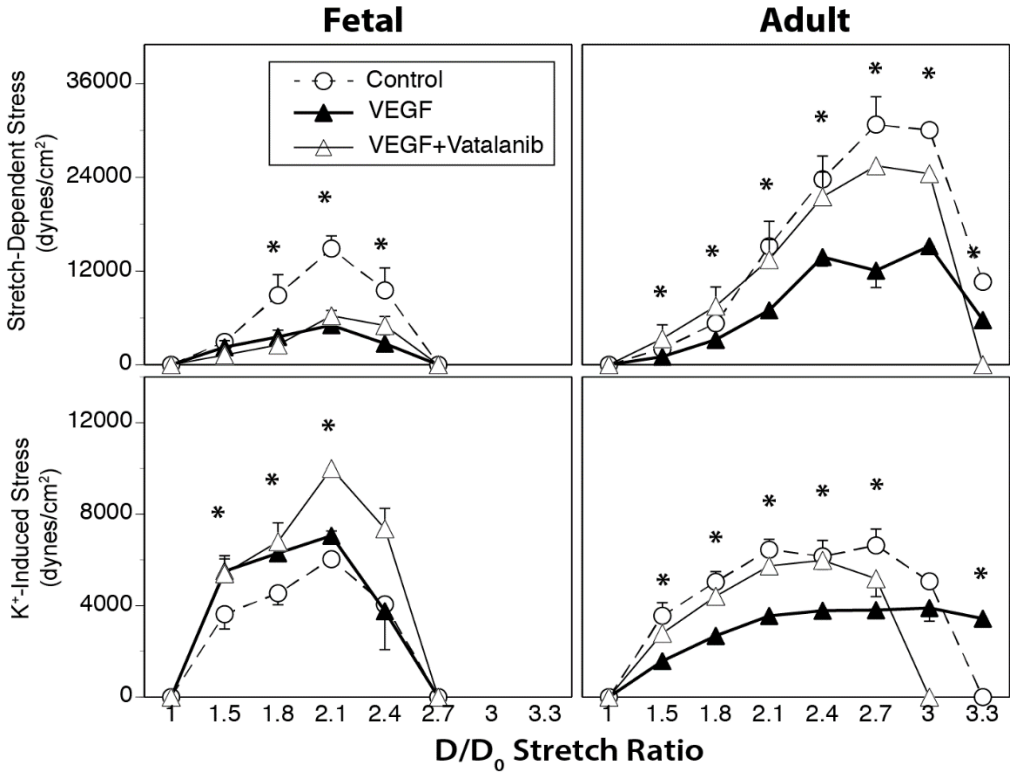

Figure 4. The VEGF Receptor Inhibitor Vatalanib Ablates the Effects of VEGF. Endothelium-denuded carotid arteries from 6 normoxic fetal lambs and 11 normoxic adult sheep were serum starved for 24h then cultured another 24h under starvation conditions (Control), with 3 ng/ml VEGF (VEGF), or with 3 ng/ml VEGF + 240 nM vatalanib (VEGF+vatalanib). With this approach, all arteries underwent a standardized organ culture regiment with treatments between groups varying only by the presence or absence of VEGF and/or vatalanib. Following organ culture, stress-strain relations were determined; at each level of strain examined both stretch dependent myogenic stress (upper panels), and the active response to depolarization with 122 mM potassium (lower panels) were determined. VEGF decreased stretch-dependent stresses in both fetal and adult arteries, but decreased potassium-induced stresses only in adult arteries. Vatalanib prevented the effects of VEGF on myogenic and active stresses only in adult arteries. Asterisks denote significant differences between control and VEGF treatment at $P<0.05$ (Behrens Fisher). Error bars indicate SEM for the N values given in Table 1.

Effects of VEGF on Age-Dependent MHC Abundance and Distribution

To explore the effects of serum starvation alone on MHC isoform expression, abundances in normoxic fresh, uncultured arteries (**Figure 2**) were compared to corresponding values in serum-starved control arteries (**Figure 5**). These comparisons revealed that in contrast to the marked effects of serum starvation on the abundance of other contractile proteins such as MLCK (11), serum starvation had only modest effects on the abundance of MHC isoforms in both fetal and adult arteries. To control for these changes, all effects of VEGF were determined by comparisons between "starved" and "VEGF-treated" segments. With this approach, all arteries underwent a standardized organ culture regiment with treatments between groups varying only by the presence or absence of VEGF and/or vatalanib.

The relative abundance of NM-MHC in control and VEGF-treated fetal arteries was 1,960% and 1,740% of abundance in corresponding adult arteries **(Figure 5)**. VEGF treatment increased NM-MHC abundance in fetal arteries, but this effect was significant only in the inner medial region. VEGF had no significant effect on NM-MHC abundance in adult arteries. In control fetal arteries, the local abundance (in μg / μg standard) of NM-MHC was significantly greater in the inner medial region (5.35 ± 0.78) than in the middle medial region (3.88 ± 0.55), which in turn was greater than in the outer medial (2.54 ± 0.37) region (**Figure 5**). A similar pattern was observed across the inner medial (6.64 ± 0.53), middle medial (4.43 ± 0.36) and outer medial (2.99 ± 0.22) regions of VEGF-treated fetal arteries. In adult arteries, NM-MHC abundances did not vary significantly among regions in either control or VEGF-treated arteries.

For SM-MHC, the relative abundances were significantly less in control fetal than in control adult arteries. VEGF treatment did not significantly influence abundances of SM-MHC in either fetal or adult arteries, and these abundances remained significantly less in VEGF-treated fetal than in VEGF-treated adult arteries (**Figure 5**). Regional abundances of SM-MHC did not vary significantly across the different transmural regions in control or VEGF-treated arteries from either age group.

VEGF Altered Colocalization of MHC with SM-Alpha Actin

Colocalization of NM-MHC with SM-AA in control fetal arteries averaged 710% of control adult arteries (**Figure 6**). VEGF treatment reduced NM-MHC colocalization to only 32% and 36% of control values in fetal and adult arteries, respectively. After VEGF treatment, NM-MHC colocalization remained markedly greater in fetal than adult arteries.

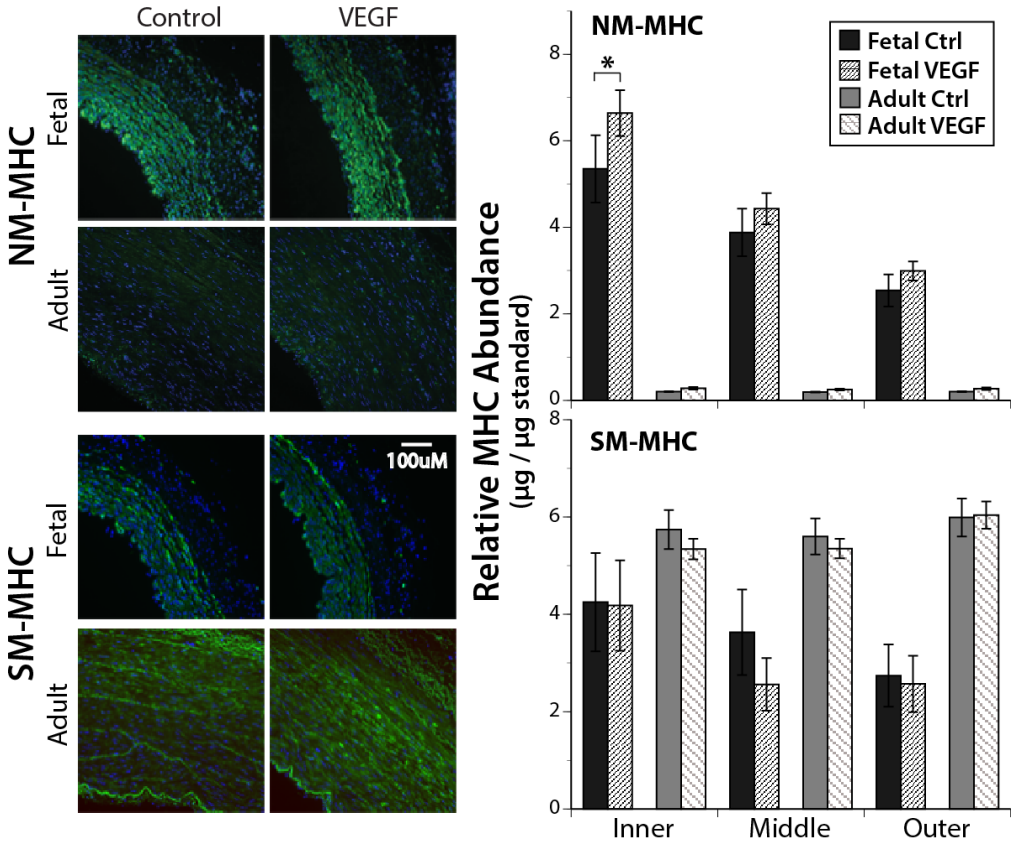

Figure 5. Effects of VEGF on Myosin Heavy Chain Abundance and Distribution. Endothelium-denuded carotid arteries from 6 normoxic fetal lambs and 6 normoxic adult sheep were serum starved for 24h and then were cultured an additional 24h in the presence or absence of 3 ng/ml VEGF. Following organ culture, the arteries were processed for immunostaining as described for **Figure 2**. Organ culture with VEGF did not significantly ($P<0.05$) alter abundance for either MHC isoform except a modest increase of NM-MHC with VEGF in the inner medial region of fetal arteries (*). In both control and VEGF-treated fetal arteries, NM-MHC exhibited a gradient in which abundance was greatest in the inner medial layer and least in the outer medial layer. Shown are means and standard errors for N=6 for all groups.

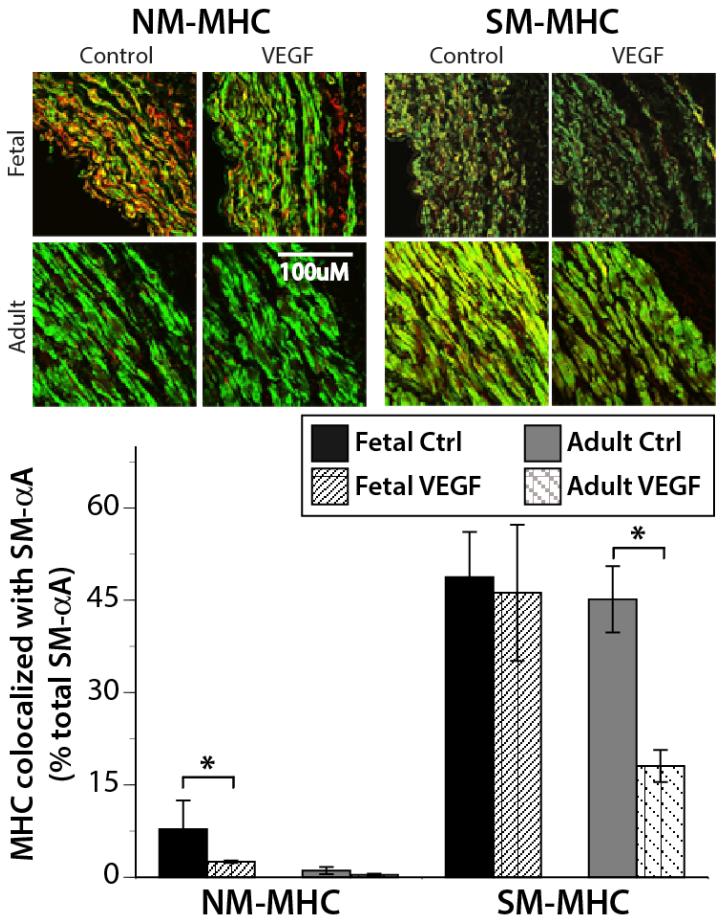

Figure 6. VEGF Alters Colocalization of Myosin Heavy Chain Isoforms with Smooth Muscle-Alpha Actin.

Coronal sections of endothelium-denuded carotid arteries from 6 normoxic fetal and 6 normoxic adult sheep were immunostained following organ culture with or without VEGF as described for **Figure 3**. Colocalizations of SM-AA (green) with myosin heavy chain isoforms are displayed in the merged images (yellow) for the NM-MHC and SM-MHC isoforms (red). Colocalization of NM-MHC with SM-AA was significantly decreased by VEGF only in fetal arteries (*). Colocalization of SM-MHC with SM-AA was significantly decreased by VEGF only in adult arteries (*). Statistical significance implies $P<0.05$. Vertical error bars indicate standard errors for $n\geq5$ for all groups.

Colocalization of SM-MHC with SM-AA was similar in control fetal and control adult arteries. VEGF treatment had no significant effect on SM-MHC colocalization in fetal arteries, but decreased colocalization significantly to 40% of control values in adult arteries. After VEGF treatment, SM-MHC colocalization in fetal arteries was 260% of colocalization in adult arteries.

Discussion

The present study offers six original observations in endothelium-denuded carotid arteries. First, hypoxic acclimatization depressed stretch-dependent contractions much more than K+-induced contractions in both fetal and adult arteries. Second, hypoxic acclimatization increased abundances of NM-MHC in fetal and adult arteries but increased SM-MHC only in adult arteries. Third, hypoxic acclimatization decreased the colocalization of NM-MHC with SM-AA only in fetal arteries but decreased colocalization of SM-MHC with SM-AA only in adult arteries. Fourth, similar to hypoxia, organ culture with 3 ng/ml VEGF depressed stretch-dependent and K^+-induced contractions in both adult and fetal arteries. Fifth, unlike hypoxia, organ culture with VEGF induced few significant changes in MHC abundance in either fetal or adult arteries. Sixth, like hypoxia, organ culture with VEGF decreased the colocalization of NM-MHC with SM-AA in fetal arteries and decreased colocalization of SM-MHC with SM-AA in adult arteries. Together, these observations support the hypothesis that VEGF may contribute to age-dependent hypoxic remodeling of artery structure and function through changes in contractile protein abundance and organization secondary to changes in smooth muscle phenotype.

Hypoxic Acclimatization Altered Artery Structure and Function

The effects of hypoxic acclimatization on artery wall thicknesses vary with artery type, size, and age (38, 60, 68) and can differentially affect the endothelial, medial and adventitial layers (59, 67). To better understand the functional consequences of hypoxic changes in artery structure, the present study focused on the medial layer that contains the smooth muscle cells responsible for contractile force. In both adult and fetal ovine carotid arteries, hypoxic acclimatization had no significant effect on medial thicknesses, which suggests that any changes in artery contractility induced by hypoxia must have been due to changes in either the abundances or organization of contractile proteins within the arterial smooth muscle.

In many vascular studies, contractile responses are measured only in units of grams or as percentages of responses to a standard contractant such as high potassium at a single segment length or passive tension. These approaches can provide excellent internal normalization but do not account for differences in wall thickness, contractile protein content, stiffness, or optimum length, which can be significant when comparing contractility across different chronic treatment groups. To avoid these limitations, our experimental approach included complete stress-strain determinations for each segment in which contractile responses were quantified as changes in active stresses measured in units of force per medial cross-sectional area at multiple levels of arterial strain, as previously described (11). Consistent with earlier findings, these measurements revealed (**Figure 1**) that K+-induced contractions were greater in adult than fetal arteries (11), and were not dramatically attenuated by hypoxia (38). In contrast, stretch-dependent (myogenic) contractions were of greater magnitude in fetal than adult arteries but were

similarly and significantly attenuated by hypoxic acclimatization in both age groups (**Table 1**). This disconnect between the effects of hypoxia on K+-induced and stretch-dependent (myogenic) contractions demonstrates that hypoxic acclimatization can differentially influence select components of the contractile apparatus and may preferentially affect mechanisms coupling stretch to contraction. Candidate mechanisms potentially involved in this selective effect of hypoxia include calcium channels involved in mechanotransduction (27) and contractile proteins involved in myogenic regulation of myofilament calcium sensitivity (14, 52). Interestingly, many of these mechanisms are strongly influenced by phenotypic transformation of smooth muscle (14, 29, 65).

Hypoxic Acclimatization Altered MHC Abundance and Organization

To explore the hypothesis that hypoxic changes in artery structure and contractility may be secondary to changes in smooth muscle phenotype, our experiments focused on changes in the abundance of MHC isoforms that are closely associated with both contractile capacity and smooth muscle phenotype (23, 24, 49). Because smooth muscle morphology and phenotype are highly heterogeneous in the artery wall (18, 60) our measurements of MHC abundance combined homogenate immunoblots calibrated against known standards, with radial line scans of fluorescent intensity in immunostained coronal sections to estimate regional protein abundance across the artery wall, as previously described (11). This approach revealed that the embryonic isoforms of MHC (NM-MHC), which are prevalent in functionally immature and proliferative smooth muscle cells (17, 44, 49), were more abundant in fetal than adult arteries, were more abundant in hypoxic than normoxic arteries in both age groups, and exhibited significant

regional variability with highest abundance near the lumen in fetal arteries (**Figure 2**). Together, these NM-MHC results support the hypothesis that hypoxia stimulates phenotypic transformation of arterial smooth muscle. The regionality of this effect in fetal arteries further suggests that vasotrophic factors released from the vascular endothelium, which was present and presumably functional in both normoxic and hypoxic fetal arteries before harvest, may influence intramural distribution and abundance of NM-MHC. Another possibility is that hypoxia stimulated changes in the expression of growth factor receptors on smooth muscle cells, and thereby enhanced regional heterogeneity in reactivity to vasotrophic factors with subsequent regional changes in contractile protein abundance. Although this lamellar heterogeneity could be a simple consequence of growth factor gradients with little functional significance, it seems more likely that this heterogeneity is an important feature of arterial homeostasis that dynamically distributes roles for contractile function and secretory function throughout the smooth muscle cells of the artery wall.

Whereas the NM-MHC isoforms of myosin heavy chain are coded by at least three different genes, the other primary isoforms of smooth muscle myosin (SM-MHC) arise from a single gene (17). More importantly, the contractile characteristics of the NM-MHC and SM-MHC isoforms of MHC differ significantly from one another. Correspondingly, NM-MHC appears more commonly in functionally immature smooth muscle, and SM-MHC is more common in fully differentiated contractile smooth muscle (7, 17, 44). Consistent with this pattern, the abundance of the NM-MHC isoform was significantly greater in fetal than adult arteries. In addition, fetal and adult NM-MHC abundances were significantly increased by hypoxic acclimatization (**Figure 2**),

suggesting that hypoxia promoted either proliferation of non-contractile smooth muscle or stimulated dedifferentiation of fully differentiated contractile smooth muscle. Both of these mechanisms would help explain the observed hypoxic attenuation of contractility (**Figure 1**).

Consistent with the relevant literature (31, 44, 49), the overall abundance of the SM-MHC isoform was markedly less in fetal than in adult arteries, which helps explain the greater peak contractile responses to potassium in adult compared to fetal arteries (**Figure 1**, lower panels). Relative to normoxic abundances of SM-MHC, chronic hypoxia significantly increased SM-MHC in adult arteries, but reduced SM-MHC in fetal arteries (**Figure 2**). As might be expected, the hypoxic decrease in SM-MHC abundance in fetal arteries was associated with decreased contractility (**Figure 1**). In contrast, the large hypoxic increase in SM-MHC abundance in adult arteries was also associated with decreased contractility, suggesting that simple abundance of SM-MHC is not a primary determinant of contractile capacity.

How hypoxic acclimatization selectively altered MHC isoform abundances remains uncertain but could be explained by either age-dependent hypoxic release of trophic factors or by increases in sensitivity to those factors. Whatever the nature of those factors, their effects on SM-MHC were uniform across the artery wall in both fetal and adult arteries, suggesting that these factors did not originate exclusively from either the luminal or adventitial border of the medial layer. Overall, these results are consistent with previous reports that hypoxia can increase total MHC content (70), and also support the hypothesis that the artery wall contains smooth muscle in multiple phenotypic states with varying responses to trophic and mitogenic stimuli (24, 56, 69). These results, however,

do not help explain hypoxic attenuation of contractility: how is it possible that hypoxia increased the content of SM-MHC but decreased contractility? Clearly, factors other than MHC abundance must be involved.

Smooth muscle contraction requires the interaction between myosin and smooth muscle-Alpha Actin. SM-AA is a smooth muscle marker protein expressed in both immature non-contractile and fully differentiated contractile smooth muscle (25, 44). SM-AA abundance increases during maturation of contractile capacity (45) and also increases during hypoxic acclimatization (54). Because hypoxia can increase both SM-AA and MHC but simultaneously decrease contractile capacity, some aspect of the interaction between SM-AA and MHC must be affected by hypoxia. Whereas possible changes in numerous other smooth muscle proteins (59) might influence calcium handling, calcium sensitization, myosin phosphorylation or cytoskeletal organization, virtually all of these mechanisms act by altering the activation of regulatory myosin light chain or its access to filamentous actin (57). Another possibility is that the spatial organization of MHC relative to SM-AA is altered as a consequence of structural responses to hypoxic acclimatization. To test this hypothesis, our experimental approach included measurements of the fraction of SM-AA colocalized with both of the main MHC isoforms using confocal microscopy as previously described (14). Colocalization of NM-MHC with SM-AA was significantly decreased by hypoxia in fetal arteries, but was unchanged in adult arteries (**Figure 3**) due perhaps to the very low content of NM-MHC in mature arteries. Conversely, colocalization of SM-MHC with SM-AA was decreased by hypoxia in adult but not fetal arteries. These results are consistent with the hypothesis that hypoxia promotes the fraction of synthetic smooth muscle cells in the

artery wall. In the fetus, hypoxia increased NM-MHC, decreased SM-MHC, and decreased colocalization of NM-MHC with SM-AA. These changes, together with no significant change in medial thickness (**Table 1**) and decreased contractility (**Figure 1**), strongly suggest that in fetal arteries hypoxic acclimatization promoted a shift in smooth muscle characteristics toward a less contractile, more proliferative, more synthetic phenotype. In adult arteries, hypoxic acclimatization increased NM-MHC but also increased SM-MHC while decreasing colocalization of SM-MHC with SM-AA. The simultaneous increase in SM-MHC abundance with a decrease in SM-MHC colocalization with SM-AA suggests increased rates of contractile protein synthesis together with possible disassembly of the contractile apparatus. Again, these changes together with no significant change in medial thickness (**Table 1**) and decreased contractility (**Figure 1**), strongly suggest that in adult arteries hypoxic acclimatization also promoted a shift in smooth muscle characteristics toward a less contractile, more proliferative, more synthetic phenotype.

VEGF Altered Artery Structure and Function

Aside from the effects of hypoxic acclimatization on the abundance and organization of vascular contractile proteins and the corresponding changes in contractile capacity, it remains uncertain how chronic hypoxia might bring about such changes. One possibility is that VEGF may be involved. Secondary to hypoxic increases in HIF-1 release (53), hypoxia stimulates the synthesis and release of VEGF, which promotes angiogenesis (28, 40) but can also exert trophic influences on many non-endothelial cell types including retinal pericytes (61), neurons (32), astrocytes (22), peripheral neurons

and Schwann cells (39, 58), skeletal muscle (9), and most importantly, smooth muscle (11, 26, 43). To test the hypothesis that VEGF may contribute to hypoxic vascular remodeling, our experimental approach compared the effects of hypoxic acclimatization to the effects of organ culture with 3 ng/ml VEGF. This approach avoided the smooth muscle dedifferentiation typical in cultured smooth muscle (63) and preserved the three-dimensional structure of the artery wall required for colocalization studies. Our 3 ng/ml concentration of VEGF was similar to the physiological concentrations of 2 ng/ml reported in pregnant sheep (64) but was far less than the 40-50 ng/ml concentrations used in other studies of VEGF (5, 13), which helped minimize possible cross-activation of PDGF receptors that can occur at VEGF concentrations of 10 ng/ml or greater (4). To avoid the dedifferentiating effects caused in smooth muscle by exposure to fetal bovine serum (34, 51), the organ cultures did not include FBS. Although organ culture can alter the abundances of some contractile proteins (11), such effects should similarly influence both stretch-dependent and K+-dependent contractions; these were measured in the same arteries. Because organ culture affected stretch-dependent and K+-dependent contractions very differently (Figure 1 Normoxic vs. Figure 4 Control), the results suggest that organ culture alters contractility through mechanisms other than just changes in contractile protein abundance. Given that peak contractile stresses independent of method of contraction were similar in fresh and organ cultured arteries, overall contractility was optimally preserved as previously described (11).

Similar to the effects of hypoxic acclimatization on contractility, organ culture with VEGF significantly decreased overall contractility in both fetal and adult arteries (**Figure 4**). In adult arteries this effect of VEGF was prevented by vatalanib, a mixed

VEGF-R1/R2 antagonist (35) at a concentration (240 nM) validated to be optimal in this preparation. Vatalanib had no effect on VEGF-induced depression of contractility in fetal arteries. Together, these findings suggest that VEGF acts through VEGF-R1/R2 receptors to attenuate both stretch-dependent and K+-induced contractions in adult arteries. In fetal arteries, VEGF must act through a different pathway to influence contractility. The unique effects of VEGF on fetal arteries might possibly involve altered coupling of VEGF receptors to cytosolic kinases (42), but might also potentially involve activation of PDGF receptors (4) which are highly abundant in immature arteries (2); more experiments were required to differentiate among these possibilities. Together, these results are consistent with the hypothesis that VEGF may contribute to hypoxic vascular remodeling through transformation of smooth muscle phenotype, but also emphasize that the mechanisms involved must be very different in fetal and adult arteries.

Effects of VEGF on MHC Abundance and Organization

The general effects of VEGF on NM-MHC abundance were roughly similar to the effects of chronic hypoxia (**Figure 5**, upper right), although the effects of VEGF were more modest due perhaps to the low concentration of VEGF employed. As in normoxic fetal arteries, NM-MHC exhibited a graded decrease in abundance from the inner medial region to the outer medial region suggesting a possible regional influence from the vascular endothelium. For SM-MHC abundance however, VEGF did not reproduce the effects of hypoxic acclimatization and was without effect on either the abundance or the homogeneous distribution of SM-MHC throughout the media in both fetal and adult arteries. Despite its relative absence of effects on NM-MHC and SM-MHC, VEGF still

decreased contractility in fetal and adult arteries, again suggesting a shift toward a less contractile smooth muscle phenotype.

In both fetal and adult arteries, hypoxia-induced changes in contractility were more closely associated with changes in contractile protein organization than with changes in abundance (**Figure 1-3**). To examine if VEGF-induced changes in contractility were similarly associated with changes in contractile protein organization, we examined the influence of VEGF on the spatial organization of MHC isoforms relative to SM-AA (**Figure 6**). For NM-MHC, VEGF treatment decreased colocalization with SM-AA in fetal but not adult arteries and thus replicated the qualitative effect of hypoxia. In addition, VEGF decreased colocalization of SM-MHC with SM-AA in adult but not fetal arteries, which also reproduced the pattern produced by hypoxia. These colocalization results further support the hypothesis that VEGF may contribute to hypoxic vascular remodeling, at least in the ovine carotid artery. These results also reinforce the interpretation that contractility was more consistently associated with contractile protein organization than with contractile protein abundance; both hypoxia and VEGF similarly decreased contractility as well as NM-MHC colocalization in the fetus and SM-MHC colocalization in the adult. In contrast, hypoxia and VEGF produced only increases in the abundance of NM-MHC and had inconsistent effects on SM-MHC.

Another approach to compare the effects of hypoxic acclimatization and treatment with VEGF arises from the presumed obligatory relation between contractile protein abundance and organization. A protein can be colocalized with another protein only if both proteins have been synthesized and are present near one another. In other words, colocalization is limited by regional abundance. If colocalization is merely a stochastic

process, then increased abundance of any protein should increase its colocalization with its binding partners. To test this idea, our data analysis compared parallel changes in abundance and colocalization following treatments with both hypoxia and VEGF. Altogether, these comparisons strongly suggested that the observed changes in colocalization were not simply secondary to increased abundance; in almost all instances the changes in abundance and colocalization were not directly proportional. This latter finding implies that both hypoxia and VEGF have significant and parallel effects on the abundances, trafficking and localization of contractile proteins within arterial smooth muscle cells. The mechanisms mediating these effects are uncertain, but could involve changes in cytoskeletal remodeling, microtubular transport, or protein-protein interactions as suggested in other cell types (3). Thus, the present results follow a major trend in contemporary cell biology that is focused on the complex and unidentified mechanisms that govern subcellular protein distribution, trafficking, and localization.

Independent of mechanisms governing abundance and colocalization of smooth muscle contractile proteins, both hypoxia and VEGF appeared to recruit some of these mechanisms similarly. VEGF reproduced some, but not all, of the effects of hypoxic acclimatization, suggesting that factors other than VEGF must be involved in hypoxic vascular remodeling, particularly in relation to regulation of SM-MHC abundance. Conversely, hypoxia and VEGF had much more similar effects on colocalization of the MHC isoforms with SM-AA in both fetal and adult arteries (**Figures 3** and **6**). Interestingly, this close parallel between hypoxia and VEGF in relation to MHC colocalization was observed, even though VEGF may not signal through traditional VEGF receptor-dependent pathways in fetal arteries (**Figure 4**). This concurrence of

effects of hypoxic acclimatization and VEGF on MHC colocalization strongly supports the main hypothesis that VEGF may contribute to hypoxic vascular remodeling in both fetal and adult arteries.

Overview

Together, the results of the present study demonstrate that hypoxic acclimatization and VEGF exert both common and independent effects on contractility, MHC isoform abundance, and MHC-SM-AA organization. In light of abundant evidence that hypoxia increases both VEGF (36, 37) and VEGF receptor density (8), the present findings suggest that hypoxic acts through VEGF not only to increase capillary density (28), but also to mediate remodeling of arterial smooth muscle (**Figure 7**). The present results further emphasize that VEGF can act directly on vascular smooth muscle through receptor-dependent pathways that appear to involve VEGF-R1/R2 in adult but not fetal arteries; this difference may help explain many of the observed age-related differences in responses to both hypoxia and VEGF. Together, these results also give rise to the hypothesis that smooth muscle phenotype is a determinant of the responses to hypoxia and VEGF, and that one component of these responses may be to stimulate phenotypic conversion and thereby alter contractile protein abundance, organization, and function. On the other hand, differences in responses to hypoxia and VEGF emphasize that VEGF is not the only or perhaps even most important vasotrophic factor contributing to hypoxic vascular remodeling. Many important questions remain: what other factors contribute; what receptors mediate fetal responses to VEGF; might larger concentrations of VEGF applied for longer durations produce greater or different effects; what mechanisms

govern MHC colocalization independent of abundance? Aside from these and other questions for future investigations, the present results support the hypothesis that VEGF may contribute to hypoxic vascular remodeling in an age-dependent manner through effects that involve changes in MHC abundance, organization, and function.

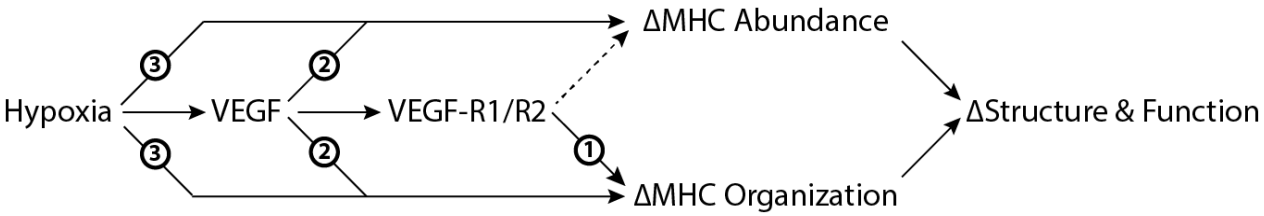

Figure 7. Hypoxic Vascular Remodeling Involves VEGF-Dependent and VEGF-Independent Effects on Contractile Protein Abundance and Organization.
Hypoxia can influence arterial structure and function through VEGF-independent and VEGF-dependent pathways. VEGF-dependent effects appear to be mediated in adult arteries through activation of VEGF receptors, with corresponding changes in MHC organization but not abundance (Pathway 1). In fetal arteries, VEGF appears to alter MHC abundance and organization independent of VEGF receptors (Pathway 2). Given that VEGF alone did not produce the full spectrum of hypoxic effects, hypoxia must also exert VEGF-independent effects on contractile protein abundance and organization (Pathway 3). Overall, the effects of hypoxia on MHC abundance and organization appear to be independently regulated. Equally important, changes in contractile protein organization were more tightly associated with changes in contractility than were changes in abundance.

Acknowledgments

The authors appreciate the excellent microscopy performed for this study by Jenna M Abrassart, MPH. The work reported in this manuscript was supported by USPHS grants P01-HD31226, R01-HL54120, R01-HL64867, R01-NS076945 and the Loma Linda University School of Medicine.

References

1. **Adair TH.** Growth regulation of the vascular system: an emerging role for adenosine. *Am J Physiol Regul Integr Comp Physiol* 289: R283-R296, 2005. PMID: 16014444

2. **Andrae J, Gallini R, and Betsholtz C.** Role of platelet-derived growth factors in physiology and medicine. *Genes Dev* 22: 1276-1312, 2008. PMID: 18483217

3. **Arizono M, Bannai H, Nakamura K, Niwa F, Enomoto M, Matsu-Ura T, Miyamoto A, Sherwood MW, Nakamura T, and Mikoshiba K.** Receptor-selective diffusion barrier enhances sensitivity of astrocytic processes to metabotropic glutamate receptor stimulation. *Science signaling* 5: ra27, 2012. PMID: 22472649

4. **Ball SG, Shuttleworth CA, and Kielty CM.** Vascular endothelial growth factor can signal through platelet-derived growth factor receptors. *J Cell Biol* 177: 489-500, 2007. PMID: 17470632

5. **Banerjee S, Mehta S, Haque I, Sengupta K, Dhar K, Kambhampati S, Van Veldhuizen PJ, and Banerjee SK.** VEGF-A165 induces human aortic smooth muscle cell migration by activating neuropilin-1-VEGFR1-PI3K axis. *Biochemistry* 47: 3345-3351, 2008. PMID: 18284215

6. **Bobik A.** Transforming growth factor-betas and vascular disorders. *Arterioscler Thromb Vasc Biol* 26: 1712-1720, 2006. PMID: 16675726

7. **Borrione AC, Zanellato AM, Scannapieco G, Pauletto P, and Sartore S.** Myosin heavy-chain isoforms in adult and developing rabbit vascular smooth muscle. *Eur J Biochem* 183: 413-417, 1989. PMID: 2667999

8. **Brogi E, Schatteman G, Wu T, Kim EA, Varticovski L, Keyt B, and Isner JM.** Hypoxia-induced paracrine regulation of vascular endothelial growth factor receptor expression. *J Clin Invest* 97: 469-476, 1996. PMID: 8567969

9. **Bryan BA, Walshe TE, Mitchell DC, Havumaki JS, Saint-Geniez M, Maharaj AS, Maldonado AE, and D'Amore PA.** Coordinated vascular endothelial growth factor expression and signaling during skeletal myogenic differentiation. *Mol Biol Cell* 19: 994-1006, 2008. PMID: 18094043

10. **Bundy RE, Marczin N, Birks EF, Chester AH, and Yacoub MH.** Transplant atherosclerosis: role of phenotypic modulation of vascular smooth muscle by nitric oxide. *Gen Pharmacol* 34: 73-84, 2000. PMID: 10974414

11. **Butler SM, Abrassart JM, Hubbell MC, Adeoye O, Semotiuk A, Williams JM, Mata-Greenwood E, Khorram O, and Pearce WJ.** Contributions of VEGF to age-dependent transmural gradients in contractile protein expression in ovine carotid arteries. *Am J Physiol Cell Physiol* 301: C653-666, 2011. PMID: 21653901

12. **Carmeliet P, Ferreira V, Breier G, Pollefeyt S, Kieckens L, Gertsenstein M, Fahrig M, Vandenhoeck A, Harpal K, Eberhardt C, Declercq C, Pawling J, Moons L, Collen D, Risau W, and Nagy A.** Abnormal blood vessel development and lethality in embryos lacking a single VEGF allele. *Nature* 380: 435-439, 1996. PMID: 8602241

13. **Chandra A and Angle N.** Vascular endothelial growth factor stimulates a novel calcium-signaling pathway in vascular smooth muscle cells. *Surgery* 138: 780-787, 2005. PMID: 16269309

14. **Charles SM, Zhang L, Cipolla MJ, Buchholz JN, and Pearce WJ.** The Roles of Cytosolic Ca2+ Concentration and Myofilament Ca2+ Sensitization in Age-Dependent Cerebrovascular Myogenic Tone. *Am J Physiol Heart Circ Physiol* 299: H1034-1044, 2010. PMID: 20639216

15. **Dao HH, Bouvet C, Moreau S, Beaucage P, Lariviere R, Servant MJ, de Champlain J, and Moreau P.** Endothelin is a dose-dependent trophic factor and a mitogen in small arteries in vivo. *Cardiovasc Res* 71: 61-68, 2006. PMID: 16580653

16. **Dvorak HF, Brown LF, Detmar M, and Dvorak AM.** Vascular permeability factor/vascular endothelial growth factor, microvascular hyperpermeability, and angiogenesis. *Am J Pathol* 146: 1029-1039, 1995. PMID: 7538264

17. **Eddinger TJ and Meer DP.** Myosin II isoforms in smooth muscle: heterogeneity and function. *Am J Physiol Cell Physiol* 293: C493-508, 2007. PMID: 17475667

18. **Elliott CF and Pearce WJ.** Effects of maturation on cell water, protein, and DNA content in ovine cerebral arteries. *J Appl Physiol* 79: 831-837, 1995. PMID: 8567525

19. **Fischer S, Clauss M, Wiesnet M, Renz D, Schaper W, and Karliczek GF.** Hypoxia induces permeability in brain microvessel endothelial cells via VEGF and NO. *Am J Physiol* 276: C812-820, 1999. PMID: 10199811

20. **Fong GH.** Regulation of angiogenesis by oxygen sensing mechanisms. *J Mol Med* 87: 549-560, 2009. PMID: 19288062

21. **Fredriksson L, Li H, and Eriksson U.** The PDGF family: four gene products form five dimeric isoforms. *Cytokine Growth Factor Rev* 15: 197-204, 2004. PMID: 15207811

22. **Freitas-Andrade M, Carmeliet P, Stanimirovic DB, and Moreno M.** VEGFR-2-mediated increased proliferation and survival in response to oxygen and glucose deprivation in PlGF knockout astrocytes. *J Neurochem* 107: 756-767, 2008. PMID: 18786179

23. **Frid MG, Dempsey EC, Durmowicz AG, and Stenmark KR.** Smooth muscle cell heterogeneity in pulmonary and systemic vessels. Importance in vascular disease. *Arterioscler Thromb Vasc Biol* 17: 1203-1209, 1997. PMID: 9261247

24. **Frid MG, Moiseeva EP, and Stenmark KR.** Multiple phenotypically distinct smooth muscle cell populations exist in the adult and developing bovine pulmonary arterial media in vivo. *Circ Res* 75: 669-681, 1994. PMID: 7923613

25. **Glukhova MA, Frid MG, and Koteliansky VE.** Developmental changes in expression of contractile and cytoskeletal proteins in human aortic smooth muscle. *J Biol Chem* 265: 13042-13046, 1990. PMID: 2376586

26. **Grosskreutz CL, Anand-Apte B, Duplaa C, Quinn TP, Terman BI, Zetter B, and D'Amore PA.** Vascular endothelial growth factor-induced migration of vascular smooth muscle cells in vitro. *Microvasc Res* 58: 128-136, 1999. PMID: 10458928

27. **Hill MA, Zou H, Potocnik SJ, Meininger GA, and Davis MJ.** Invited review: arteriolar smooth muscle mechanotransduction: Ca(2+) signaling pathways underlying myogenic reactivity. *J Appl Physiol* 91: 973-983, 2001. PMID: 11457816

28. **Hoeben A, Landuyt B, Highley MS, Wildiers H, Van Oosterom AT, and De Bruijn EA.** Vascular endothelial growth factor and angiogenesis. *Pharmacol Rev* 56: 549-580, 2004. PMID: 15602010

29. **House SJ, Potier M, Bisaillon J, Singer HA, and Trebak M.** The non-excitable smooth muscle: calcium signaling and phenotypic switching during vascular disease. *Pflugers Arch* 456: 769-785, 2008. PMID: 18365243

30. **Hull A, Long D, Longo L, and Pearce W.** Pregnancy-induced changes in ovine cerebral arteries. *Am J Physiol* 262: R137-143, 1992. PMID: 1733332

31. **Hutanu C, Cox BE, DeSpain K, Liu XT, and Rosenfeld CR.** Vascular development in early ovine gestation: carotid smooth muscle function, phenotype, and biochemical markers. *Am J Physiol Regul Integr Comp Physiol* 293: R323-333, 2007. PMID: 17475675

32. **Jin KL, Mao XO, and Greenberg DA.** Vascular endothelial growth factor: direct neuroprotective effect in in vitro ischemia. *Proc Natl Acad Sci U S A* 97: 10242-10247, 2000. PMID: 10963684

33. **Johnson BD, Wilson LE, Zhan WZ, Watchko JF, Daood MJ, and Sieck GC.** Contractile properties of the developing diaphragm correlate with myosin heavy chain phenotype. *J Appl Physiol* 77: 481-487, 1994. PMID: 7961272

34. **Jones BA, Aly HM, Forsyth EA, and Sidawy AN.** Phenotypic characterization of human smooth muscle cells derived from atherosclerotic tibial and peroneal arteries. *J Vasc Surg* 24: 883-891, 1996. PMID: 8918338

35. **Karaman MW, Herrgard S, Treiber DK, Gallant P, Atteridge CE, Campbell BT, Chan KW, Ciceri P, Davis MI, Edeen PT, Faraoni R, Floyd M, Hunt JP, Lockhart DJ, Milanov ZV, Morrison MJ, Pallares G, Patel HK, Pritchard S,**

Wodicka LM, and Zarrinkar PP. A quantitative analysis of kinase inhibitor selectivity. *Nat Biotechnol* 26: 127-132, 2008. PMID: 18183025

36. **Kuo N, Benhayon D, Przybylski R, Martin R, and LaManna J.** Prolonged hypoxia increases vascular endothelial growth factor mRNA and protein in adult mouse brain. *J Appl Physiol* 86: 260-264, 1999. PMID: 9887138

37. **Liu Y, Cox SR, Morita T, and Kourembanas S.** Hypoxia regulates vascular endothelial growth factor gene expression in endothelial cells. Identification of a 5' enhancer. *Circ Res* 77: 638-643, 1995. PMID: 7641334

38. **Longo LD, Hull AD, Long DM, and Pearce WJ.** Cerebrovascular adaptations to high-altitude hypoxemia in fetal and adult sheep. *Am J Physiol* 264: R65-72, 1993. PMID: 8430888

39. **Marko SB and Damon DH.** VEGF promotes vascular sympathetic innervation. *Am J Physiol Heart Circ Physiol* 294: H2646-2652, 2008. PMID: 18408130

40. **Nagy JA, Dvorak AM, and Dvorak HF.** VEGF-A(164/165) and PlGF: roles in angiogenesis and arteriogenesis. *Trends Cardiovasc Med* 13: 169-175, 2003. PMID: 12837578

41. **Ohkuma H, Suzuki S, and Ogane K.** Phenotypic modulation of smooth muscle cells and vascular remodeling in intraparenchymal small cerebral arteries after canine experimental subarachnoid hemorrhage. *Neurosci Lett* 344: 193-196, 2003. PMID: 12812838

42. **Olsson AK, Dimberg A, Kreuger J, and Claesson-Welsh L.** VEGF receptor signalling - in control of vascular function. *Nat Rev Mol Cell Biol* 7: 359-371, 2006. PMID: 16633338

43. **Osada-Oka M, Ikeda T, Imaoka S, Akiba S, and Sato T.** VEGF-enhanced proliferation under hypoxia by an autocrine mechanism in human vascular smooth muscle cells. *J Atheroscler Thromb* 15: 26-33, 2008. PMID: 18270456

44. **Owens GK, Kumar MS, and Wamhoff BR.** Molecular regulation of vascular smooth muscle cell differentiation in development and disease. *Physiol Rev* 84: 767-801, 2004. PMID: 15269336

45. **Owens GK, Loeb A, Gordon D, and Thompson MM.** Expression of smooth muscle-specific alpha-isoactin in cultured vascular smooth muscle cells: relationship between growth and cytodifferentiation. *J Cell Biol* 102: 343-352, 1986. PMID: 3944187

46. **Pearce WJ, Hull AD, Long DM, and Longo LD.** Developmental changes in ovine cerebral artery composition and reactivity. *Am J Physiol* 261(2 Pt 2): R458-R465, 1991. PMID: 1877701

47. **Pearce WJ, Williams JM, White CR, and Lincoln TM.** Effects of chronic hypoxia on soluble guanylate cyclase activity in fetal and adult ovine cerebral arteries. *J Appl Physiol* 107: 192-199, 2009. PMID: 19407253

48. **Presta M, Dell'Era P, Mitola S, Moroni E, Ronca R, and Rusnati M.** Fibroblast growth factor/fibroblast growth factor receptor system in angiogenesis. *Cytokine Growth Factor Rev* 16: 159-178, 2005. PMID: 15863032

49. **Rensen SS, Doevendans PA, and van Eys GJ.** Regulation and characteristics of vascular smooth muscle cell phenotypic diversity. *Netherlands heart journal : monthly journal of the Netherlands Society of Cardiology and the Netherlands Heart Foundation* 15: 100-108, 2007. PMID: 17612668

50. **Sartore S, Chiavegato A, Franch R, Faggin E, and Pauletto P.** Myosin gene expression and cell phenotypes in vascular smooth muscle during development, in experimental models, and in vascular disease. *Arterioscler Thromb Vasc Biol* 17: 1210-1215, 1997. PMID: 9261248

51. **Saward L and Zahradka P.** Coronary artery smooth muscle in culture: migration of heterogeneous cell populations from vessel wall. *Mol Cell Biochem* 176: 53-59, 1997. PMID: 9406145

52. **Schubert R, Lidington D, and Bolz SS.** The emerging role of Ca2+ sensitivity regulation in promoting myogenic vasoconstriction. *Cardiovasc Res* 77: 8-18, 2008. PMID: 17764667

53. **Semenza GL.** HIF-1: mediator of physiological and pathophysiological responses to hypoxia. *J Appl Physiol* 88: 1474-1480, 2000. PMID: 0010749844

54. **Shields KM, Panzhinskiy E, Burns N, Zawada WM, and Das M.** Mitogen-activated protein kinase phosphatase-1 is a key regulator of hypoxia-induced vascular endothelial growth factor expression and vessel density in lung. *Am J Pathol* 178: 98-109, 2011. PMID: 21224048

55. **Skalli O, Pelte MF, Peclet MC, Gabbiani G, Gugliotta P, Bussolati G, Ravazzola M, and Orci L.** Alpha-smooth muscle actin, a differentiation marker of smooth muscle cells, is present in microfilamentous bundles of pericytes. *The journal of histochemistry and cytochemistry : official journal of the Histochemistry Society* 37: 315-321, 1989. PMID: 2918221

56. **Sobue K, Hayashi K, and Nishida W.** Molecular mechanism of phenotypic modulation of smooth muscle cells. *Horm Res* 50 Suppl 2: 15-24, 1998. PMID: 9721587

57. **Somlyo AP and Somlyo AV.** Ca2+ sensitivity of smooth muscle and nonmuscle myosin II: modulated by G proteins, kinases, and myosin phosphatase. *Physiol Rev* 83: 1325-1358, 2003. PMID: 14506307

58. **Sondell M, Lundborg G, and Kanje M.** Vascular endothelial growth factor has neurotrophic activity and stimulates axonal outgrowth, enhancing cell survival and Schwann cell proliferation in the peripheral nervous system. *J Neurosci* 19: 5731-5740, 1999. PMID: 10407014

59. **Stenmark KR, Fagan KA, and Frid MG.** Hypoxia-induced pulmonary vascular remodeling: cellular and molecular mechanisms. *Circ Res* 99: 675-691, 2006. PMID: 17008597

60. **Stiebellehner L, Frid MG, Reeves JT, Low RB, Gnanasekharan M, and Stenmark KR.** Bovine distal pulmonary arterial media is composed of a uniform population of well-differentiated smooth muscle cells with low proliferative capabilities. *Am J Physiol Lung Cell Mol Physiol* 285: L819-828, 2003. PMID: 12857671

61. **Takagi H, King GL, and Aiello LP.** Identification and characterization of vascular endothelial growth factor receptor (Flt) in bovine retinal pericytes. *Diabetes* 45: 1016-1023, 1996. PMID: 8690146

62. **Tipoe GL and Fung ML.** Expression of HIF-1alpha, VEGF and VEGF receptors in the carotid body of chronically hypoxic rat. *Respir Physiol Neurobiol* 138: 143-154, 2003. PMID: 14609506

63. **van Eys GJ, Voller MC, Timmer ED, Wehrens XH, Small JV, Schalken JA, Ramaekers FC, and van der Loop FT.** Smoothelin expression characteristics: development of a smooth muscle cell in vitro system and identification of a vascular variant. *Cell Struct Funct* 22: 65-72, 1997. PMID: 9113392

64. **Vonnahme KA, Wilson ME, Li Y, Rupnow HL, Phernetton TM, Ford SP, and Magness RR.** Circulating levels of nitric oxide and vascular endothelial growth factor throughout ovine pregnancy. *J Physiol* 565: 101-109, 2005. PMID: 15774525

65. **Wamhoff BR, Bowles DK, and Owens GK.** Excitation-transcription coupling in arterial smooth muscle. *Circ Res* 98: 868-878, 2006. PMID: 16614312

66. **Williams B.** Mechanical influences on vascular smooth muscle cell function. *J Hypertens* 16: 1921-1929, 1998. PMID: 9886878

67. **Williams JM and Pearce WJ.** Age-dependent modulation of endothelium-dependent vasodilatation by chronic hypoxia in ovine cranial arteries. *J Appl Physiol* 100: 225-232, 2006. PMID: 16179402

68. **Wohrley JD, Frid MG, Moiseeva EP, Orton EC, Belknap JK, and Stenmark KR.** Hypoxia selectively induces proliferation in a specific subpopulation of smooth muscle cells in the bovine neonatal pulmonary arterial media. *J Clin Invest* 96: 273-281, 1995. PMID: 7615796

69. **Yablonka-Reuveni Z, Christ B, and Benson JM.** Transitions in cell organization and in expression of contractile and extracellular matrix proteins during development of chicken aortic smooth muscle: evidence for a complex spatial and temporal differentiation program. *Anat Embryol (Berl)* 197: 421-437, 1998. PMID: 9682974

70. **Zacour ME, Teoh H, Halayko AJ, and Ward ME.** Mechanisms of aortic smooth muscle hyporeactivity after prolonged hypoxia in rats. *J Appl Physiol* 92: 2625-2632, 2002. PMID: 12015382

CHAPTER THREE

HYPOXIC ACCLIMATIZATION MODULATES ENDOTHELIAL INFLUENCE ON SMOOTH MUSCLE CONTRACTILE FUNCTION AND PHENOTYPES IN FETAL OVINE MIDDLE CEREBRAL ARTERIES

Margaret C. Hubbell, Richard B. Thorpe, Dahlim Kim, Jinjutha Silpanisong, Adam Vergara, and William J. Pearce

Running Title: Hypoxia Modulates Endothelial Influence on Smooth Muscle Phenotypes

Address for Correspondence:
William J. Pearce, Ph.D.
Center for Perinatal Biology
Loma Linda University School of Medicine
Loma Linda, CA 92350
Phone: 909-558-4325
FAX: 909-558-4029
E-Mail: wpearce@llu.edu

Introduction

Fetal cerebral angiogenesis is a complex and delicate process. As such it is vulnerable to numerous stressors, not the least of which includes acute and chronic hypoxia. This hypoxic stress is often due to placental insufficiency, pre-eclampsia, gestational diabetes, maternal nicotine use, and more. The response to hypoxic stress may involve vascular remodeling that includes alterations to vascular structure and function as well as a predisposition to cardiovascular disease in adulthood and a long-term maladaptation to subsequent hypoxic insults.

Hypoxic vascular remodeling is mediated by numerous growth factors, cytokines, miRNAs, and notably Vascular Endothelial Growth Factor (VEGF). VEGF has been shown to act on multiple cell types including endothelium, smooth muscle, neurons, and more. VEGF also activates several known signaling pathways, including the nitric oxide (NO) pathway, that induce short-term changes in arterial function (vasorelaxation) as well as long-term changes in the smooth muscle cell (SMC) phenotype. These changes include a transition in the expression and organization of alpha actin and myosin heavy chain. VEGF is one of numerous stimuli that activate the release of NO within the endothelium in response to stress. NO released from the endothelium rapidly diffuses into the adjacent vascular smooth muscle (VSM) where it serves as a paracrine signal to promote vasorelaxation.

The main endpoint of the NO pathway is the cGMP-dependent protein kinase (PKG). PKG is pleiotropic; it (PKG) has literally hundreds of known kinase targets, and displays a variety of well-studied activities depending on the specific tissue type wherein it is activated. In vascular smooth, activation of PKG has been shown to promote the

expression of contractile proteins and alter the VSM phenotype. Likewise, VEGF is shown to act directly via FLT-1 and KDR receptors, and indirectly through the NO, and possibly other pathways to alter the VSM phenotype. This represents a long-term shift in the character and behavior of the cerebral VSM, and alters the response to any subsequent stress including hypoxic challenge. Our main hypothesis is that chronic hypoxia modulates the influence endothelial modification of VSM function and phenotype in part through changes in response to VEGF and the NO pathway.

Specifically, this hypothesis predicts that hypoxic acclimatization 1) alters the endothelium and its modulation of contractile protein organization and smooth muscle function, 2) that the endothelial response to exposure to VEGF is altered and 3) that hypoxic alterations to the endothelial and smooth muscle cell occurs in part through a change in the NO-PKG pathway. To test our hypothesis, we performed organ culture using intact and denuded fetal and adult middle ovine cerebral arteries (MCAs). To examine the influence of the NO pathway, we inhibited NO production by eNOS with L-NAME. Our main endpoints included a functional assay, length-tension protocol measuring myogenic tone and passive stretch using an isometric force transducer. We also examined changes in the VSM phenotype by measuring colocalization of SM-alpha Actin (SM-αA) with two myosin heavy chain (MHC) isoforms using confocal microscopy.

In the context of this study, artery "structure" was assessed through measurements of medial layer thickness, artery stiffness, and intracellular organization of smooth muscle contractile proteins. In turn, intracellular organization and smooth muscle phenotype were defined by the patterns of colocalization of Non-Muscle and Smooth

Muscle MHC with SM-αA into 3 distinct quadrants (21, 22). Quantification of various contractile and smooth muscle protein markers is well established in the literature to characterize smooth muscle phenotype. Our lab has further extended this method of identification by use of immunohistochemical colocalization among these markers, which yields a better correlation to contractile function than mere protein abundance (1, 5, 10). In this study we applied this colocalization method to identify shifts among smooth muscle phenotypes with 3 primary mechanistic perturbations: denudation of the endothelium, vasotrophic stimulation by VEGF in organ culture and inhibition/activation of the NO-PKG pathway. We introduce a novel quartile method to demonstrate shifts among smooth muscle phenotypes using established MHC isoform colocalization with SM-αA to distinguish fully differentiated contractile from partially de-differentiated and fully de-differentiated (synthetic, migratory, proliferative) SMC phenotypes. The experimental design focused first on the effects of chronic hypoxia on artery structure and function in the presence and absence of the endothelium using established methods for measurements of in vitro contractility and confocal microscopy (5, 6) These same endpoints are utilized to define the structural and functional effects of acute organ culture with VEGF in a second set of experiments. Upon demonstrating that colocalization of multiple smooth muscle markers is the most sensitive indication of phenotype, we then perturbated the intercellular pathway of NO production and release by the endothelium by L-NAME to the smooth muscle and use confocal microscopy to characterize shifts within these phenotypic profiles. The effects of chronic hypoxia were examined by comparing arteries harvested from sheep maintained at sea level versus those maintained at high altitude (3820 m) for 110 days as previously described (19). Together, these

approaches enable a unique perspective on the role of the endothelium in directing smooth muscle phenotype and contractile function after hypoxic acclimatization as well as secondary exposure to VEGF.

Materials and Methods

All procedure used in these studies were approved by the Animal Research Committee of Loma Linda University, adhered to the policies and practices set forth by the National Institutes of Health *Guide for the Care and Use of Laboratory Animals*, and have been previously described in detail (5, 26).

Tissue Harvest and Preparation

Middle cerebral arteries were harvested using sterile techniques from fetal (139–142 days gestation) sheep that had been maintained at either sea level (normoxic) or at 3,820 m for the final 110 days of gestation (hypoxic). For tissue harvest, pregnant ewes were anesthetized with 10mg/kg ketamine and 5mg/kg midazolam, intubated, and then placed on 1%-2% isoflurane. The fetus was then exteriorized through a midline vertical laparotomy and euthanized by rapid removal of the heart and exsanguination. Harvested arteries were placed in sterile HEPES buffer solution containing the following (in mM): 122 NaCl, 25.0 HEPES, 11.1 dextrose, 5.15 KCl, 2.40 $MgSO_4$, 1.6 $CaCl_2$, and 0.050 EDTA. Following gentle removal of extracellular and loose connective tissue, one middle cerebral artery (MCA) was mechanically denuded of endothelium with the passage of a stainless steel rod through the lumen while the contralateral MCA remained endothelium intact as previously described (26). Both the intact and denuded artery were cut into

coronal segments 2–3 mm in length and then distributed to the various protocols.

Organ culture

As described previously (5), artery segments designated for organ culture were maintained in 12-well plates with DMEM (Sigma-Aldrich, St. Louis, MO; no. M56469C) supplemented with the following: 0.5% amino acid solution (Sigma Aldrich; no. M5550), 1% nonessential amino acid solution (Sigma Aldrich; no. M7145), 3.7 g/l Na_2HCO_3, 4 mM glutamine (Sigma Aldrich; no.G7513), 2% antibiotic-antimycotic solution (GIBCO, Carlsbad, CA; no. 15240–096), and 70 μg/ml gentamycin (GIBCO; no. 15750–060). Cultures were maintained in a humidified incubator with 5% CO_2 in room air at 37 °C. Matched artery segments were cultured in supplemented DMEM without FBS for the initial 24 h to prevent dedifferentiation in vitro. This was followed by an additional 24 h in media containing DMEM (control) and 0, 3, 10 or 30 ng/ml VEGF-A165. Preliminary dose-finding studies at VEGF concentrations between 3–100ng/mL were performed to identify the optimal concentration for VEGF effects by functional contractility assays. The concentration of 10 ng/ml VEGF used for all further studies was chosen to simulate physiologic serum levels measured in pregnant sheep (25) as well as to minimize nonspecific binding of VEGF to other receptors (3). Following organ culture, arteries were allocated for analysis via fluorescent immunohistochemistry or contractility studies. This second protocol to elucidate the effect of hypoxia on the endothelial NO-PKG pathway consisted of matched intact and denuded arteries underwent organ culture in Ctrl, 10 ng/ml VEGF, the eNOS inhibitor LNAME (100uM), or 10 ng/ml VEGF ± 100uM LNAME.

Artery Structure and Contractility

Artery segments designated for contractility measurement were mounted on wires in vitro between an isometric force transducer and a micrometer slide used to set artery diameters. Mounted segments were initially equilibrated for 30 min in calcium-replete Na^+-Krebs buffer containing the following (in mM): 5.17 KCl, 2.56 dextrose, 2.49 $MgSO_4$, 1.60 $CaCl_2$, 122 NaCl, 25.6 $NaHCO_3$, 0.114 ascorbic acid, and 0.027 EGTA. Buffer pH was maintained at ≈7.4 with continuous bubbling of 95% O2-5% CO2 at physiologic ovine core temperature of 38°C. After initial equilibration, the unstressed artery diameter (D_0) of each segment was measured at a passive tension of 0.03 g. Working diameters (D) were calculated for each artery segment based on its D_0 at strain ratios of D/D_0 = 1.5, 1.8, 2.1, 2.4, 2.7, 3.0, and 3.3. Contractile stresses in dynes per centimeter squared were recorded at each of these strain values, in increasing order under resting conditions to determine spontaneous myogenic stress and then followed by contraction in a high potassium buffer containing the following (in mM): 122 KCl, 11.1 dextrose, 2.50 $MgSO_4$, 1.60 ml $CaCl_2$, 5.16 NaCl, 2.15 $NaHCO_3$, 0.114 ascorbic acid, and 0.027 EDTA. After K^+-induced contractions had stabilized, arteries were returned to Na^+-Krebs buffer, allowed to relax, and then stretched to and equilibrated at the next highest stretch ratio. After the K+-induced contraction had been measured at the maximum D/D_0 ratio of 3.3, the arteries were frozen in liquid nitrogen to rupture the cells and then incubated in a calcium free Na^+-Krebs buffer containing 3 mM EGTA to chelate and therefore further inhibit any smooth muscle cell derived force through Ca2+ sequestration. The passive stress produced at each strain ratio used was then recorded in descending order.

Myogenic stresses were calculated as the spontaneous stresses measured under resting conditions at each strain ratio (D/D_0) minus the passive stresses measured after freezing in liquid N2 at the same strain ratio. The potassium-induced stresses were calculated as the maximum stresses measured during exposure to high potassium at each strain ratio (D/D_0) minus the spontaneous stresses measured under resting conditions at the same strain ratio. Arterial stiffness was determined using the relations between strain and passive stress, using curve fitting with Young's monotonic exponential model to determine the coefficient of stiffness. All methods used to quantify contractility have been described previously in detail (5).

Immunohistochemistry

Matched artery segments were fixed in 4% neutral buffered electron microscopy-grade paraformaldehyde (Electron Microscopy Sciences, Hatfield, PA; no. 15713S) for 24 h at 4°C. Fixed segments were dehydrated and grouped by animal, embedded in a paraffin block, which was then sectioned at 5 μm and mounted on slides. Sections were deparaffinized by Histo-Clear (National Diagnostic, Atlanta, GA; no. HS-200) and then rehydrated by decreasing concentrations of alcohol, and microwaved in a citrate buffer at pH 6.03 to retrieve antigenicity. Permeabilization. Blocking was performed by 0.1% Triton X-100 (Sigma Aldrich; no. T-8787) and 1% BSA (Santa Cruz Biotechnology, Santa Cruz, CA; no. SC-2323) in PBS. To quantify shifts in phenotype, artery sections were then probed with antibodies to reveal expression of NM-MHC, an established marker for incompletely differentiated, partially contractile/synthetic smooth muscle, and SM-MHC, an established marker for differentiated, contractile smooth muscle present in

increasing abundance with animal maturation (21, 22). As stated in previous studies (Butler et al, Hubbell et al), these antibodies were selective for vascular tonic smooth muscle (MHC-A family) and not phasic smooth muscle (MHC-B family) Ref. (9).

Sections were exposed overnight to primary antibodies utilizing primary monoclonal mouse anti-sheep antibodies against SM-αA (Sigma-Aldrich; A5228, 1:400) and either polyclonal rabbit anti-human NM-MHC (CoVance, Princeton, NJ; PPR-445P) at 1:400 or polyclonal rabbit anti-bovine SM-MHC (Abcam, Cambridge, MA; ab53219) at 1:500. The following day, slides were washed for two 10-min cycles in PBS and incubated using the appropriate secondary antibody. The secondary antibody was a goat anti-rabbit-488 (Thermo Scientific, Rockford, IL; no. 35552 lot LI150311) at 1:400 to detect SM-AA and goat anti-mouse-633 (Thermo Scientific, Rockford, IL; no. 35512 lot QD217311) to detect MHC and then incubated in the dark for 2 hours at room temperature. To minimize photobleaching, slides were maintained in the dark during staining and washings phases. Slides underwent two additional 10-min cycles in PBS and were then coverslipped using SlowFade Gold anti-fade reagent with DAPI (Invitrogen, Carlsbad, CA; S36939) and stored until imaged. All slides were imaged with an Olympus FV1000 confocal microscope at an optical section thickness of 0.7 μm, a lateral resolution of 200 nm, and a numerical aperture of 18.

Confocal Microscopy

As described under the Immunohistochemistry section, matched artery segments were collected, prepared, and immunostained with the primary monoclonal antibody against SM-AA and a second primary antibody against one of the MHC isoforms.

Because SM-AA is considered selective to smooth muscle and it is present in all SMC phenotypes, each MHC isoform was colocalized relative to the abundance of SM-AA. Similarly, only the alpha isoform of actin is involved in smooth muscle contraction, changes in other actin isoforms that may be expressed in smooth muscle should have little influence on smooth muscle contractile function (16)

The extent of colocalization between the MHC and SM-αA was determined using Colocalizer Pro (www.Colocalizer.com), which included the calculation of a modified Mander's Coefficient independent of absolute marker intensities (14). Following imaging as described fully in the Immunohistochemistry section, coronal sections were extracted from the parent images with a masking routine that eliminated background contributions to the measurement statistics with removal of pixels outside of the medial layer of the artery. For each pixel in a double-immunostained image, the MHC marker and SM-AA was automatically graded as: 1) below threshold of 5% maximum intensity; 2) above threshold but less than 50% maximum intensity (Low Intensity); or 3) greater than 50% maximum intensity (High Intensity). All pixels above threshold for both markers were grouped into 3 categories: Low MHC and Low SM-AA, Low MHC and High SM-AA, and High MHC and High SM-AA. The total of all pixels above threshold for both markers was set as 100% with the number of pixels in each of the 3 categories calculated as a percentage of that total. These methods have previously been described in detail (2, 8, 10).

Data analysis and statistics

Contractile stresses were calculated as ratios of force per cross-sectional area,

with force measured as contractile tension in grams times the acceleration due to gravity. The cross-sectional area (segment length x wall thickness) was corrected for changes due to stretch as described previously (11, 18). With regard to confocal colocalization, all values were calculated among SM-αA positive pixels, and then the fractions of those pixels also positive for each of the MHC isoforms was determined. Adding the individual colocalization index values for each of the MHC isoforms yielded the total colocalization values. The group error was calculated as a pooled variance. Each statistical comparison was done using Behrens-Fisher comparison at the $P<0.05$ level.

Results

A total of 379 middle cerebral artery segments were harvested from 22 normoxic fetuses (FN) and 23 hypoxic fetuses (FH). 156 segments were used for functional contractility studies and 223 segments were used for confocal imaging. Throughout "n" denotes the number of animals not the number of segments used in each experiment. Statistical significance was defined at $P < 0.05$ for all assays, with all values given as means ± SEM.

Chronic Hypoxia Alters VEGF-Induced Endothelial Influence on Contractile Function

To assess how hypoxia in utero alters the endothelial and smooth muscle response to an acute secondary hypoxic insult, artery segments from normoxic and hypoxic animals were either denuded of endothelium or left intact and then cultured in the presence of VEGF at either 0, 3, 10, or 30 ng/mL for 24hrs (Figure 1). Significant

changes in artery structure did not occur over this short duration (medial wall thickness nor passive stiffness) but significant changes in contractile force did occur. Overall, hypoxia in utero reduced maximum stretch-induced stress compared with respective normoxic controls for both endothelium-intact and endothelium-denuded arteries. In normoxic arteries, secondary VEGF exposure after denudation of the endothelium resulted in an 89% increase in stretch-induced stress compared with endothelium-intact arteries. This effect via the endothelium was ablated in hypoxic arteries. Hypoxia in utero did not significantly alter maximum K+-induced stress but it did diminish with VEGF exposure in endothelium-denuded compared with endothelium-intact arteries for both normoxic (-44%) and hypoxic arteries (-43%).

Chronic Hypoxia Alters Smooth Muscle Colocalization Pattern of MHC Isoforms and Alpha Actin

To complement the contractile effects of hypoxia in utero on the endothelium and smooth muscle, the parallel effects on contractile protein organization were assessed using confocal microscopy. The extent of colocalization for two distinct MHC isoforms with SM-AA was quantified for baseline organization in arteries immediately after harvest from normoxic and hypoxic animals (**Figure 2**) and in matched arteries after exposure to VEGF in organ culture (**Figure 3**). Only pixels for which both proteins were above a minimal threshold of 5% maximum intensity were analyzed and the total number of such pixels was defined as 100%. Using a second threshold of 50% of maximal intensity for each marker, these pixels were categorized into three groups: 1) both markers above threshold but below half-maximal intensity (Low/Low); 2) MHC was

above threshold but below half-maximal intensity and for SM-AA was greater than half-maximal intensity (Low/High); and 3) both MHC and SM-AA were greater than half-maximal intensity (High/High). The effects of hypoxic acclimatization on baseline contractile protein organization in smooth muscle by examining how hypoxia shifted the total pixels among these categories. Also note that by definition, the number of pixels in quadrant LL, LR, and UR were defined to combine as the total number of physiologically relevant pixels so that each quadrant is represented by the % of the total pixels it contains and is reported as the "Raw percentage" seen in the left side component of Figure 2 and Figures 4-6. Therefore, throughout this article, LL + LR + UR = 100% within a treatment group. A corollary to this is that when pixels are lost from one quadrant they are mathematically obligated to be gained by another quadrant. Therefore, the three Δ's within a quadrant sum to a net zero or simply put Δ LL+ Δ LR + Δ UR = 0% as seen in the middle column of Figure 2, 4, 5, and 6. Similarly, within a treatment group the ΔΔLL + ΔΔLR + ΔΔUR = 0% as seen in the far right column of Figures 2 and Figures 4-6.

In normoxic sections dual stained for SM-MHC and a-Actin (**Figure 2**, Left Panel), pixels are predominantly in the LL (61±4%) with few in the LR (26+4%) and UR (13+3%). Hypoxia in utero significantly shifted this distribution with a -18% loss in LL, -3% in LR and subsequent gain of +21% in the UR. Together, this pattern of results indicates that hypoxia in utero increased the organization between a-Actin and SM-MHC, a marker for mature contractile smooth muscle cells. While SM-MHC is considered to be the main myosin heavy chain isoform expressed in mature, fully differentiated contractile smooth muscle, NM-MHC is generally expressed more abundantly in immature smooth muscle, especially in the fetus. A similar distribution at baseline was noted for NM-MHC

and a-Actin in normoxic arteries with the majority of pixels in LL (58+5) and few in LR (23+4), and UR (18+4). Hypoxia in utero significantly shifted this distribution with a -12% loss in the LL and -17% loss in LR with subsequent increase of +29% increase in UR. Together, this pattern of results indicates that hypoxia in utero also increased the organization between a-Actin and NM-MHC.

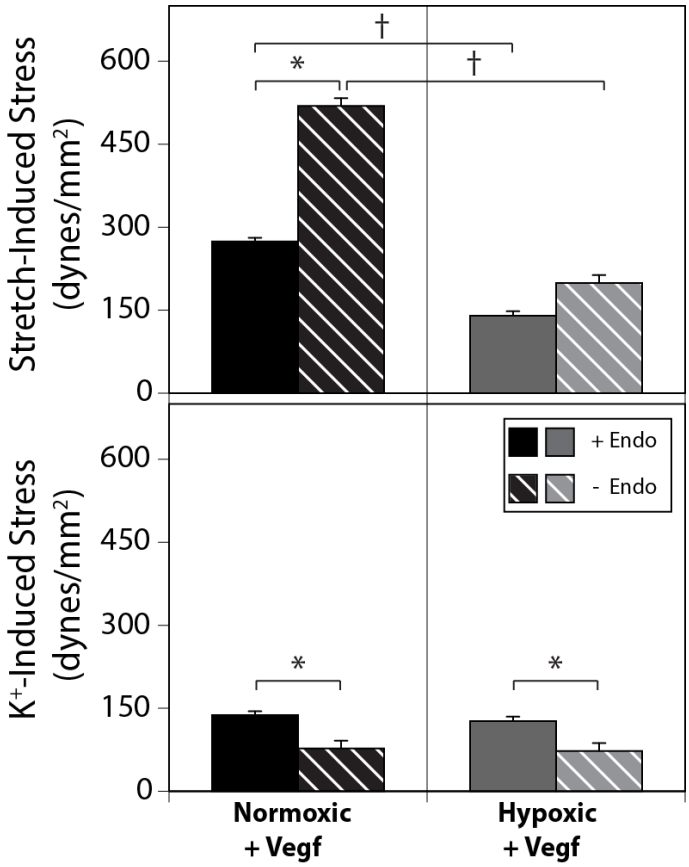

Figure 1. Hypoxia in Utero Alters Endothelium-Dependent Effect of VEGF on Contractile Function.

Middle cerebral arteries harvested from fetal sheep maintained at 3820 m for 110 days (Hypoxic) or at sea level (Normoxic) were denuded of endothelium or left intact prior to 24hr organ culture with VEGF and undergoing functional contractility assays. A standard length-tension protocol was performed as described previously, for details see methods. Arteries were cut transversely into 2mm segments and used to determine stretch-induced myogenic stresses at different strains applied in increments of the unstressed diameter, from 1 to 3.3. Stiffness was determined as relation between passive stress and stretch, measured by Young's modulus. Myogenic stress was calculated as the maximum spontaneous stress measured in PBS under resting conditions minus the passive stress in EGTA for each strain ratio. Active potassium-induced stress was calculated as maximum stress in 122 mM K^+ isotonic Krebs buffer minus the spontaneous stress in PBS at each strain ratio. Organ culture with VEGF did not significantly alter artery structural characteristics such as thickness and stiffness for either normoxic or hypoxic arteries. Denudation of the endothelium increased stretch-dependent stress only in normoxic arteries; hypoxic acclimatization ablated the effect of endothelium removal. Hypoxia did not significantly alter potassium-induced stress but denudation of the endothelium decreased potassium-induced stress in both normoxic and hypoxic arteries. Error bars indicate SEM for arteries from 6 normoxic and 7 hypoxic fetuses with all denoted significant differences are at $P<0.05$.

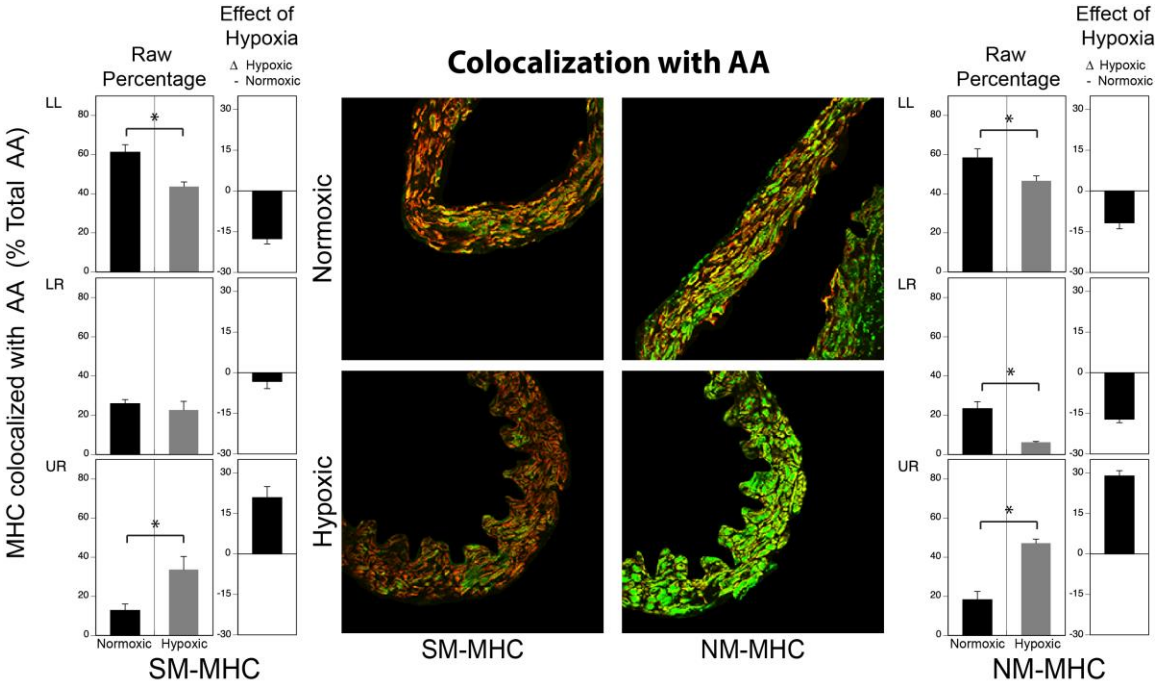

Figure 2. Hypoxia in Utero Increases MHC Isoform Colocalization with AA.
Middle cerebral arteries harvested from fetal sheep maintained from normoxic and hypoxic fetal sheep underwent confocal microscopy. Arteries were fixed immediately upon harvest in paraformaldehyde, paraffin-embedded, sectioned coronally at 5 µm and immunostained for myosin heavy chain isoforms NM-MHC or SM-MHC (red) and SM-αA (green). Colocalizations of SM-AA with MHC isoforms are displayed in the merged images (yellow). Summarized above are the pixel distributions for each of the 4 main experimental groups for two different marker pairs: SM-MHC with SM-αA in the upper panels, and NM-MCH with SM-AA in the lower panels. For each marker pair within each experimental group, the total of all pixels in the Low MHC / Low AActin (LL), Low MHC / High AActin (LR), and High MHC / High AActin (UR) categories is 100%. Please note that the vertical scale is the same within each panel for ease of comparison. For baseline normoxic arteries, the distribution of both SM-MHC and NM-MHC colocalization with AA is predominantly in LR with ~60% of pixels. Chronic hypoxia caused a rightward shift in pixel distribution toward the UR High MHC / High AActin category for both SM-MHC and NM-MHC colocalization with SM-αA. Error bars indicate SEM for n values of 8 normoxic fetuses and 3 hypoxic fetuses. Asterisks (*) denotes significant differences between normoxic and hypoxic values at $P<0.05$.

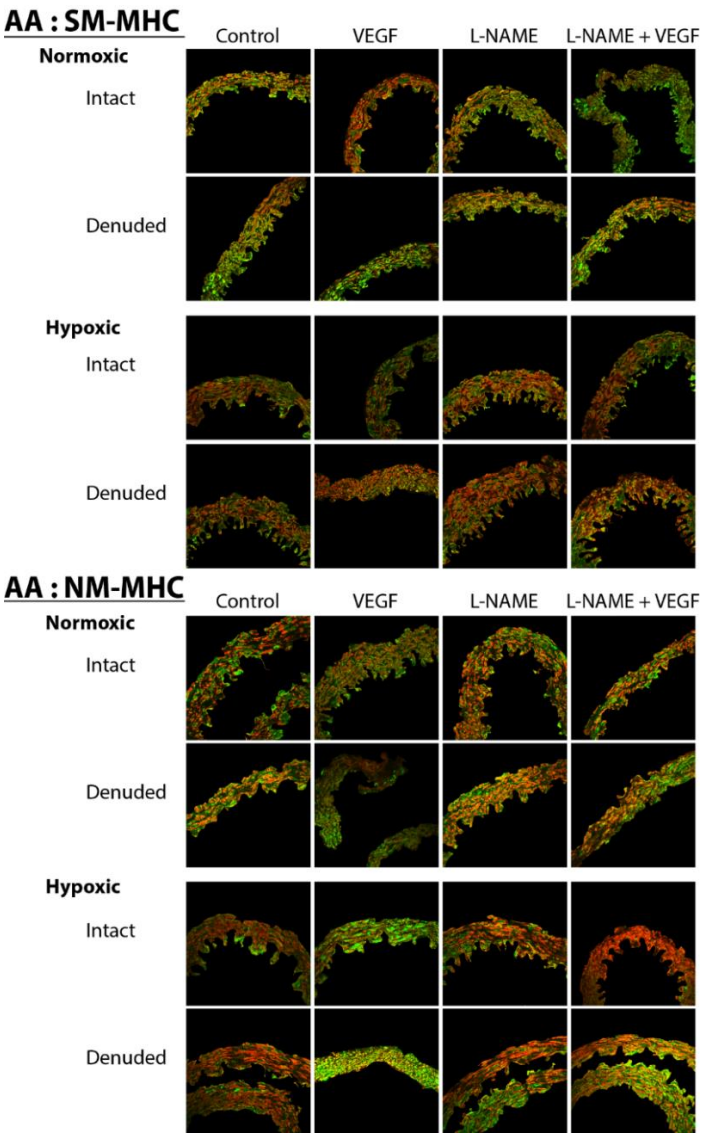

Figure 3. Hypoxia in utero alters endothelium-dependent effect of VEGF on MHC colocalization pattern with SM-αA.

To elucidate the effect of hypoxia on the endothelial NO-PKG pathway, matched intact and denuded arteries from normoxic and hypoxic fetal sheep underwent organ culture with 0, 10 ng/ml VEGF, the eNOS inhibitor LNAME (100uM), or with 10 ng/ml VEGF ± 100uM LNAME. Representative images are displayed in Figure 3. Hypoxia in utero altered endothelial-dependent effect of VEGF on Alpha Actin (RED 633nm) and myosin heavy chains (GREEN 488nm) organization. YELLOW represents pixels that are positive for both-Alpha Actin and MHC. Using this dual-label fluorescent confocal microscopy to quantify the extent of colocalization between-Alpha Actin and myosin. Shown above is a single image from each of the 4 different colocalization groups undergoing 4 treatments that represent a total of 365 images. For each treatment group, n values greater than 6 in all groups.

Hypoxia in Utero Alters Endothelial Response to VEGF and Smooth Muscle Contractile Protein Organization

To assess how hypoxia in utero alters endothelial response to VEGF and influence on the smooth muscle phenotype, perturbation of the NO-PKG pathway with and without stimulus by VEGF was performed in artery segments from normoxic and hypoxic animals. To separate out the endothelial component from direct action of VEGF on smooth muscle, one MCA from each animal was denuded of endothelium and the contralateral side left intact as described in the methods before being dissected into segments and cultured in the presence of 0 or 10 ng/ml VEGF, 100uM LNAME, or 100uM LNAME + 10ng/mL VEGF for 24hrs as described. Segments designated for colocalization analysis underwent fixation, staining and imaging per the Immunohistochemistry and Confocal protocol. Colocalization of the mature contractile SM-MHC isoform with SM-AA varied by quadrant. Given that these 3 quadrants total 100 percent of the pixels physiologically relevant and that both SM-MHC isoforms and a-Actin have previously been established to distinguish different smooth muscle cell phenotypes, this analysis helps quantify possible shifts between different SMC phenotype subpopulations within the artery.

Hypoxia Alters Endothelial Mediation of VEGF on MHC Colocalization with AA

Figure 4A depicts SM-MHC and AA colocalization. Baseline treatment in organ culture of normoxic arteries with intact endothelium had a distribution pattern of myosin-actin colocalization of 3 distinct populations in decreasing prevalence: LL with 49%, LR

with 12% and UR with 39%. This colocalization pattern was not significantly altered by chronic hypoxia or 24hr organ culture after denudation of the endothelium. Acute 24hr exposure to VEGF of endothelium-intact normoxic arteries increased LL at the expense of UR, with LL increased to +10, LR increased to +11% of control, and UR decreased -21% of control. VEGF treatment of endothelium-denuded normoxic arteries enhanced this effect, with a greater increase in UR and loss of LL: LL increased to +15%, LR did not significantly change, UR decreased to -15%. Hypoxia decreased the influence VEGF treatment in endothelium-intact arteries, with similar shifts of population but none statistically significant at the $p < 0.05$. Hypoxia inverts the influence of VEGF treatment on endothelium-denuded arteries in UR only: LL did not significantly change with -4%, LR increased to **+5%**, UR did not significantly change-with -1%. Intact arteries contain 2 prominent cell populations, the endothelium and smooth muscle cells excluding a minimal population of pericytes and neurons that are present in the adventitial wall. By taking the difference of the effect of VEGF on endothelium intact arteries (predominantly Endothelium + Smooth muscle) minus the effect of VEGF on endothelium denuded arteries (predominantly Smooth muscle), we hoped to determine the component of the shift in colocalization populations due to hypoxic changes of the endothelium alone. The far right panel in Figures 5-8 for both A and B represents this *Difference of the Difference* or in formula form $\Delta\Delta$ = Intact $_{\Delta\Delta\,(VEGF\,-\,Ctrl)}$ - Denuded $_{\Delta\Delta\,(VEGF\,-\,Ctrl)}$. Hypoxia changed endothelial contribution to VEGF influence on SM-MHC and Actin colocalization (See Figure 4A, right panels). VEGF action through the endothelium: decreased LL (-5%) in normoxic arteries while it increased LL (+8%) in hypoxic arteries, increased LR (+11%)

in normoxic arteries while it did not significantly change LR (-2%) in hypoxic arteries and decreased UR equally in both in normoxic (-6%) and in hypoxic (-6%) arteries.

Figure 4B depicts NM-MHC and AA colocalization. Baseline treatment in organ culture of normoxic arteries with intact endothelium had a distribution pattern of myosin-actin colocalization in control arteries demonstrates the 3 distinct populations in decreasing prevalence/abundance: LL with absolute 43%, LR with absolute 32%, UR with absolute 26%. This colocalization pattern was not significantly altered by chronic hypoxia or 24hr organ culture after denudation of the endothelium. Acute 24hr exposure to VEGF increased the LL quadrant in normoxic (equally in denuded and intact arteries) and in hypoxic arteries. VEGF treatment of endothelium-intact normoxic arteries increased LL at the expense of both other quadrants, LR decreased more than UR: LL increased to +20%, LR decreased to -14%, UR insignificantly decreased to -7%. VEGF treatment of endothelium-denuded normoxic arteries had a similar increase in LL but at a greater expense of UR instead of LR: LL increased to +20%, LR decreased to -10%, UR decreased to -10%. As with SM-MHC, hypoxia significantly decreased the influence of VEGF treatment in endothelium-intact arteries, with similar shifts of population but with none statistically different from control at the $p < 0.05$. Hypoxia accents the influence of VEGF treatment on endothelium-denuded arteries in LR only, inverting the effect of the endothelium: LL insignificantly increased +11%, LR decreased to -15%, UR insignificantly increased +4%. Hypoxia changes endothelial contribution to VEGF influence on NM-MHC and Actin colocalization (See Figure 4B, right panels). VEGF action through the endothelium did not significantly alter LL in normoxic arteries (0%) while it decreased LL in hypoxic arteries (-4%). Decreased LR in normoxic arteries (-

3%) but increased LR in hypoxic arteries (+9%). Increased UR in normoxic arteries (+3%) while decreasing UR in hypoxic arteries (-5%). Thus VEGF is acting primarily through the smooth muscle in normoxic arteries and hypoxic arteries. However, hypoxia appears to sensitize the endothelium to VEGF which partially opposes the direct effect on the smooth muscle to decrease synthetic NM-MHC colocalization with AA.

A)

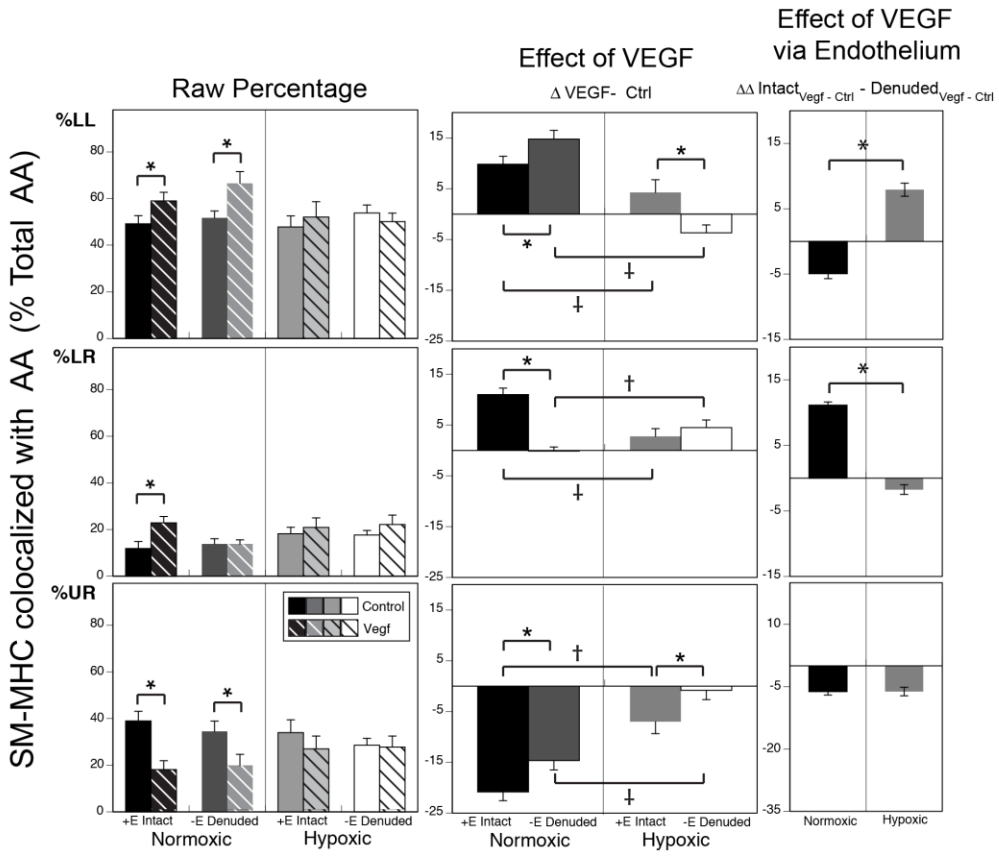
Raw Percentage
Effect of VEGF
Δ VEGF- Ctrl
Effect of VEGF via Endothelium
ΔΔ Intact Vegf - Ctrl - Denuded Vegf - Ctrl
SM-MHC colocalized with AA (% Total AA)
%LL
%LR
%UR
Control
Vegf
+E Intact
-E Denuded
+E Intact
-E Denuded
Normoxic
Hypoxic
Normoxic
Hypoxic
Normoxic
Hypoxic

B)

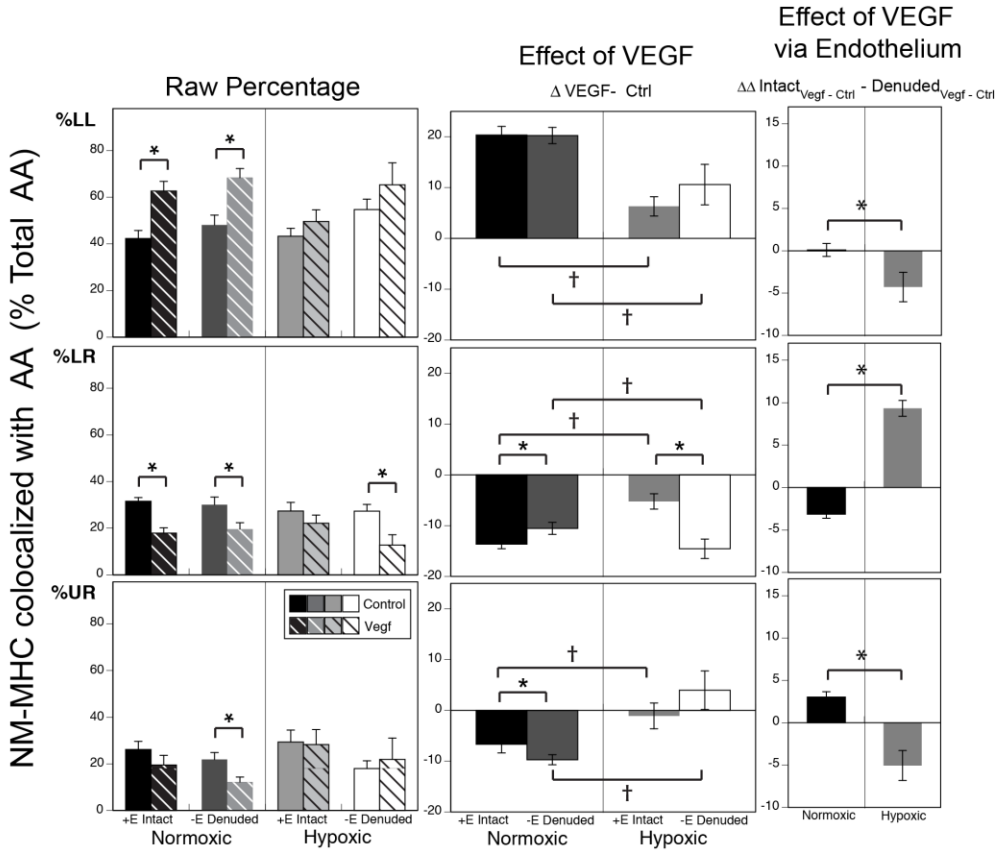
Raw Percentage
Effect of VEGF
Δ VEGF- Ctrl
Effect of VEGF via Endothelium
ΔΔ Intact Vegf - Ctrl - Denuded Vegf - Ctrl
NM-MHC colocalized with AA (% Total AA)
%LL
%LR
%UR
Control
Vegf
+E Intact
-E Denuded
+E Intact
-E Denuded
Normoxic
Hypoxic
Normoxic
Hypoxic
Normoxic
Hypoxic

Figure 4. Chronic Hypoxia Alters Endothelium-Dependent Effect of VEGF on MHC Colocalization Pattern with SM-αA.

Endothelium intact and denuded arteries from normoxic and hypoxic animals were organ cultured in the presence or absence of 10ng/mL VEGF, underwent colocalization assays and quadrant analysis. The far left column is raw percentage of pixels by quadrant. The middle column is the differences due to treatment in 24hr organ culture, in this case VEGF. The far right column is differences of this difference or ΔΔ due to the endothelium (Intact – Denuded). Among controls, the distribution pattern did not change with chronic hypoxia or denudation of the endothelium for both SM-MHC and NM-MHC. Figure 4A: Unlike hypoxia, acute exposure to VEGF shifted both SM-MHC and NM-MHC colocalization with SM-αA pixels from UR to LL in normoxic arteries and this is modestly amplified by the presence of the endothelium (Intact vs denuded). This effect is lost following hypoxic acclimatization of the endothelium and smooth muscle. As illustrated in Figure 4B, far right column, the normoxic endothelium contributes a shift in SM-MHC towards the LR while the hypoxic endothelium modestly shifts SM-MHC colocalization to the LL. Stated another way, the presence of the endothelium appears to amplify the effect of VEGF compared with endothelium-denuded in normoxic arteries but not in hypoxic arteries. For NM-MHC colocalization, VEGF causes a similar increase in LL that is diminished by the presence of the endothelium. The net shift induced by VEGF through the endothelium increases UR in normoxic and LR in hypoxic arteries. All differences are at $P<0.05$. Asterisks (*) denotes significant differences between endothelium intact and denuded values for either normoxic or hypoxic arteries. The † denotes significant differences between normoxic and hypoxic values. The star (*) denote significant difference in the effect of VEGF modification to the MHC and SM-αA colocalization pattern through the normoxic vs hypoxic endothelium. Error bars indicate SE for $n \geq 6$ for all groups.

Hypoxia Does Not Alter Baseline Endothelial Mediation of MHC Colocalization with AA

Figure 5A depicts SM-MHC and AA colocalization. Please see discussion of Figure 4 for comparison among baseline controls for Normoxic (intact and denuded) and Hypoxic (intact and denuded) treatment groups. Note bars in graph are ordered with perspective of the contribution by the endothelium, where baseline minus LNAME inhibition treatment. Acute 24hr inhibition of baseline eNOS with LNAME did not significantly alter any colocalization quadrant in endothelium intact arteries while slightly increasing both LL and LR, and decreasing UR in endothelium denuded arteries for both normoxic and hypoxic arteries. (Figure 5A, middle panels) LNAME treatment of endothelium-intact normoxic arteries does not significantly alter baseline unstimulated endothelial function on any quadrant. LNAME treatment of endothelium-denuded normoxic arteries enhanced the modest effect of endothelial intact arteries, with an increase in LL and LR at the expense of UR: LL decreased -7%, LR decreased -5% of control, UR increased +12%. Hypoxia did not alter the influence LNAME inhibition in endothelium-intact arteries, like with normoxic no significant shift among the quadrants occurred at unstimulated baseline. Hypoxia matches the influence of VEGF treatment on endothelium-denuded arteries with normoxic arteries, increasing LL at the expense of UR: LL decreased -9%, LR did not change, UR increased +9%. Hypoxia does not change baseline unstimulated endothelial contribution to LNAME influence on SM-MHC and Actin colocalization (See Figure 5A, right panels). LNAME inhibition through the endothelium decreased LL in normoxic (-6%) and in hypoxic arteries (-7%), decreased LR in normoxic (-2%) and hypoxic (-2%) arteries, increased UR in normoxic (+8%) and

hypoxic (9%). Hypoxia is not altering baseline endothelial or direct smooth muscle LNAME pathways upstream of SM-MHC and AA colocalization.

A)

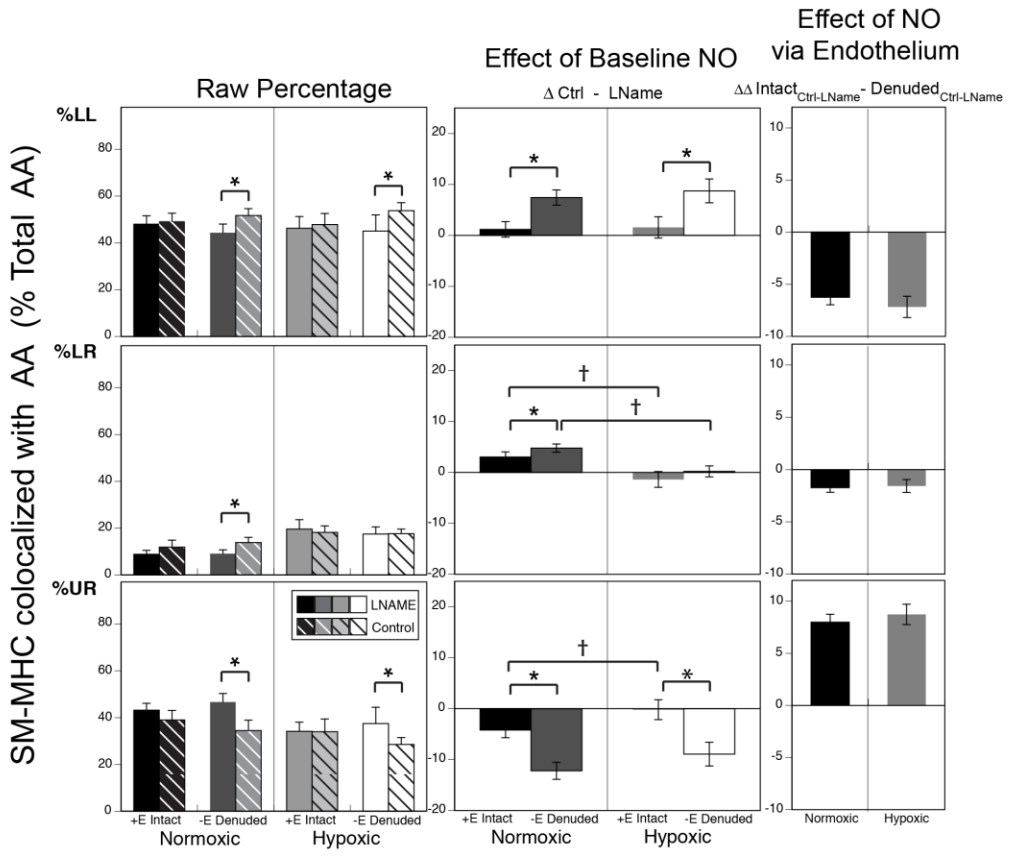
Raw Percentage
Effect of Baseline NO
Δ Ctrl - LName
Effect of NO via Endothelium
ΔΔ Intact Ctrl-LName - Denuded Ctrl-LName
SM-MHC colocalized with AA (% Total AA)
%LL
%LR
%UR
LNAME
Control
+E Intact
-E Denuded
Normoxic
Hypoxic

B)

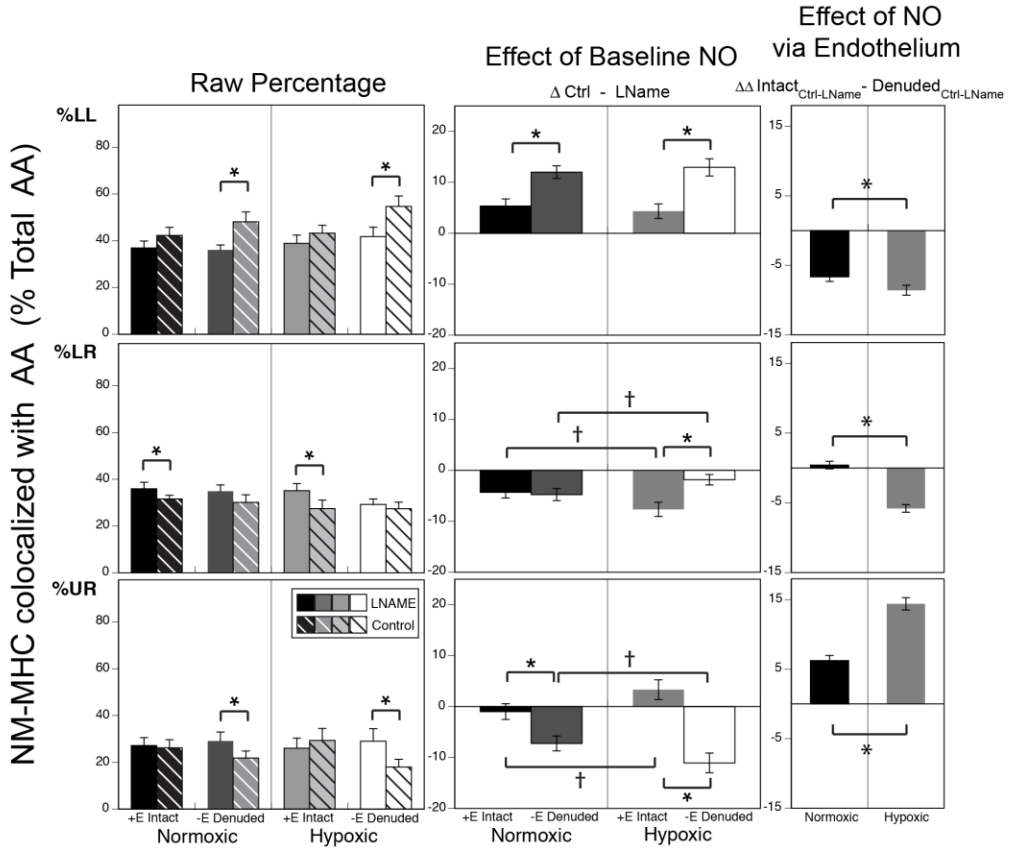
Raw Percentage
Effect of Baseline NO
Δ Ctrl - LName
Effect of NO via Endothelium
ΔΔ Intact Ctrl-LName - Denuded Ctrl-LName
NM-MHC colocalized with AA (% Total AA)
%LL
%LR
%UR
LNAME
Control
+E Intact
-E Denuded
Normoxic
Hypoxic

Figure 5. Chronic Hypoxia Alters Endothelium-Dependent Effect of L-NAME on MHC Colocalization Pattern with SM-αA.
Endothelium intact and denuded arteries from normoxic and hypoxic animals were organ cultured in the presence or absence of 100uM LNAME, underwent colocalization assays and quadrant analysis as described in the text. The far left column is raw percentage of pixels by quadrant. The middle column is the differences due to treatment in 24hr organ culture, in this case the NOS inhibitor L-NAME. The far right column is differences of the treatment difference or ΔΔ due to the endothelium (Intact – Denuded). Figure 5A: L-NAME inhibition of basal NO increases LL for SM-MHC and SM-αA colocalization pixel distribution primarily in endothelium-denuded arteries (LEFT PANEL) and this is not significantly altered by hypoxic acclimatization (RIGHT PANEL). Figure 5B: L-NAME does alter NM-MHC and SM-αA colocalization pixel distribution (LEFT PANEL) with a shift toward UR through the normoxic endothelium that is amplified through hypoxic endothelium (RIGHT PANEL). Asterisks (*) denotes significant differences between endothelium intact and denuded values for either normoxic or hypoxic arteries at $P<0.05$. The † denotes significant differences between normoxic and hypoxic values at $P<0.05$. The Star (*) denotes significant difference in the effect of VEGF modification to MHC and SM-αA colocalization pattern through the normoxic vs hypoxic endothelium. Error bars indicate SEM for $n \geq 8$ for all groups.

Figure 5B depicts NM-MHC and AA colocalization. Please see discussion of Figure 4 for comparison among baseline controls for Normoxic (intact and denuded) and Hypoxic (intact and denuded) treatment groups. Acute 24 hr inhibition of baseline eNOS with LNAME marginally increased LR +5% in endothelium-intact arteries for both normoxic and hypoxic arteries while decreasing LL -12% and increasing UR +7% in normoxic denuded arteries and hypoxia enhanced this effect (Figure 5B, middle panels). Hypoxia modestly increased the influence LNAME inhibition in endothelium-intact arteries on NM-MHC and AA colocalization further decreasing LR and increasing UR at unstimulated baseline: LL did not significantly change -4%, LR increased +7%, UR did not significantly change -3%. Hypoxia accentuated the influence of LNAME treatment on endothelium-denuded arteries compared with normoxic arteries, increasing LL at the expense of UR and inverting the action through the endothelium on UR: LL decreased -13%, LR did not change +2%, UR increased +11%. Hypoxia changes endothelial contribution to VEGF influence on NM-MHC and Actin colocalization (See Figure 5B, right panels). LNAME inhibition through the endothelium: decreased LL in normoxic (-7%) and hypoxic (-9%) arteries, did not change LR in normoxic (0%) arteries but significantly decreased in hypoxic (-6%) arteries, modestly increased UR in normoxic (+6%) arteries and majorly increased UR in hypoxic (+14%) arteries. Clearly the LNAME is acting directly on the smooth muscle or some other non-endothelial cell type in the artery wall. LNAME acting through non-endothelial LNAME targets is causing a shift toward decreased synthetic NM-MHC colocalization with AA while LNAME targets within the endothelium is acting to increase synthetic NM-MHC colocalization with AA.

Hypoxia Does Alter VEGF Stimulated Endothelial Mediation of MHC Colocalization with AA through NO-Dependent and NO-Independent Pathways

Figure 6A depicts SM-MHC and AA colocalization. VEGF stimulation in organ culture of normoxic arteries with intact endothelium had a distribution pattern of LL with absolute 59%, LR with absolute 23%, UR with absolute 18%. This colocalization pattern changed with hypoxia: decreased in LL (endothelium-denuded) and increased in UR (endothelium-intact). This colocalization pattern also decreased with denudation of the endothelium in LR. Compared to acute 24hr exposure to VEGF alone, VEGF + LNAME decreased LL and increased UR in normoxic (more in denuded than intact arteries). This effect was present but minimized in hypoxic arteries. Figure 6A, middle panels. LNAME partial inhibition of VEGF stimulated normoxic arteries with intact endothelium resulted in a modest increase in UR with a prominent complimentary decrease of LR: LL did not change--4%, LR decreased -7%, UR increased +11%. Partial inhibition of VEGF with LNAME in normoxic arteries without endothelium resulted in an even large increase of UR and decrease in LL: LL decreased -16%, LR decreased -7%, UR increased +23%. VEGF stimulation of hypoxic endothelium-intact arteries were less inhibited by LNAME than normoxic endothelium. VEGF stimulation of hypoxic endothelium-denuded arteries were less inhibited by LNAME than normoxic endothelium-denuded arteries. Hypoxia changes endothelial contribution to VEGF influence on SM-MHC and Actin colocalization (See Figure 6A, right panels). LNAME partial inhibition of VEGF action through the endothelium greatly decreased LL in normoxic (-13%) while minimally increased in hypoxic (+4%) arteries, with no change in LR in normoxic (+1%) while

slightly decreasing in hypoxic (-5%) arteries, greatly increased UR in normoxic (+12%) with no change in hypoxic (+1%) arteries.

Figure 6B depicts NM-MHC and AA colocalization. VEGF stimulation in organ culture of normoxic arteries with intact endothelium has a distribution pattern: LL with absolute 62%, LR with absolute 18%, UR with absolute 19%. This colocalization pattern changed with hypoxia: decreased in LL with complimentary increase in UR (for endothelium-intact arteries). This colocalization pattern also decreased with denudation of the endothelium in UR for normoxic arteries and LR for hypoxic arteries. LL increased with denudation in hypoxic arteries. Compared to acute 24hr exposure to VEGF alone, VEGF + LNAME decreased LL and increased LR and UR in normoxic (more in denuded than intact). This trend was present but minimized in hypoxic arteries (again more in denuded than intact). Figure 6A, middle panels. LNAME partial inhibition of VEGF stimulated normoxic arteries with intact endothelium decreased in LL and increased LR: LL decreased -13%, LR increased +10%, UR did not change significantly -2%. Partial inhibition of VEGF with LNAME in normoxic arteries without endothelium resulted in an even large increase of LR and UR with decrease in LL: LL decreased -28%, LR increased +15%, UR increased +13%. VEGF stimulation of hypoxic endothelium-intact arteries were less inhibited by LNAME than normoxic endothelium: LL did not change -3%, LR increased +9%, UR did not change -6%. VEGF stimulation of hypoxic endothelium-denuded arteries were equally inhibited by LNAME than normoxic endothelium-denuded arteries: LL decreased -25, LR increased +18%, UR did not change significantly +7%. Hypoxia accentuated endothelial contribution to VEGF influence on NM-MHC and Actin colocalization (See Figure 6B, right panels). LNAME partial

inhibition of VEGF action through the endothelium decreased LL in normoxic (-16%) while minimally increased in hypoxic (-22%) arteries; increased LR in normoxic (+5%) while slightly decreasing in hypoxic (+9%) arteries; increased UR in normoxic (+11%) with no change in hypoxic (+13%) arteries. VEGF action through intact endothelium is partially inhibited by LNAME equally in both normoxic and hypoxic arteries with respect to NM-MHC and AA colocalization. Hypoxic smooth muscle plays a greater role than the endothelium in LNAME action following VEGF stimulation.

A)

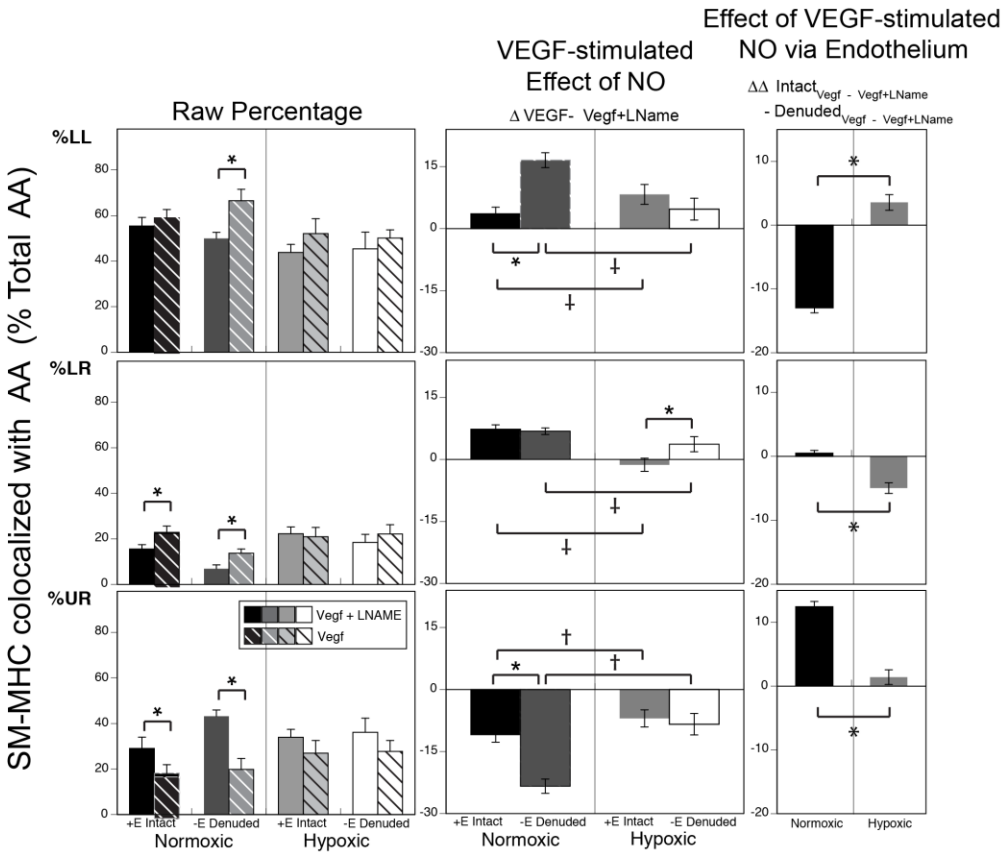
SM-MHC colocalized with AA (% Total AA)
Raw Percentage
VEGF-stimulated Effect of NO
Δ VEGF- Vegf+LName
Effect of VEGF-stimulated NO via Endothelium
ΔΔ Intact Vegf - Vegf+LName - Denuded Vegf - Vegf+LName
%LL
%LR
%UR
Vegf + LNAME
Vegf
+E Intact
-E Denuded
Normoxic
Hypoxic

B)

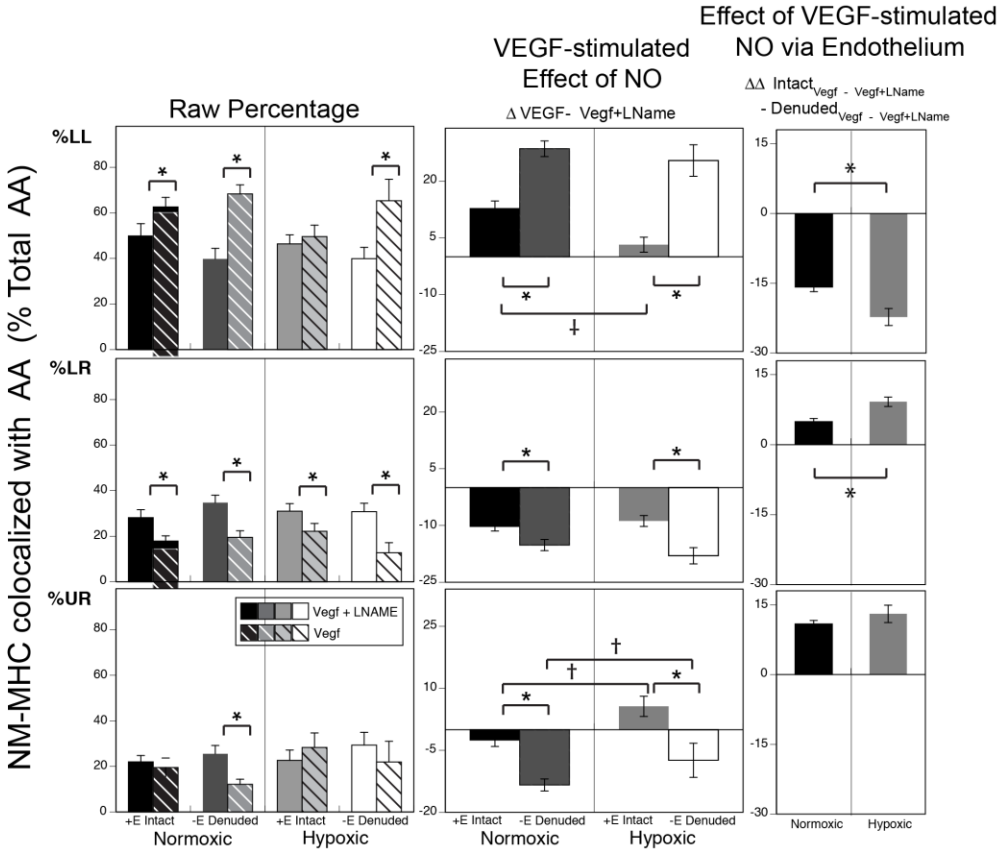
NM-MHC colocalized with AA (% Total AA)
Raw Percentage
VEGF-stimulated Effect of NO
Δ VEGF- Vegf+LName
Effect of VEGF-stimulated NO via Endothelium
ΔΔ Intact Vegf - Vegf+LName - Denuded Vegf - Vegf+LName
%LL
%LR
%UR
Vegf + LNAME
Vegf
+E Intact
-E Denuded
Normoxic
Hypoxic

Figure 6. Chronic Hypoxia alters endothelium-dependent effect of VEGF-induced NO on MHC colocalization pattern with SM-αA.
Endothelium intact and denuded arteries from normoxic and hypoxic animals were organ cultured in 10 ng/ml VEGF ± 100uM LNAME, underwent colocalization assays and quadrant analysis as described in the text. The far left column is raw percentage of pixels by quadrant. The middle column is the differences due to treatment in 24hr organ culture, in this case VEGF stimulation with and without the NOS inhibitor L-NAME. The far right column is differences of this difference or ΔΔ due to the endothelium (Intact – Denuded). Figure 6A: L-NAME inhibition of VEGF-stimulated NO decreases SM-MHC and SM-αA colocalization pixel distribution from LL and increases UR. This response is greater in endothelium-denuded arteries and this is lost with hypoxic acclimatization. Figure 6B: L-NAME inhibition of VEGF-induced NO decreases NM-MHC and AA colocalization pixel distribution with a shift toward UR from LL through the normoxic endothelium. This effect is amplified by hypoxic acclimatization of the endothelium. Asterisks (*) denotes significant differences between endothelium intact and denuded values for either normoxic or hypoxic arteries at $P<0.05$. The † denotes significant differences between normoxic and hypoxic values at $P<0.05$. The Star (*) denotes significant difference in the effect of VEGF modification to MHC and SM-αA colocalization pattern through the normoxic vs hypoxic endothelium. Error bars indicate SE for $n \geq 8$ for all groups.

Discussion

This study offers five original findings. First, hypoxia in utero significantly alters cerebrovascular contractile response following future VEGF exposure. Second, this response to subsequent exposure to VEGF is mediated through both the endothelium and smooth muscle. Third, hypoxia in utero alters contractile protein organization in the cerebrovascular smooth muscle, specifically among SM-MHC, NM-MHC and SM-AA with characteristic colocalization patterns. Fourth, these colocalization patterns serve to characterize multiple SMC phenotypes within the wall and thus enable quantification of shifts between subpopulations of SMC phenotypes from baseline. Fifth, hypoxia in utero alters the endothelial regulation of VSM contractile function and phenotype in part through changes to the NO pathway. Together, these findings support the hypothesis that hypoxia in utero alters endothelial influence on cerebrovascular smooth muscle contractile function and phenotype.

Hypoxic Acclimatization Alters Artery Structure and Function

Hypoxia induces vascular remodeling with changes in artery structure that manifests as increased artery thickness and changes in contractile force production, including ligand-, stretch-, and potassium-induced contraction (17). Hypoxic remodeling is tissue-specific with unique responses in various tissues such as pulmonary, large vessels such as the common carotid or the smaller muscular arteries such as the middle cerebral (24). This suggests that the mix of cell phenotypes present and their history of prior hypoxic exposure will control the response to any subsequent hypoxic stress. Hypoxia also alters more than artery structure; it alters contractile behavior. These

changes may be mediated in part through prolonged exposure to various factors, including contractants, vasodilators, and vasotrophic factors such as VEGF. This response can even change for a single factor solely due to the duration of the exposure. Likewise, the duration of hypoxic exposure from acute, intermittent, to long-term chronic hypoxia stimulate distinct or even opposing responses.

It has also been shown that hypoxic vascular remodeling alters intercellular communication between the endothelium and smooth muscle. Chronic hypoxia has been shown to alter activation-coupling of intracellular pathways such as PKG and modification of downstream proteins within the contractile apparatus (13). These include changes in the repertoire of contractile protein types, abundance, and subcellular organization, which in turn represents a shift in SMC phenotype. (21, 23). These changes serve to influence any potential future vascular remodeling consequent to hypoxic challenge.

Four VSM phenotypes have traditionally been described along a developmental spectrum from proliferative, migratory, synthetic, and the mature contractile type (7, 21, 23). It appears that certain SMCs within a tissue retain the ability to de-differentiate along this spectrum to functionally adapt as needed to a changing environment (7). Such response represents an adaptation that promotes short-term survival as a biological necessity. Acutely, vascular smooth muscle is thought to act principally to maintain vascular tone through contractile force production. However, other VSM phenotypes are vital for the frequent remodeling of the cerebral vasculature, including synthesis of the ECM by non-contractile phenotypes.

Extended duration of exposure to otherwise normal physiologic stimulus can alter the long-term effects (13, 20, 21). Hypoxia alters the response to VEGF with transient upregulation of receptors (2). Like growth factors, chronic exposure to usually transient vasocontractants such as endothelin can promote a SMC phenotypic shift toward a synthetic VSM phenotype, with increased ECM production which enhances the structural and elastic properties of cerebral vessels and promotes their ability to maintain vascular tone (12). Acute vasodilators such as NO and downstream activation of PKG have been shown to induce the contractile SMC phenotype with chronic exposure (13, 20). Similarly, VEGF, a central growth factor in hypoxic vascular remodeling, has been shown to activate eNOS, which stimulates NO release with consequent activation of PKG (4). Together, these findings support the hypothesis that hypoxia alters smooth muscle phenotype and function; and that this occurs in part through changes in endothelial regulation. The extent to which these effects alter endothelial factor release and downstream pathways remain largely unreported.

Hypoxic Acclimatization Altered Endothelial and Smooth Muscle Response to VEGF

In the present study, hypoxia suppressed contractile function, and the endothelial component of this response to VEGF was ablated (**Figure 1, Upper Panels**) raising the possibility that hypoxia altered either VEGF receptors, or altered downstream endothelial influence on SMC contractile signaling. Hypoxia did not alter K^+-induced stress; but VEGF in the presence of the endothelium did increase K^+-induced stress regardless of normoxic/hypoxic status (**Figure 1, Lower Panels**). Previous work from many

laboratories, including our own (5), (10) have established that changes in vascular structure and function are frequently coupled with changes in vascular smooth muscle phenotype (15). To explore the possibility that hypoxia-induced changes in MCA function may have involved shifts in smooth muscle phenotype, the present study employed quantitative confocal microscopy to examine MCAs from the same treatment groups used for contractility measurements (Figure 2). These measurements quantified changes in the colocalization of smooth muscle α-actin with the smooth-muscle (SM-MHC) and non-muscle (NM-MHC) isoforms of myosin heavy chain (MHC) to identify transitions in phenotype, as previously reported (10, 15). A novel strength of the non-parametric colocalization analysis employed in these studies was that all colocalized pixels fell into one of three main phenotypic categories depending on the relative intensities of the markers examined. This assignment emphasized shifts between the phenotypic categories in response to hypoxia and VEGF.

As indicated by changes in colocalization between SM-AA and the MHC isoforms, hypoxia in utero appears to promote differentiation to a contractile phenotype (**Figure 2**) as indicated by an increase in colocalized pixels with high intensities for SM-MHC. Unexpectedly, hypoxia also strongly increased the fraction of colocalized pixels with high intensities for NM-MHC denoting an increase in the partially de-differentiated synthetic phenotype. The rightward shift in pixel distribution implies an increase in the proportion of cells in a contractile phenotype. This suggests an upregulation of 2 distinct populations of SMC with different phenotypes; the contractile, and the partially de-differentiated synthetic.

Hypoxic Acclimatization Altered Endothelial Mediation of VEGF on SMC Phenotype Distribution

As indicated by changes in colocalization between SM-AA and the MHC isoforms, VEGF appeared to promote synthetic differentiation in normoxic but not hypoxic arteries (**Figure 4**). While hypoxia seemed to increase colocalization for both MHC isoforms, acute secondary exposure to VEGF in organ culture resulted in decreased pixel intensity for SM-MHC colocalization. VEGF also correspondingly increased the fraction of colocalized pixels with low intensities for both SM-AA and SM-MHC. This leftward shift in pixel distribution was consistent with a decrease in the proportion of smooth muscle cells in a contractile phenotype (**Figure 4, Upper Panels**). The concept of isolating the purely *endothelial* component by observing the *differences* between intact and denuded arteries was introduced by John Magnus. VEGF action through the endothelium resulted in a loss of pixels in both UR and LL with a subsequent increase in LR for SM-MHC colocalization with SM-AA suggesting an increase in SM-AA but unchanged re-organization with SM-MHC. Hypoxia decreased intensity for both intensity and colocalization for both markers with an increase in LL. VEGF in organ culture also significantly decreased the fraction of colocalized pixels with high intensities for both NM-MHC and SM-AA, and correspondingly increased the fraction with low intensities for both markers; this leftward shift in pixel distribution implies a decrease in the proportion of cells in a non-contractile phenotype (**Figure 4, Lower Panels**). The influence of VEGF through the endothelium significantly changed with hypoxia, increase LL colocalization for SM-MHC and increasing LR for NM-MHC.

Hypoxic Acclimatization Did Not Alter Baseline Action of Endothelial NO on SMC Phenotype

As indicated by changes in colocalization between SM-AA and the MHC isoforms, basal NO did not appear to promote de-differentiation of SMCs in normoxic or hypoxic arteries (**Figure 5A**). L-NAME inhibition of basal NO modestly increased LL for SM-MHC and SM-αA colocalization pixel distribution primarily in endothelium-denuded arteries (LEFT PANEL) and this is not significantly altered by hypoxic acclimatization (RIGHT PANEL). Interestingly L-NAME inhibition of basal NO did increase NM-MHC and SM-αA colocalization pixel distribution with a shift toward UR through the normoxic endothelium that is amplified through hypoxic endothelium (**Figure 5B**). This suggests that NM-MHC organization may be more sensitive to NO regulation. The influence of the endothelium significantly changed with hypoxia only with increasing organization of the synthetic-denoting NM-MHC.

Hypoxic Acclimatization Did Alter VEGF-Stimulated Endothelial NO Mediation of SMC Phenotype

Unlike basal NO, VEGF stimulated NO through normoxic endothelium significantly increased the contractile SM-MHC colocalization with SM-AA. This effect of VEGF through the endothelium was lost with hypoxic acclimatization of the endothelium however, the hypoxic endothelium retained its effect on NM-MHC colocalization with SM-AA, re-iterating its independent regulation from SM-MHC.

Overview

As a whole, the results of this study emphasize that hypoxia can alter the structure, contractile protein organization, contractility and smooth muscle phenotype of cerebral arteries through changes in endothelial regulation of NO-dependent and NO-independent pathways. Given that many but not all of these effects were stimulated by VEGF and then partially attenuated by inhibition of eNOS with L-NAME, these findings reinforce the hypothesis that hypoxia alters endothelial response and downstream influence on smooth muscle through NO-dependent and NO-independent pathways. Consistent with this idea are multiple findings that hypoxia upregulates VEGF, that VEGF leads to release of NO, and that NO alters SMC function.

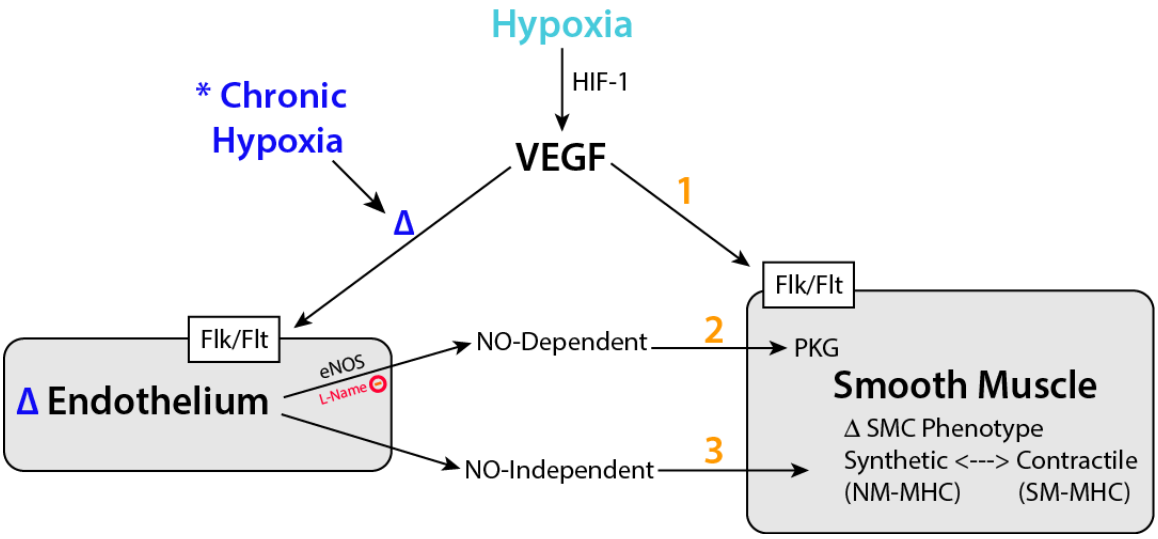

Figure 7. Chronic hypoxia alters endothelial and smooth muscle response to secondary VEGF through altered NO-dependent and NO-independent pathways. Hypoxia in Utero Alters Endothelial influence on Smooth Muscle Phenotype and Function. Hypoxia can influence smooth muscle function and phenotype through changes in endothelial influence via NO-dependent and NO-independent pathways. Secondary activation of the vessel with VEGF seems to stimulate pathways in the endothelium that have changed with hypoxic acclimatization. NO inhibition with LNAME appears to perturbate some but not all of this effect suggesting there are both NO-dependent and NO-independent components. Likewise, VEGF direct stimulation of smooth muscle in denuded arteries and combined direct + indirect stimulation in endothelium-intact arteries appears to alter downstream organization of MHC with SM-AA. This occurs with shifts between smooth muscle phenotype within the medial wall as demonstrated by novel quadrant characterization and these shifts are strongly associated with changes in contractility.

Acknowledgements

The authors appreciate the excellent image processing performed by Adam Vergara and the microscopy support performed by Alane Bristow, MPH for this study. Imaging was performed in the LLUSM Advanced Imaging and Microscopy Core with support of NSF Grant MRI-DBI 0923559. The work reported in this manuscript was supported by USPHS grants P01-HD31226, R01-HL54120, R01-HL64867, R01-NS076945 and the Loma Linda University School of Medicine.

References

1. **Adeoye OO, Bouthors V, Hubbell MC, Williams JM, and Pearce WJ**. VEGF receptors mediate hypoxic remodeling of adult ovine carotid arteries. *J Appl Physiol (1985)* 117: 777-787, 2014.

2. **Adeoye OO, Butler SM, Hubbell MC, Semotiuk A, Williams JM, and Pearce WJ**. Contribution of increased VEGF receptors to hypoxic changes in fetal ovine carotid artery contractile proteins. *Am J Physiol Cell Physiol* 304: C656-665, 2013.

3. **Ball SG, Shuttleworth CA, and Kielty CM**. Vascular endothelial growth factor can signal through platelet-derived growth factor receptors. *J Cell Biol* 177: 489-500, 2007.

4. **Bussolati B, Dunk C, Grohman M, Kontos CD, Mason J, and Ahmed A**. Vascular endothelial growth factor receptor-1 modulates vascular endothelial growth factor-mediated angiogenesis via nitric oxide. *Am J Pathol* 159: 993-1008, 2001.

5. **Butler SM, Abrassart JM, Hubbell MC, Adeoye O, Semotiuk A, Williams JM, Mata-Greenwood E, Khorram O, and Pearce WJ**. Contributions of VEGF to age-dependent transmural gradients in contractile protein expression in ovine carotid arteries. *Am J Physiol Cell Physiol* 301: C653-666, 2011.

6. **Charles SM, Zhang L, Cipolla MJ, Buchholz JN, and Pearce WJ**. Roles of cytosolic Ca2+ concentration and myofilament Ca2+ sensitization in age-dependent cerebrovascular myogenic tone. *Am J Physiol Heart Circ Physiol* 299: H1034-1044, 2010.

7. **Davis-Dusenbery BN, Wu C, and Hata A**. Micromanaging vascular smooth muscle cell differentiation and phenotypic modulation. *Arterioscler Thromb Vasc Biol* 31: 2370-2377, 2011.

8. **Durrant LM, Khorram O, Buchholz JN, and Pearce WJ**. Maternal food restriction modulates cerebrovascular structure and contractility in adult rat offspring: effects of metyrapone. *Am J Physiol Regul Integr Comp Physiol* 306: R401-410, 2014.

9. **Eddinger TJ, and Meer DP**. Myosin II isoforms in smooth muscle: heterogeneity and function. *Am J Physiol Cell Physiol* 293: C493-508, 2007.

10. **Hubbell MC, Semotiuk AJ, Thorpe RB, Adeoye OO, Butler SM, Williams JM, Khorram O, and Pearce WJ**. Chronic hypoxia and VEGF differentially modulate abundance and organization of myosin heavy chain isoforms in fetal and adult ovine arteries. *Am J Physiol Cell Physiol* 303: C1090-1103, 2012.

11. **Hull AD, Long DM, Longo LD, and Pearce WJ**. Pregnancy-induced changes in ovine cerebral arteries. *Am J Physiol* 262: R137-143, 1992.

12. **Kida T, Chuma H, Murata T, Yamawaki H, Matsumoto S, Hori M, and Ozaki H**. Chronic treatment with PDGF-BB and endothelin-1 synergistically induces

vascular hyperplasia and loss of contractility in organ-cultured rat tail artery. *Atherosclerosis* 214: 288-294, 2011.

13. **Lincoln TM, Wu X, Sellak H, Dey N, and Choi CS**. Regulation of vascular smooth muscle cell phenotype by cyclic GMP and cyclic GMP-dependent protein kinase. *Front Biosci* 11: 356-367, 2006.

14. **McDonald JH, and Dunn KW**. Statistical tests for measures of colocalization in biological microscopy. *J Microsc* 252: 295-302, 2013.

15. **Owens GK, Kumar MS, and Wamhoff BR**. Molecular regulation of vascular smooth muscle cell differentiation in development and disease. *Physiol Rev* 84: 767-801, 2004.

16. **Owens GK, Loeb A, Gordon D, and Thompson MM**. Expression of smooth muscle-specific alpha-isoactin in cultured vascular smooth muscle cells: relationship between growth and cytodifferentiation. *J Cell Biol* 102: 343-352, 1986.

17. **Pearce WJ, Butler SM, Abrassart JM, and Williams JM**. Fetal cerebral oxygenation: the homeostatic role of vascular adaptations to hypoxic stress. *Adv Exp Med Biol* 701: 225-232, 2011.

18. **Pearce WJ, Hull AD, Long DM, and Longo LD**. Developmental changes in ovine cerebral artery composition and reactivity. *Am J Physiol* 261(2 Pt 2): R458-R465, 1991.

19. **Pearce WJ, Williams JM, White CR, and Lincoln TM**. Effects of chronic hypoxia on soluble guanylate cyclase activity in fetal and adult ovine cerebral arteries. *Journal of applied physiology* 107: 192-199, 2009.

20. **Pilz RB, and Casteel DE**. Regulation of gene expression by cyclic GMP. *Circ Res* 93: 1034-1046, 2003.

21. **Rensen SS, Doevendans PA, and van Eys GJ**. Regulation and characteristics of vascular smooth muscle cell phenotypic diversity. *Netherlands heart journal : monthly journal of the Netherlands Society of Cardiology and the Netherlands Heart Foundation* 15: 100-108, 2007.

22. **Sartore S, Chiavegato A, Franch R, Faggin E, and Pauletto P**. Myosin gene expression and cell phenotypes in vascular smooth muscle during development, in experimental models, and in vascular disease. *Arterioscler Thromb Vasc Biol* 17: 1210-1215, 1997.

23. **Semenza GL**. HIF-1: mediator of physiological and pathophysiological responses to hypoxia. *J Appl Physiol (1985)* 88: 1474-1480, 2000.

24. **Semenza GL**. Vasculogenesis, angiogenesis, and arteriogenesis: mechanisms of blood vessel formation and remodeling. *J Cell Biochem* 102: 840-847, 2007.

25. **Vonnahme KA, Wilson ME, Li Y, Rupnow HL, Phernetton TM, Ford SP, and Magness RR**. Circulating levels of nitric oxide and vascular endothelial growth factor throughout ovine pregnancy. *J Physiol* 565: 101-109, 2005.

26. **Williams JM, and Pearce WJ**. Age-dependent modulation of endothelium-dependent vasodilatation by chronic hypoxia in ovine cranial arteries. *J Appl Physiol* 100: 225-232, 2006.

CHAPTER FOUR

CHRONIC HYPOXIA ALTERS REACTIVITY TO VEGF IN OVINE CAROTID ARTERIES

Margaret C Hubbell, Andrew M Semotiuk, James M Williams, Olayemi O Adeoye, and William J. Pearce

Divisions of Physiology, Pharmacology, and Biochemistry
Center for Perinatal Biology
Loma Linda University School of Medicine
Loma Linda, CA 92350

Running Title: **Chronic Hypoxia alters arterial response to second insult with VEGF**

Address for Correspondence:
William J. Pearce, Ph.D.
Center for Perinatal Biology
Loma Linda University School of Medicine
Loma Linda, CA 92350
Phone: 909-558-4325
FAX: 909-558-4029
E-Mail: wpearce@som.llu.edu

Introduction

Vascular remodeling is a dynamic process to optimize delivery of oxygen and nutrients to meet the metabolic demands of the tissue. It can be directed by transient or chronic, as well as local versus systemic exposures to hypoxia that may contribute to numerous pathophysiologic processes (16, 48) including ischemia (29), hypertension (46), and atherosclerosis (37). This process not only alters the pathway and diameter of the vasculature but can also alter the inherent ability to maintain vascular tone, to recover from injury, and the response to future insults. Much of this remodeling takes place in the arterial smooth muscle cells (12, 40) with corresponding changes in contractility and vascular reactivity (24, 26, 27). These changes are thought to be coupled with conversions of smooth muscle phenotype that can be identified with characteristic changes in contractile proteins (24, 36) including smooth muscle-alpha actin (SM-AA) (31, 32) and various components of smooth muscle myosin including the myosin heavy chain (MHC) isoforms (36, 37). These have been shown to reliably and dynamically reveal corresponding changes in smooth muscle phenotype during both physiological (24), and pathophysiological (16, 40, 46) vascular remodeling.

Several factors that drive vascular remodeling as well as phenotypic transitions of smooth muscle have been identified but remain incompletely understood. These include platelet-derived growth factor (15), fibroblast growth factor (35), transforming growth factor-β (3), and vascular endothelial growth factor (20, 31). These growth factors activate several intracellular pathways with possible release of intercellular factors for paracrine communication acting primarily at the serosal surface of the blood vessel, or between the endothelium and smooth muscle. In the latter category are endothelin and

NO (5, 9) that emanate from the vascular endothelium and act more prominently at the luminal surface. VEGF has been shown to alter activity of both. Other factors are released into both the interstitium and systemically into the bloodstream, thereby coordinating distributed effects on vascular structure and function. A prominent example in this latter category is Vascular Endothelial Growth Factor (VEGF) which has been recognized as a key mediator of angiogenesis (10). VEGF has been shown to have trophic effects on numerous non-endothelial cell types including pericytes (42), CNS neurons (25), sympathetic neurons (28), skeletal muscle (4) and smooth muscle (6, 18, 30). Equally relevant, the synthesis and release of VEGF are prominantly stimulated by hypoxia via several pathways (14, 43). Together, these characteristics give VEGF the potential to broadly influence vascular remodeling and phenotypic transformation of smooth muscle, particularly in response to chronic hypoxia and hypoxic acclimatization.

The present study further explores the hypothesis that age-dependent hypoxic remodeling of artery structure and function occurs in part through VEGF with induced changes in smooth muscle phenotype that alters the response to subsequent exposure to VEGF in the future. Both the new baseline smooth muscle phenotype from hypoxic acclimatization and following secondary exposure to VEGF can be quantified by changes in contractile protein abundance and organization. Additionally, the trophic factors can act differentially from the adventitial face or from the luminal face and our development of transmural morphometry helps illustrate this. In the context of this study, artery "structure" was determined through measurements of medial layer thickness, unstressed diameter, and the transmural distribution and intracellular organization of smooth muscle contractile proteins. In turn, intracellular organization and smooth muscle phenotype

were defined by the patterns of colocalization of Non-Muscle and Smooth Muscle Myosin Heavy Chain with Smooth Muscle-Alpha Actin (36, 37).

The experimental design focused on the hypoxic acclimatization and the altered effects of VEGF in vitro on artery structure, contractile protein organization, and function using established methods for immunoblotting, confocal microscopy, and measurements of in vitro contractility (6, 8). These experiments employed a low physiological concentration of VEGF at 3 ng/ml (13, 44) to minimize non-specific activation of non-VEGF receptors (2). Experiments were performed in large conduit arteries to minimize influences attributable to the release of parenchymal metabolites. Comparisons between arteries harvested from sheep maintained at sea level, and those maintained at high altitude (3820 m) for 110 days served to define the effects of chronic hypoxia, as previously described (34) while the effects in organ culture were defined as the effects of VEGF. Vascular remodeling differs great in mature and immature arteries (7), therefore this paper includes comparisons between arteries from non-pregnant adult sheep and full term fetal lambs. Together, these approaches enabled a unique perspective of the altered response to VEGF in age-dependent hypoxic vascular remodeling and acclimatization.

Materials and Methods

All procedures used in these studies were approved by the Animal Research Committee of Loma Linda University, adhered to the policies and practices set forth by the National Institutes of Health Guide for the Care and Use of Laboratory Animals, and have been previously described in detail (6, 47).

Tissue Harvest and Preparation

Segments from common carotid arteries were collected under sterile technique for each protocol from fetal (139-142 days gestation) and young non-pregnant adult sheep (18-24 mo old) that had been maintained in normoxic (sea level) or hypoxic (3280 m) settings for the last 110 days of gestation. Tissue harvest was carried out on anesthetized pregnant ewes with 30mg/kg pentobarbital, followed by intubation, and then maintained under 1.5%-2.0% halothane. A midline vertical laparotomy enabled exteriorization of the anesthetized fetus followed by sacrifice via rapid removal of the heart and exsanguinations. Intravenous administration of 100 mg/kg pentobarbital was used to sacrifice the adult animals. Arteries were harvested and placed in sterile HEPES buffer solution (mM unless otherwise noted, 122.1 NACl, 25 HEPES, 5.15 KCl, 2.4 MgSO4, 50 μM EDTA, 11.1 dextrose, 1.6 CaCl2). Arteries then underwent gentle surgical removal of all loose adipose and extracellular connective tissue followed by rod denudation of the endothelium as previously described (47). For each animal, the denuded carotid was then cut into 2-mm (for contractility and immunohistochemistry assays) and 3 mm lengths (for immunofluorescence assays), then distributed to the various protocols in matched treatment sets.

Organ Culture

As described previously (6) , each artery segment allocated for organ culture was maintained in untreated 12-well plates with DMEM (Sigma Aldrich, St. Louis, #M56469C) supplemented with: Na2HCO3 (3.7 g/L), 0.5% amino acid solution (Sigma Aldrich, St. Louis, #M5550), 1% non-essential amino acid solution (Sigma Aldrich, St.

Louis, #M7145), 4 mM glutamine (Sigma Aldrich, St. Louis, #G7513), 2% antibiotic-antimycotic solution (Gibco, Carlsbad, #15240-096), and Gentamycin at 70 µg/ml (Gibco, Carlsbad, #15750-060). Cultures occurred in a humidified incubator with a 5% CO2¬ in room air at 37 ºC.

Matched serial arteries were cultured in supplemented DMEM without FBS for the initial 24 hours and for an additional 24 hours in media containing DMEM (Control), with 3ng/mL VEGF-A_{165} (VEGF), or with 3ng/mL VEGF-A_{165} plus the VEGF-R inhibitor Vatalanib at 240nM (VEGF+Vat). This low physiological level of VEGF was selected in accordance with VEGF levels measured in sheep (44) and to minimize binding of VEGF to non-VEGF receptor such as PDGF-B as recently shown (2). Following organ culture, arteries were then submitted for fluorescent immunohistochemistry, Western blots, or contractility studies. For all cultured treatments, matched artery segments harvested fresh and uncultured were studied in parallel.

Contractility Studies

Artery segments allocated for contractility assay were mounted on wires in vitro between a micrometer slide and an isometric force transducer used to measure artery diameters. First, for 30 min mounted segments were equilibrated in calcium-replete Na^+-Krebs buffer containing (in mM) 122 NaCl, 25.6 $NaHCO_3$, 5.17 KCl, 2.49 $MgSO_4$, 1.60 $CaCl_2$, 2.56 dextrose, 0.027 EGTA, and 0.114 ascorbic acid. At 38 ºC, normal ovine core temperature, a buffer pH of ≈7.4 was maintained with continuous bubbling of 95% O_2—5% CO_2. After initial equilibration, unstressed artery diameter (D_0) was measured in each

segment at a passive tension of 0.03 g. Based on its D_0 at strain values of D/D_0 = 1.5, 1.8, 2.1, 2.3, 2.7, 3.0, and 3.3, each artery's working diameters (D) were calculated. Contractile stresses in mN/cm^2 were measured in increasing order at each of these strain values, first under resting conditions to identify spontaneous myogenic tone, and then with contraction in a high potassium buffer including (in mM) 5.16 NaCl, 122.1 KCl, 2.15 $NaHCO_3$, 2.5 $MgSO_4$, 0.027 EDTA, 11.08 Dextrose, 0.114 Ascorbic Acid, and 1.6 ml $CaCl_2$. Once the K^+-induced contraction stabilized, the arteries were replaced in the Na^+-Krebs buffer, permitted to relax, then elongated to and equilibrated at the next highest stretch ratio. Once the max K^+-induced contraction had been achieved and identified, the arteries were then frozen in liquid nitrogen to rupture the cells. Next, the arteries were incubated in a calcium free Na^+ Krebs buffer including 3mM EGTA; this was done to further inhibit SMC derived-force via Ca^{+2} sequestration. The degree of passive stress produced for each strain ratio applied was subsequently recorded for each descending stretch ratio.

Active stress caused by high K^+ was determined to be the difference between the magnitudes of the active stress measured immediately before and after applying the high K^+ buffer. Active stress caused by spontaneous myogenic tone was determined to be the difference between the pre-treatment measure of plateaued spontaneous active tone and the post-treatment measure of passive stress after treatment with liquid N_2 and EGTA treatment for each level of strain. Arterial stiffness was determined using the relations between strain and passive stress; the coefficient of stiffness was determined by with a monotonic exponential model using curve-fitting.

Fluorescent Immunohistochemistry

Each artery segment was fixed in 4% neutral buffered EM-grade formaldehyde (Electron Microscopy Sciences, Hatfield, #15713S) overnight. Each segment was dehydrated and then embedded in paraffin, sectioned at 5 μm, and plated. Each slide was deparaffinized in Histo-Clear (National Diagnostic, Atlanta, #HS-200), rehydrated in alcohol of decreasing grades, and then microwaved in a citrate buffer (pH 6.03) to expose antigenic sites. Permeabilization and blocking was done with 1% Bovine Serum Albumin (Santa Cruz Biotechnology, Santa Cruz, #SC-2323) and 0.1% Triton X-100 (Sigma Aldrich, St. Louis, #T-8787). Primary antibodies were stained with overnight and included: Monoclonal anti- α actin smooth muscle (Sigma Aldrich, St. Louis, A5228) @ 1:200 with either polyclonal rabbit anti-human Non-Muscle Myosin Heavy Chain (NM-MHC; CoVance, Princeton, PPR-445P) at 1:500 or polyclonal rabbit anti-bovine Smooth Muscle Myosin Heavy Chain (SM-MHC; Abcam, Cambridge, ab53219) at 1:500. The following day slides were washed for two 10 minute cycles in PBS and stained using the appropriate secondary antibody with DyLight 488 Conjugated (Pierce Chemical, Rockford, #35502) for two hours at room temperature. The secondary antibody was a goat anti-rabbit-488 (Thermo Scientific, Rockford, #35552 Lot LI150311). To minimize deterioration of the fluorescent dye, slides were then after kept in the dark. Following two 10-minute cycles in PBS while covered, each tissue slide was mounted with a coverslip as well as SlowFade Gold anti-fade reagent with DAPI (Invitrogen, Carlsbad, S36939) then stored until imaged. Each image was captured using the Zeiss Imager A1. AX10 Fluorescence microscope and the Spot software (Diagnostic Instruments, Inc. Ver 4.6.4.5).

Transmural Morphometry

Transmural morphometry was performed as previously described (6). In brief, along radial lines that extended from the basal lamina to the adventitial-medial junction, six scans of separate intensity were recorded using Image Pro Plus (MediaCybernetics, Version 6.0). Mapping fluorescent intensity relative to distance from the lumen, the radial scan lines were equally distributed at regular intervals of 60-degrees around the lumen. A value of "0" was assigned to the region immediately inside the basal lamina, and a value of "100" was assigned to the region just inside the adventitial-medial junction; this scale was used to normalize distance measurements relative to medial thickness.

Calibration curves were calculated previously to compensate for the non-linear relation between fluorescent intensity and fluorophore, enabling conversion of fluorescent intensities in to relative concentrations. Using percentages of the normalized distance from the lumen, values of 5-15% were averaged and termed the "Lumen", values of 45-55% were averaged and termed "Media", and values of 85-95% were averaged and termed "Adventitial."

Confocal Microscopy

Matched artery segments were collected, prepared and cut into 5 μm sections, deparaffinized, sectioned, and immunostained as described for Transmural Morphometry, with the exception that all sections were stained with primary monoclonal mouse anti-sheep antibodies against SM-AA (Sigma-Aldrich, A5228, 1:200) and a second primary antibody against one of the MHC isoforms. Because in arterial smooth muscle the □ isoform of actin is the main isoform involved in smooth muscle contraction (32), all

colocalization of MHC was quantified relative to the abundance of □ actin. Because only alpha-actin is involved in smooth muscle contraction, changes in the other actin isoforms that can also be expressed in smooth muscle (45) should have little if any influence on smooth muscle contractility. The antibodies used to detect the MHC isoforms were as described in the Fluorescent Immunohistochemistry section. Following incubation with the primary antibodies, sections were washed in PBS, equilibrated in darkness for 2 h at room temperature with two secondary antibodies labeled with Dylight-488 to detect SM-AA and Dylight-649 to detect MHC, as indicated for Fluorescent Immunohistochemistry. Following secondary staining, sections were cover-slipped using Slowfade Gold Antifade Reagent (S36936, Invitrogen), and then examined with an Olympus FV1000 confocal microscope at an optical section thickness of 0.7 μm, a lateral resolution of 200 nm, and a numerical aperture of 18.

Antigen colocalization in confocal images was analyzed using FlouView software (version 2.1c), which provided multiple indices of co-localization including the Manders Colocalization Index 1 (actin signal in the denominator) that quantifies the portion of pixels that fluoresce for both MHC and SM-AA relative to the total number of pixels positive for SM-AA. Positive pixels were defined as having a fluorescent intensity equal to or greater than 5% of the maximum fluorescence intensity in the section. To eliminate cells with a small but significant above-threshold abundance of SM-AA characteristic of incompletely differentiated smooth muscle cells and some non-smooth muscle cell types (39), a second index of colocalization was developed. This second index, which we termed %Upper Right (%UR), was calculated to select for differentiated contractile smooth muscle as identified by high SM-AA abundance levels. This index counted only

pixels that fluoresced at or above the mean intensity threshold for SM-AA, which in essence was equivalent to recalculating the Colocalization Index 1 with an SM-AA threshold of 50% of maximum intensity. This method of analysis was derived from a flow-cytometry quadrant analysis, and thus was referred to as the percentage in the upper right quadrant of the scatterplot of SM-AA intensities against MHC intensities. From a general perspective, Colocalization Index 1 and %UR were both proportional to the fraction of actin-positive pixels that were also positive for MHC. Interestingly, the results obtained for both Colocalization Index 1 and %UR varied somewhat in absolute values, but were qualitatively similar.

Westerns

Each artery segment was homogenized via glass on glass in 8 M Urea, 500 mM NaCl, 20 mM Tris, 23 mM Glycine, 10 mM EGTA, and 10% Glycerol at pH 8.6, and also with the addition of a protease inhibitor cocktail at 5 µl per ml of buffer (Sigma-Aldrich, Saint Louis, #M1745). Centrifugation for 20 minutes of the homogenate at 5,000 G allowed for the supernatant to be collected, that was then separated by SDS-PAGE alongside a pooled reference. The pooled reference was harvested from adult ovine common carotid arteries and was used to calibrate sample abundances. Separated proteins were then transferred to nitrocellulose in Towbin's buffer at 350mA for 90 minutes (25 mM Tris, 192 mM Glycine, 10 and 20% Methanol) and blocked for 1 hour at room temperature with 5% milk in Tris-buffered saline at pH 7.5 (M-TBS) and using continuous shaking. Each subsequent wash and incubation was done in M-TBS with 0.1% Tween-20. Incubation was done with the same primary antibodies as

immunohistochemistry, for 3 hours with anti-SM-AA 1:3000, anti-NM-MHC 1:1000 and anti-SM-MHC 1:20,000 for 3 hours. To achieve visualization, membranes were then incubated with a secondary antibody conjugated to DyLight 800 for 90 minutes (Pierce Chemical, Rockford, #46422) and imaged using LI-COR Bioscience's Odyssey system.

Data Analysis and Statistics

Contractile stress was calculated as a ratio of force per cross-sectional area, where force was contractile tension (grams x acceleration due to gravity) and cross-sectional area (wall thickness x segment length) had been adjusted for changes with stretch as detailed previously (23, 33). For immunofluorescence, intensity values within each segment were normalized to yield an area below the intensity-distance curve of unity, and calibrated against marker abundances measured with Westerns. For each marker, Western measurements were calibrated against a standard curve that was pooled from adult common carotids. For confocal, the median intensity for smooth-muscle α-actin was determined on a log scale, with pixels above the median denoted as "α-actin positive." The percentage of SM-α Actin positive pixels co-localized with SM-MHC, or NM-MHC respectively was determined using confocal software and shown in figures below. All statistical comparisons were done using Behrin's Fischer at the $P>0.05$ level with each animal contributing equally to each treatment group.

Results

Fetal and adult sheep from either normoxic or hypoxic settings were included in this study (Fetal- 7 normoxic and 7 hypoxic; Adult- 11 normoxic and 8 hypoxic). From each animal, endothelium denuded carotid arteries were harvested and adjacent artery

segments allocated to each treatment as a paired set totaling 436 artery segments (Fetal- 112 normoxic and 96 hypoxic; Adult- 120 normoxic and 108 hypoxic). The term "n" denotes number of animals used in each experiment, not the number of segments. Statistical significance was defined at $P < 0.05$ for all assays unless noted otherwise, with all values in the form of means ± SEM.

Chronic Hypoxia Neutralizes or Reverses the Effect of VEGF on Artery Function (Figure 1)

All changes are difference with VEGF organ culture in % Ctrl. The second insult with VEGF further accentuated the increase in potassium induced contraction seen with hypoxia in adult (N -45.2±3.0 vs H +35.9±6.1) and showed desensitization to VEGF in fetal (N -15.6±4.3 vs H +8.9±10.0) arteries. As seen previously with myogenic tone, a distinct optimum stretch ratio occurred in fetal arteries at D/D_0 2.1 while a broader range is seen in the adult between D/D_0 2.1 and 2.7. This suggests age-dependent organization of contractile elements including extracellular organization of ECM, SMC size, and SMC heterogeneity as well as intracellular organization of desmosomes, SM-MHC and SM-SM-αA. Hypoxia followed by organ culture with VEGF also lessened the loss of stretch-induced contraction in the adult (N -50.6 ± 2.8% vs H -36.9± 5.1%). Hypoxia + VEGF showed a small but significant increase in medial thickness in the fetus (N 2.0 ± 1.57% vs H 8.4± 4.4%) and a decrease in the adult (N 6.9 ± 1.1% vs H -5.0± 1%). The reverse in medial thinning in the adult coupled with increased contractile force suggests a possible shift toward a more efficient contractile SMC.

Chronic Hypoxia alters VEGF Action on Myosin Heavy Chain Expression and Distribution Across the Artery (Figure 2)

Interestingly, similar trends of MHC distribution between medial layers were maintained under hypoxia and with/without VEGF, except for SM-MHC in the fetus. However hypoxia+VEGF shifted MHC expression towards the extreme marker ends in the fetus with NM-MHC (N 24.3 ± 0.2% vs H 97.9± 1.2%, Lumen) and SM-MHC (N -29.4± 0.1%, medial vs H 81.2± 1.0%, luminal). In contract, adult arteries showed hypoxia followed VEGF showed sensitized the down regulation of SM-MHC (N -6.9 ± 0.1% vs H -21.0± 0.3%, luminal), with NM-MHC losing reactivity to VEGF (N 39.3± 0.4% vs H 17.8± 0.3%).

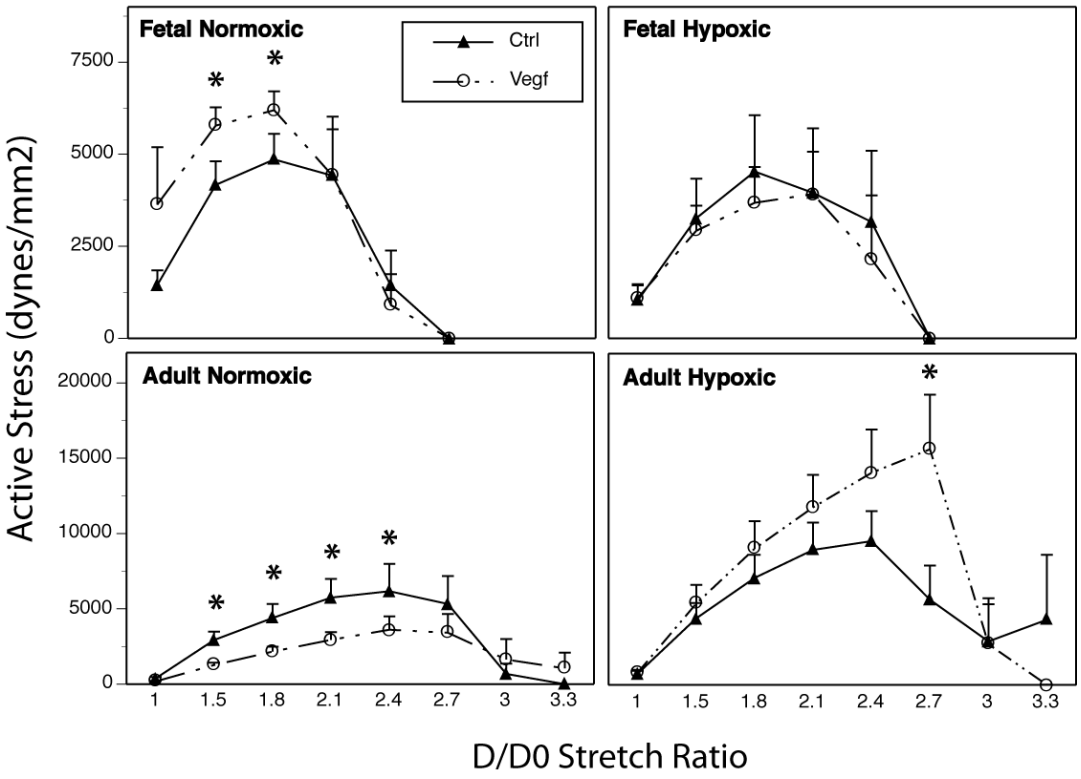

Figure 1. Chronic Hypoxia neutralizes or reverses the effect of VEGF on Artery Function.

Endothelium-denuded common carotid arteries from fetal and adult sheep maintained at normoxic settings (N, sea level) or hypoxic settings (H, 3280 m for 110days) were placed in 48hrs Organ Culture (OC) with or without 3ng/mL VEGF. Both stretch induced (myogenic) and potassium-induced (active) contraction were determined at increasing multiples of the unstressed diameter (D_0). Organ culture with VEGF enhanced K+-induced contractions in the fetal and depressed it in adult arteries. Hypoxia ablated this response in the fetus and reversed the effect in the adult arteries. Error bars indicate SEM for arteries from a total of 31 animals: 7 Normoxic Fetal, 5 Hypoxic Fetal, 11 Normoxic Adult, and 8 Hypoxic Adult. All differences denoated * are at $P < 0.05$.

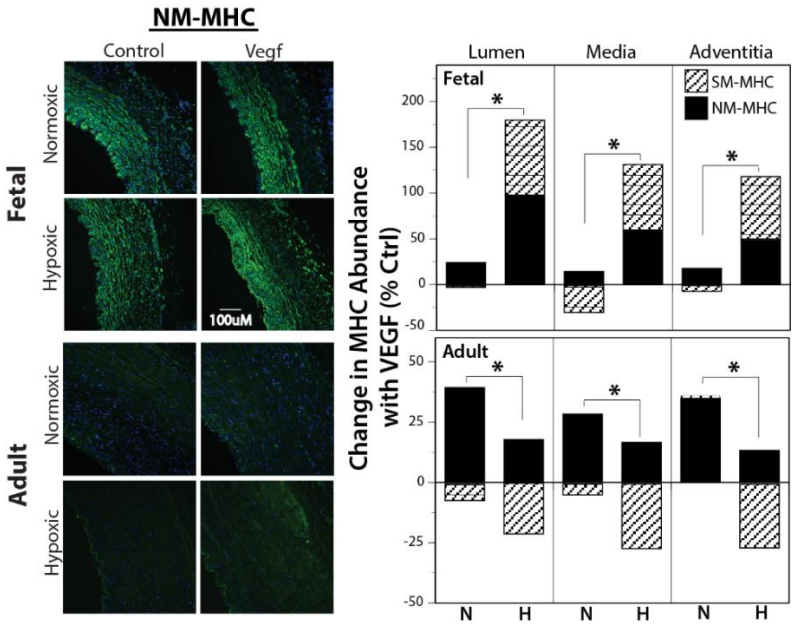

Figure 2. Chronic Hypoxia alters VEGF action on Myosin Heavy Chain Expression and Distribution across the artery.

Coronal sections of endothelium denuded carotid arteries from fetal and adult sheep (hypoxic and normoxic) were treated in 48hrs OC with or without 3ng/mL VEGF and immunostained for SM-MHC or NM-MHC (green signal). Cell nuclei were stained with DAPI (blue signal). Shown here are representative matched sections from a single animal for each experimental group. Artery layers of smooth muscle were defined as Lumen (area just inside basal elastic elamina), Media (area midway between basal elastic lamina and adventitial-medial border), Adventitia (area immediately adjacent to the adventitial-media border). Analysis described in detail previously. Each * denotes a difference at the $P < 0.05$ level using the Behren's Fischer test. Error bars indicate the combined SEM from both techniques: Immunofluorescence (6 normoxic fetal, 6 hypoxic fetal, 6 normoxic adult and 5 hypoxic adult). Immunohistochemistry included n=7 for each of the four groups.

Chronic Hypoxia alters VEGF Action on Myosin Heavy Chain Expression and SM-AA Colocalization (Figure 3 and 4)

All changes are difference with VEGF organ culture in % Ctrl. The second insult with VEGF diminished colocalization of NM-MHC in fetal normoxic but not hypoxic arteries. Similarly VEGF also decreased colocalization of mature contractile SM-MHC in fetal hypoxic but not normoxic arteries. In adults, colocalization of all MHC with SM-AA decreased with VEGF in normoxic arteries and this same response was amplified in hypoxic arteries.

Chronic Hypoxia Alters Receptor that VEGF Acts on to Alter K^+- Induced Contractile Function (Figure 5)

Vatalanib is a selective inhibitor for both primary VEGF receptors KDR and Flt-1. Vatlanib inhibition of VEGF in OC had no effect in fetal arteries suggesting that VEGF may be acting through a non-VEGF receptor that is upregulated in the fetus. Inhibition of VEGF in adult arteries during OC was able to neutralize the decrease of potassium induced contraction and prevented the VEGF contractile enhancement. Vatalanib did not alter the optimum stretch ratio occurred in fetal arteries or in adult arteries.

Chronic Hypoxia Alters Receptor that VEGF Acts on to Alter Stretch-Induced Contractile Function (Figure 6)

Vatalanib was unable to inhibit contractile effects of OC with VEGF in fetal arteries. However in adult arteries, Vatalanib did successfully inhibit part of the effect of VEGF and this effect was not significantly altered by hypoxia.

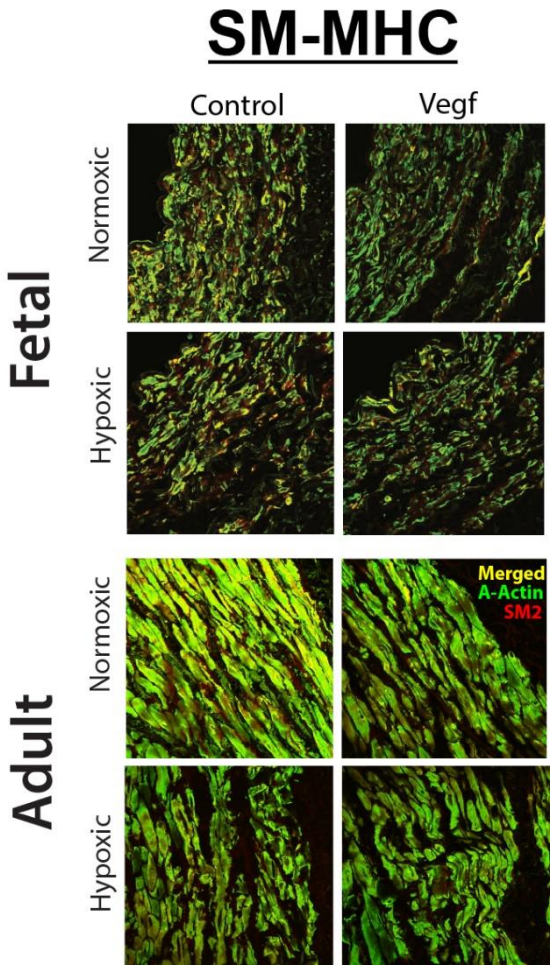

Figure 3. Chronic Hypoxia Alters VEGF Action on Myosin Heavy Chain Expression and SM-AA Colocalization.
Coronal sections of endothelium denuded carotid arteries from fetal and adult sheep (hypoxic and normoxic) were treated in 48hrs OC with or without 3ng/mL VEGF, fixed in 4% paraformaldehyde, paraffin embedded, sectioned at 5 μm, and immunostained for SM-MHC (red signal) and SM-AA (green signal). Co-localization of the two are displayed below in merged images (yellow signal) and are representative matched sections from a single animal for each experimental group.

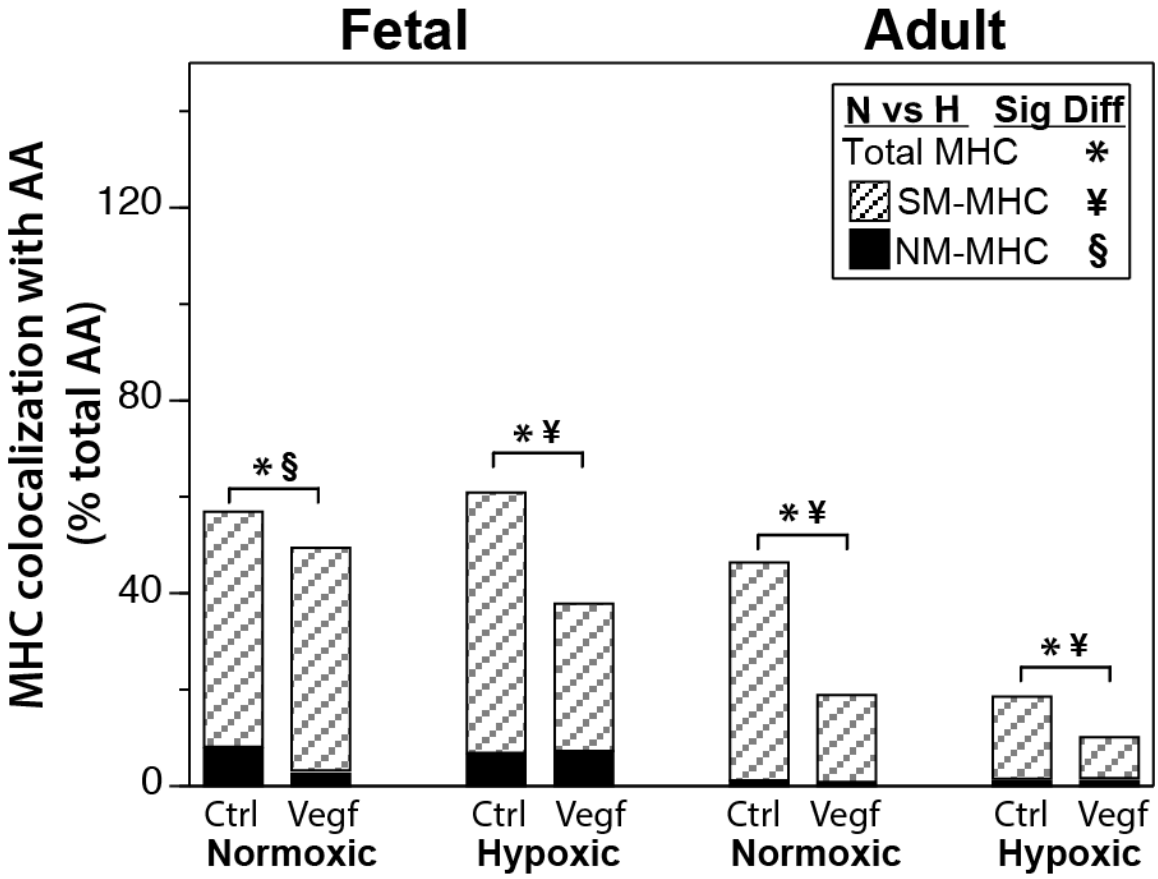

Figure 4. Chronic Hypoxia Alters VEGF-Induced SMC Phenotype.
Coronal sections of endothelium denuded carotid arteries from 6 normoxic and 6 hypoxic fetal lambs and 6 normoxic and 6 hypoxic adult sheep were treated 48hrs in OC with or without 3ng/mL VEGF, then fixed and stained for immunostained for SM-MHC or NM-MHC (red signal) and SM-AA (green signal) colocalization. Hypoxia+VEGF reverse effect of hypoxia or VEGF individually. Overall contractile MHC decreased (decreasing NM-MHC in normoxic and SM-MHC in hypoxic arteries) in fetal arteries. All denoted differences are at the $P < 0.05$ level.

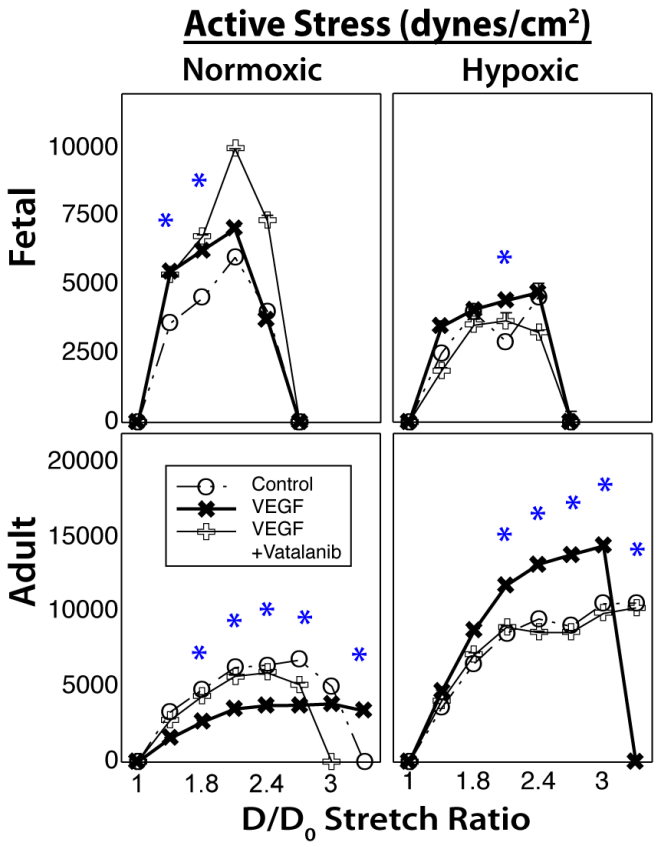

Figure 5. Hypoxia Alters the Receptor that VEGF Alters K^+-Induced Stress.
Endothelium-denuded common carotid arteries from fetal and adult sheep maintained at normoxic settings (N, sea level) or hypoxic settings (H, 3280 m for 110days) were placed in 48hrs Organ Culture (OC) with 0ng/mL VEGF (Control), 3ng/mL VEGF (VEGF), or 3ng/mL VEGF + 240nM Vatalanib (VEGF+Vatalanib) then underwent contractility assay. Potassium-induced (active) contraction was determined at increasing multiples of the unstressed diameter (D_0). Hypoxia diminished the effect of VEGF in the fetus and reversed the effect of VEGF in the adult. Error bars indicate SEM for arteries from a total of 31 animals: 7 Normoxic Fetal, 5 Hypoxic Fetal, 11 Normoxic Adult, and 8 Hypoxic Adult. All differences denoated * are at $P < 0.05$.

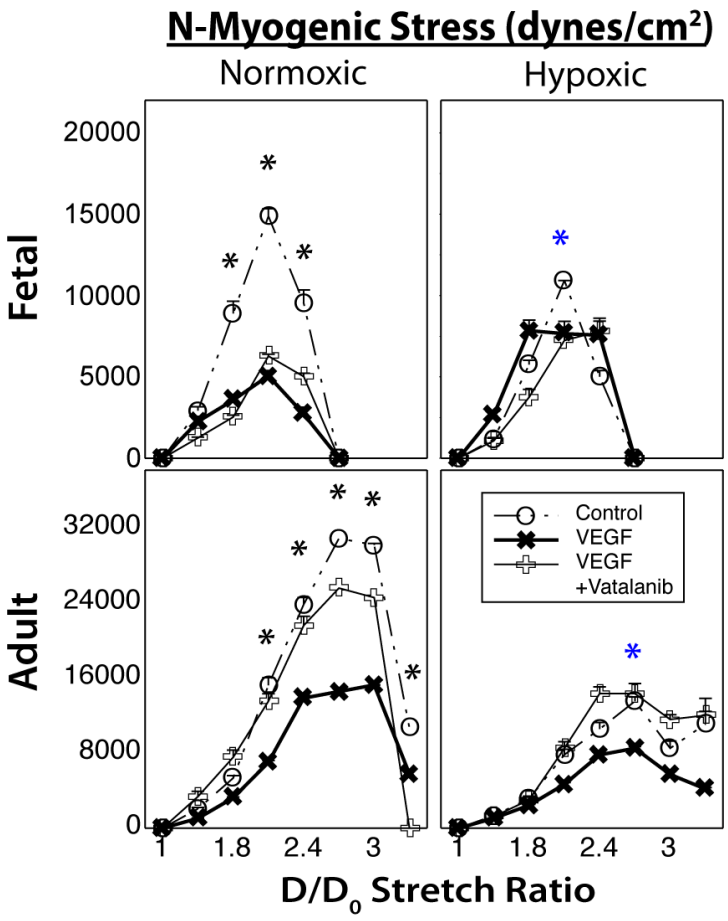

Figure 6. Hypoxia Alters the Receptor that VEGF Alters Stretch-Induced Stress. Endothelium-denuded common carotid arteries from fetal and adult sheep maintained at normoxic settings (N, sea level) or hypoxic settings (H, 3280 m for 110days) were placed in 48hrs Organ Culture (OC) with 0ng/mL VEGF (Control), 3ng/mL VEGF (VEGF), or 3ng/mL VEGF + 240nM Vatalanib (VEGF+Vatalanib) then underwent contractility assay. Stretch induced (myogenic) contraction was determined at increasing multiples of the unstressed diameter (D_0). Error bars indicate SEM for arteries from a total of 31 animals: 7 Normoxic Fetal, 5 Hypoxic Fetal, 11 Normoxic Adult, and 8 Hypoxic Adult. All differences denoated * are at $P < 0.05$.

Discussion

The present study offers five original observations in endothelium-denuded carotid arteries. First, Hypoxic acclimatization ablated the age-dependent contractile response to VEGF in fetal and while reversing the effect in adult arteries shown previously (22). Second, hypoxic acclimatization alters the response to a second exposure to VEGF in organ culture with increased abundance of both NM-MC and SM-MHC throughout the medial wall in the fetus while VEGF decreases NM-MHC and increases SM-MHC abundance through the medial wall in the adult. Third, hypoxic acclimatization alters re-organization of myosin heavy chains and actin by VEGF, decreasing total MHC and SM-MHC coloclization with SM-AA in fetal and adult arteries. Fourth, selective inhibition of both VEGF receptor 1 (Flt-1) and VEGF receptor 2 (KDR) with Vatalanib ablated the contractile effect of VEGF in organ culture in adult but not fetal arteries. Fifth, both VEGF receptors were significantly more abundant in adult arteries relative to protein standard, with similar levels of VEGFR1 in both age groups and nearly 3 fold greater for VEGFR2 in the adult compared with fetus. Together, these observations support the hypothesis that hypoxic acclimatization alters the vascular response to VEGF and downstream changes in artery structure and function through changes in contractile protein abundance and organization secondary to changes in smooth muscle phenotype.

Hypoxic Acclimatization Altered Artery Structure and Function

Hypoxic acclimatization alters artery wall thicknesses in different ways depending on artery type, size, and age (27, 41, 48) and can act differently on any or all layers of the artery wall including the endothelial, medial and adventitial layers (40, 47).

To more fully understand hypoxic changes to artery structure and the functional implications, the present study focused on the medial layer that contains the smooth muscle cells responsible for contractile force. Although hypoxic acclimatization did not alter baseline medial thickness in either adult or fetal ovine carotid arteries, organ culture with VEGF increased medial thickness in hypoxic fetal arteries while decreasing medial thickness in hypoxic adult arteries. Coupled with the increased contractile force seen in the adult, this suggests a possible shift toward a more contractile SMC associated with either an increase in contractile protein abundance or organization within the vascular smooth muscle.

As described previously (22), most vascular studies measure the contractile response as a percentage response to a standardized contractant such as high potassium or in units of gram for a single segment length. This method is internaly normalized but does not consider changes in wall thickness, stiffness, content of contractile protein, or optimum stretch length, all of which can significantly affect comparisons across various chronic treatment groups. Therefore the experimental approach applied in this study applied a complete stress-strain length-tension protocol where the contractile response was quantified as changes in active stresses in units of force per medial cross-sectional area for multiple degrees of arterial strain, as described previously (6). As seen in earlier studies, these measurements revealed (**Figure 1**) that K+-induced contractions were greater in adult than fetal arteries (6), were not altered much by hypoxia but were inversely responsive to VEGF in adult and lost response to VEGF in fetal arteries (27).

Hypoxic Acclimatization Altered VEGF-Induced Change in MHC Abundance and Organization

We explored the hypothesis that hypoxic acclimatization that changes artery structure and contractility may be due to changes in smooth muscle phenotype, and that hypoxia may alter regulation of these changes when exposed to a second insult. To quantify this change in response, experiments were done to assess changes in MHC isoform abundance that is considered to be synonymous with contractile capacity and smooth muscle phenotype (16, 17, 36). The artery wall contains a heterogenous distribution of SMC phenotype and morphology (12, 41) which led us to incorporate the relative abundance determined via immunoblots across the artery wall using radial line scans of fluorescent intensity in coronal section that had been immunostained for the desired protein, as described previously (6).

This method revealed that embryonic isoforms of MHC (NM-MHC) that are generally prevalent in functionally immature and proliferative smooth muscle cells (11, 31, 36) were indeed more abundant in fetal than adult arteries and increased with hypoxia for both age groups (data not shown). VEGF following hypoxic acclimatization significantly changes in all 3 layers in a gradient like fashion with the greatest change in the lumen greater than the medial greater than the adventitial portion of the media. While hypoxia did not alter this distribution pattern, it did heighten the response to VEGF in the fetal artery with increased abundance of both the immature NM-MHC and the mature contractile SM-MHC. In adult arteries, Vegf increased NM-MHC while decreasing SM-MHC, with both of these effects amplified by hypoxic acclimatization (**Figure 2)**. Together, these results suggest that hypoxic acclimatization alters the receptor or

intracellular coupling of VEGF with MHC isoforms expression and the gradient effect suggests that the point of vasotrophic stimulus may be laminar in location. The lamellar heterogeneity may simply be a non-functional consequence but it may also be suggestive of the importance of organized heterogeneity of SMC phenotypes within the arterial wall to maintain vascular homeostasis with dynamic interaction between contractile and secretory functions.

Hypoxic Acclimatization Altered VEGF Receptor Mediating the Contractile Response

In the adult, the selective VEGF receptor inhibitor Vatalanib did successfully inhibit the contractile effects of organ culture with VEGF for both K^+-induced and stretch-induced stress. This was not altered by hypoxia. In fetal arteries, normalized stretch-induced stress diminished with VEGF and hypoxia ablated both the effect of VEGF and therefore the effect of VEGF inhibition. This disconnect between the effects of hypoxia on K+-induced and stretch-dependent (myogenic) contractions suggests that hypoxic acclimatization can affect certain components of the contractile apparatus differentially and may preferentially affect mechanisms that couple stretch to contraction. Possible mechanisms involved in this selective effect of hypoxia include calcium channels involved in mechanotransduction (19) and contractile proteins involved in myogenic determination of myofilament calcium sensitivity (8, 38). Interestingly, many of these mechanisms are strongly influenced by phenotypic transformation of smooth muscle (8, 21, 45). As recently shown by our lab, VEGF receptor prevalence of type and

abundance differs throughout development with greater expression in the adult (1) and upregulated with chronic hypoxia.

Overview

Together, the results of the present study demonstrate that hypoxic acclimatization alters the response to VEGF and downstream changes in contractility, MHC isoform abundance and MHC-SM-AA organization that all implicate a change in SMC phenotype.

Acknowledgments

The authors appreciate the excellent microscopy performed for this study by Jenna M Abrassart, MPH. The work reported in this manuscript was supported by USPHS grants P01-HD31226, R01-HL54120, R01-HL64867, R01-NS076945 and the Loma Linda University School of Medicine.

References

1. **Adeoye OO, Bouthors V, Hubbell MC, Williams JM, and Pearce WJ**. VEGF receptors mediate hypoxic remodeling of adult ovine carotid arteries. *J Appl Physiol (1985)* 117: 777-787, 2014.

2. **Ball SG, Shuttleworth CA, and Kielty CM**. Vascular endothelial growth factor can signal through platelet-derived growth factor receptors. *J Cell Biol* 177: 489-500, 2007.

3. **Bobik A**. Transforming growth factor-betas and vascular disorders. *Arterioscler Thromb Vasc Biol* 26: 1712-1720, 2006.

4. **Bryan BA, Walshe TE, Mitchell DC, Havumaki JS, Saint-Geniez M, Maharaj AS, Maldonado AE, and D'Amore PA**. Coordinated vascular endothelial growth factor expression and signaling during skeletal myogenic differentiation. *Mol Biol Cell* 19: 994-1006, 2008.

5. **Bundy RE, Marczin N, Birks EF, Chester AH, and Yacoub MH**. Transplant atherosclerosis: role of phenotypic modulation of vascular smooth muscle by nitric oxide. *Gen Pharmacol* 34: 73-84, 2000.

6. **Butler SM, Abrassart JM, Hubbell MC, Adeoye O, Semotiuk A, Williams JM, Mata-Greenwood E, Khorram O, and Pearce WJ**. Contributions of VEGF to age-dependent transmural gradients in contractile protein expression in ovine carotid arteries. *Am J Physiol Cell Physiol* 301: C653-666, 2011.

7. **Carmeliet P, Ferreira V, Breier G, Pollefeyt S, Kieckens L, Gertsenstein M, Fahrig M, Vandenhoeck A, Harpal K, Eberhardt C, Declercq C, Pawling J, Moons L, Collen D, Risau W, and Nagy A**. Abnormal blood vessel development and lethality in embryos lacking a single VEGF allele. *Nature* 380: 435-439, 1996.

8. **Charles SM, Zhang L, Cipolla MJ, Buchholz JN, and Pearce WJ**. Roles of cytosolic Ca2+ concentration and myofilament Ca2+ sensitization in age-dependent cerebrovascular myogenic tone. *Am J Physiol Heart Circ Physiol* 299: H1034-1044, 2010.

9. **Dao HH, Bouvet C, Moreau S, Beaucage P, Lariviere R, Servant MJ, de Champlain J, and Moreau P**. Endothelin is a dose-dependent trophic factor and a mitogen in small arteries in vivo. *Cardiovasc Res* 71: 61-68, 2006.

10. **Dvorak HF, Brown LF, Detmar M, and Dvorak AM**. Vascular permeability factor/vascular endothelial growth factor, microvascular hyperpermeability, and angiogenesis. *Am J Pathol* 146: 1029-1039, 1995.

11. **Eddinger TJ, and Meer DP**. Myosin II isoforms in smooth muscle: heterogeneity and function. *Am J Physiol Cell Physiol* 293: C493-508, 2007.

12. **Elliott CF, and Pearce WJ**. Effects of maturation on cell water, protein, and DNA content in ovine cerebral arteries. *J Appl Physiol (1985)* 79: 831-837, 1995.

13. **Fischer S, Clauss M, Wiesnet M, Renz D, Schaper W, and Karliczek GF**. Hypoxia induces permeability in brain microvessel endothelial cells via VEGF and NO. *Am J Physiol* 276: C812-820, 1999.

14. **Fong GH**. Regulation of angiogenesis by oxygen sensing mechanisms. *J Mol Med* 87: 549-560, 2009.

15. **Fredriksson L, Li H, and Eriksson U**. The PDGF family: four gene products form five dimeric isoforms. *Cytokine Growth Factor Rev* 15: 197-204, 2004.

16. **Frid MG, Dempsey EC, Durmowicz AG, and Stenmark KR**. Smooth muscle cell heterogeneity in pulmonary and systemic vessels. Importance in vascular disease. *Arterioscler Thromb Vasc Biol* 17: 1203-1209, 1997.

17. **Frid MG, Moiseeva EP, and Stenmark KR**. Multiple phenotypically distinct smooth muscle cell populations exist in the adult and developing bovine pulmonary arterial media in vivo. *Circ Res* 75: 669-681, 1994.

18. **Grosskreutz CL, Anand-Apte B, Duplaa C, Quinn TP, Terman BI, Zetter B, and D'Amore PA**. Vascular endothelial growth factor-induced migration of vascular smooth muscle cells in vitro. *Microvasc Res* 58: 128-136, 1999.

19. **Hill MA, Zou H, Potocnik SJ, Meininger GA, and Davis MJ**. Invited review: arteriolar smooth muscle mechanotransduction: Ca(2+) signaling pathways underlying myogenic reactivity. *J Appl Physiol* 91: 973-983, 2001 Aug.

20. **Hoeben A, Landuyt B, Highley MS, Wildiers H, Van Oosterom AT, and De Bruijn EA**. Vascular endothelial growth factor and angiogenesis. *Pharmacol Rev* 56: 549-580, 2004.

21. **House SJ, Potier M, Bisaillon J, Singer HA, and Trebak M**. The non-excitable smooth muscle: calcium signaling and phenotypic switching during vascular disease. *Pflugers Arch* 456: 769-785, 2008.

22. **Hubbell MC, Semotiuk AJ, Thorpe RB, Adeoye OO, Butler SM, Williams JM, Khorram O, and Pearce WJ**. Chronic hypoxia and VEGF differentially modulate abundance and organization of myosin heavy chain isoforms in fetal and adult ovine arteries. *Am J Physiol Cell Physiol* 303: C1090-1103, 2012.

23. **Hull AD, Long DM, Longo LD, and Pearce WJ**. Pregnancy-induced changes in ovine cerebral arteries. *Am J Physiol* 262: R137-143, 1992.

24. **Hutanu C, Cox BE, DeSpain K, Liu XT, and Rosenfeld CR**. Vascular development in early ovine gestation: carotid smooth muscle function, phenotype, and biochemical markers. *Am J Physiol Regul Integr Comp Physiol* 293: R323-333, 2007.

25. **Jin KL, Mao XO, and Greenberg DA**. Vascular endothelial growth factor: direct neuroprotective effect in in vitro ischemia. *Proc Natl Acad Sci U S A* 97: 10242-10247, 2000.

26. **Johnson BD, Wilson LE, Zhan WZ, Watchko JF, Daood MJ, and Sieck GC**. Contractile properties of the developing diaphragm correlate with myosin heavy chain phenotype. *J Appl Physiol (1985)* 77: 481-487, 1994.

27. **Longo LD, Hull AD, Long DM, and Pearce WJ**. Cerebrovascular adaptations to high-altitude hypoxemia in fetal and adult sheep. *Am J Physiol* 264: R65-72, 1993.

28. **Marko SB, and Damon DH**. VEGF promotes vascular sympathetic innervation. *Am J Physiol Heart Circ Physiol* 294: H2646-2652, 2008.

29. **Ohkuma H, Suzuki S, and Ogane K**. Phenotypic modulation of smooth muscle cells and vascular remodeling in intraparenchymal small cerebral arteries after canine experimental subarachnoid hemorrhage. *Neurosci Lett* 344: 193-196, 2003.

30. **Osada-Oka M, Ikeda T, Imaoka S, Akiba S, and Sato T**. VEGF-enhanced proliferation under hypoxia by an autocrine mechanism in human vascular smooth muscle cells. *J Atheroscler Thromb* 15: 26-33, 2008.

31. **Owens GK, Kumar MS, and Wamhoff BR**. Molecular regulation of vascular smooth muscle cell differentiation in development and disease. *Physiol Rev* 84: 767-801, 2004.

32. **Owens GK, Loeb A, Gordon D, and Thompson MM**. Expression of smooth muscle-specific alpha-isoactin in cultured vascular smooth muscle cells: relationship between growth and cytodifferentiation. *J Cell Biol* 102: 343-352, 1986.

33. **Pearce WJ, Hull AD, Long DM, and Longo LD**. Developmental changes in ovine cerebral artery composition and reactivity. *Am J Physiol* 261(2 Pt 2): R458-R465, 1991.

34. **Pearce WJ, Williams JM, White CR, and Lincoln TM**. Effects of chronic hypoxia on soluble guanylate cyclase activity in fetal and adult ovine cerebral arteries. *Journal of applied physiology* 107: 192-199, 2009.

35. **Presta M, Dell'Era P, Mitola S, Moroni E, Ronca R, and Rusnati M**. Fibroblast growth factor/fibroblast growth factor receptor system in angiogenesis. *Cytokine Growth Factor Rev* 16: 159-178, 2005.

36. **Rensen SS, Doevendans PA, and van Eys GJ**. Regulation and characteristics of vascular smooth muscle cell phenotypic diversity. *Netherlands heart journal : monthly journal of the Netherlands Society of Cardiology and the Netherlands Heart Foundation* 15: 100-108, 2007.

37. **Sartore S, Chiavegato A, Franch R, Faggin E, and Pauletto P**. Myosin gene expression and cell phenotypes in vascular smooth muscle during development, in

experimental models, and in vascular disease. *Arterioscler Thromb Vasc Biol* 17: 1210-1215, 1997.

38. **Schubert R, Lidington D, and Bolz SS**. The emerging role of Ca2+ sensitivity regulation in promoting myogenic vasoconstriction. *Cardiovasc Res* 77: 8-18, 2008.

39. **Skalli O, Pelte MF, Peclet MC, Gabbiani G, Gugliotta P, Bussolati G, Ravazzola M, and Orci L**. Alpha-smooth muscle actin, a differentiation marker of smooth muscle cells, is present in microfilamentous bundles of pericytes. *J Histochem Cytochem* 37: 315-321, 1989.

40. **Stenmark KR, Fagan KA, and Frid MG**. Hypoxia-induced pulmonary vascular remodeling: cellular and molecular mechanisms. *Circ Res* 99: 675-691, 2006.

41. **Stiebellehner L, Frid MG, Reeves JT, Low RB, Gnanasekharan M, and Stenmark KR**. Bovine distal pulmonary arterial media is composed of a uniform population of well-differentiated smooth muscle cells with low proliferative capabilities. *Am J Physiol Lung Cell Mol Physiol* 285: L819-828, 2003.

42. **Takagi H, King GL, and Aiello LP**. Identification and characterization of vascular endothelial growth factor receptor (Flt) in bovine retinal pericytes. *Diabetes* 45: 1016-1023, 1996.

43. **Tipoe GL, and Fung ML**. Expression of HIF-1alpha, VEGF and VEGF receptors in the carotid body of chronically hypoxic rat. *Respir Physiol Neurobiol* 138: 143-154, 2003.

44. **Vonnahme KA, Wilson ME, Li Y, Rupnow HL, Phernetton TM, Ford SP, and Magness RR**. Circulating levels of nitric oxide and vascular endothelial growth factor throughout ovine pregnancy. *J Physiol* 565: 101-109, 2005.

45. **Wamhoff BR, Bowles DK, and Owens GK**. Excitation-transcription coupling in arterial smooth muscle. *Circ Res* 98: 868-878, 2006.

46. **Williams B**. Mechanical influences on vascular smooth muscle cell function. *J Hypertens* 16: 1921-1929, 1998.

47. **Williams JM, and Pearce WJ**. Age-dependent modulation of endothelium-dependent vasodilatation by chronic hypoxia in ovine cranial arteries. *J Appl Physiol* 100: 225-232, 2006.

48. **Wohrley JD, Frid MG, Moiseeva EP, Orton EC, Belknap JK, and Stenmark KR**. Hypoxia selectively induces proliferation in a specific subpopulation of smooth muscle cells in the bovine neonatal pulmonary arterial media. *J Clin Invest* 96: 273-281, 1995.

CHAPTER FIVE

SUMMARY AND FUTURE DIRECTIONS

Summary

The purpose of this dissertation was to define how hypoxic vascular remodeling alters artery structure and function, and how changes in smooth muscle phenotype contribute to these changes. In chapter 2, we determined that hypoxic vascular remodeling does alter vascular contractility, that it is associated with a re-organization of contractile proteins that may represent a change in SMC phenotype, and that VEGF is likely to contribute to this process. Transmural quantification of contractile proteins was also able to distinguish a gradient pattern of distribution suggesting possible sources of vasotrophic factors that may have contributed to the hypoxic vascular remodeling. Similarly, the organization of the contractile proteins was found to correlate much more strongly with contractile behavior in contrast to the previously used protein abundance suggesting that SMC phenotype may be better identified with colocalization of established proteins.

In chapter 3, our goal was to identify the endothelial component of hypoxia and VEGF on transitions between SMC phenotype populations in the artery wall and determine if NO mediated this process at all. To this end, we assessed the effect of VEGF in organ culture of normoxia and hypoxia acclimatized arteries, with and without the endothelium, for changes in contractile function and SMC phenotype. We applied a novel characterization method to help identify where on the spectrum of mature contractile to immature synthetic phenotypes the SMC were present and how this changed with hypoxia and VEGF. We inhibited eNOS with LNAME to determine if VEGF might be

acting through NO and found that both an NO-dependent and NO-independent contribution from the endothelium.

Chapter 4 hoped to expand upon chapter 2 and 3 with consideration to how hypoxic acclimatization may program the tissue to respond differently to additional hypoxic insults. Similar methods as chapter 2 were utilized with endothelium-denuded carotid arteries from normoxic and hypoxic sheep cultured with and without VEGF to assess possible structural, contractile and phenotypic responses. As described, the response was age dependent, dramatically changed in the adult but with minimal to no response in the fetus. This contributes possible mechanism to the current thought that chronic hypoxia in utero has significant pathophysiological effects that the fetus carries on after birth.

In this chapter, we briefly describe other contributing factors to this interplay of the smooth muscle, endothelium, and vasotrophic factors during hypoxic vascular remodeling. Endothelin is a prominent vasoconstrictor with acute exposure but has also been shown to induce a significant phenotypic shift toward the synthetic SMC. Below we stimulated endothelin with VEGF in the presence and absence of the endothelium as well as selectively inhibited receptors to identify which intracellular pathway led to the described phenotypic shifts. We also display colocalization findings using additional established and novel methods (Fluoview, Upper Right %, Colocalization index #2). We also report the negative finding of PKG activation that was investigated using denuded middle cerebral arteries, suggesting that downstream of endothelial NO activity, other kinases may also be at work.

Future Directions

At the conclusion of this work, we are left with several important questions that may act as a spring board for future studies. We have now established that hypoxia alters SMC phenotype within the artery wall and that this is associated with functional changes in contractility and structured. We've also noted that this new phenotype appears to predispose the vessel to a different response to normal physiological stimulus. This would easily lend itself to testing with the several known factors in vascular remodeling and angiogenesis, including PDGF, FGF, TGF-b and some of the inflammatory factors active in atherosclerosis. An additional step forward would be an organ culture model that would allow control *in vitro* treatment with hydrostatic intra-luminal pressure and sheer force to more fully model the physiologic environment. An additional next step is in progress to partner these phenotypic changes with miRNA and transcription factor assays to identify additional regulators. This could also be assessed in the setting of a whole tissue environment following a controlled wound, with perturbation of various angiogenic factors including VEGF. With regard to vascular remodeling secondary to hypoxia and maturity, there are many areas of future research. This dissertation added several tools to quantify, describe, and categorize smooth muscle phenotype, as well as a greater understanding of its role in hypoxic vascular remodeling.

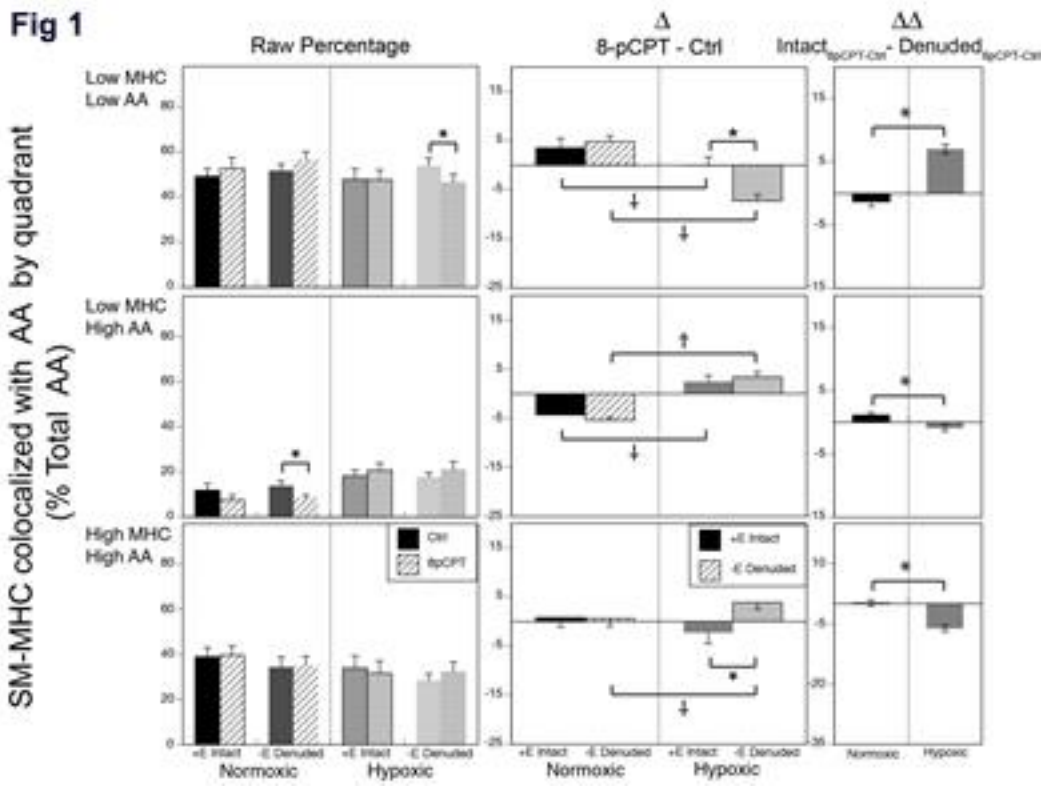

Figure 1. Hypoxia Increases Role of PKG Driven SMC Phenotype Shift in 48hr Organ Culture.

In Figure 1, hypoxia does not alter PKG mediation of MHC colocalization with AA. In Figure 5.1a, SM-MHC and AA colocalization: Please see discussion of Figure 3.5 (chapter 3 above) for comparison among baseline controls for Normoxic (intact and denuded) and Hypoxic (intact and denuded) treatment groups. Acute 24hr exposure to PKG activator 8-pCPT increases Q1 quadrant in normoxic (more in denuded than intact arteries), and increases Q3 in hypoxic arteries. Figure 1, middle panels: 8-pCPT treatment of endothelium-intact normoxic arteries did not alter colocalization pattern at all. Hypoxia did not alter the influence 8-pCPT treatment in endothelium-intact arteries, but it did show a similar effect as VEGF but more modest. Hypoxia inverts the influence of VEGF treatment on Q1, Q2, and Q3 compared with normoxic. Hypoxia changes endothelial contribution to VEGF influence on SM-MHC and Actin colocalization (See Figure 5A, right panels). 8-pCPT action through the endothelium differed significantly between normoxic and hypoxic arteries for all 3 quadrants and demonstrated a similar shift in SM-MHC and Actin colocalization as seen with VEGF but at a decreased magnitude.

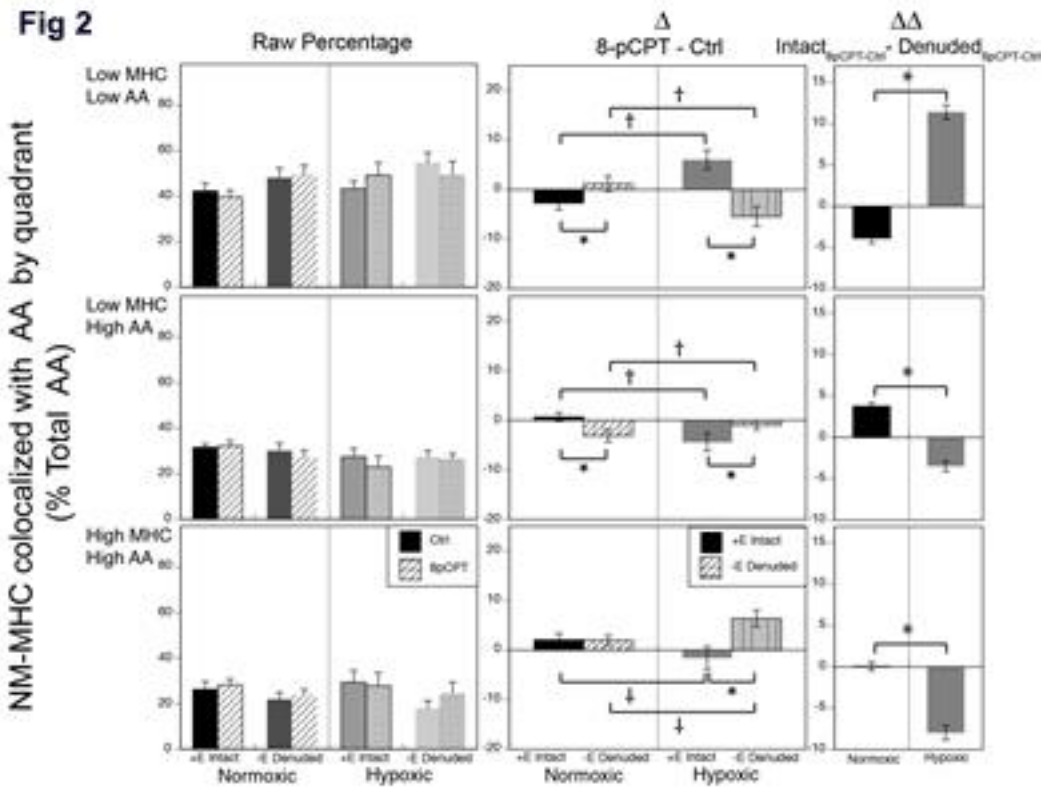

Figure 2. Hypoxia Increases Role of PKG Driven SMC Phenotype Shift in 48hr Organ Culture as Measured Using NM-MHC and AA Colocalization.

For Figure 2 with NM-MHC and AA colocalization, see discussion of Figure 1 above for comparison among baseline controls for Normoxic (intact and denuded) and Hypoxic (intact and denuded) treatment groups. Acute 24hr exposure to 8-pCPT did not significantly alter any of the 3 quadrants when compared with control but did respond inversely to treatment for endothelium-intact vs endothelium-denuded arteries in both normoxic and hypoxic arteries. Figure 2, middle panels: 8-pCPT treatment of endothelium-intact normoxic arteries did not significantly differ from control. As with SM-MHC, hypoxia did not affect influence of 8-pCPT treatment in endothelium-intact arteries but did follow the pattern shift seen with VEGF on hypoxic endothelium-denuded arteries at a lesser magnitude. Hypoxia accents the influence of 8-pCPT treatment on endothelium-denuded arteries in all 3 quadrants, inverting the effect of the endothelium. Hypoxia changes endothelial contribution to 8-pCPT influence on NM-MHC and Actin colocalization (Figure 5.1b, right panels) for 8-pCPT action through the endothelium was inverted by hypoxia in all 3 quadrants.

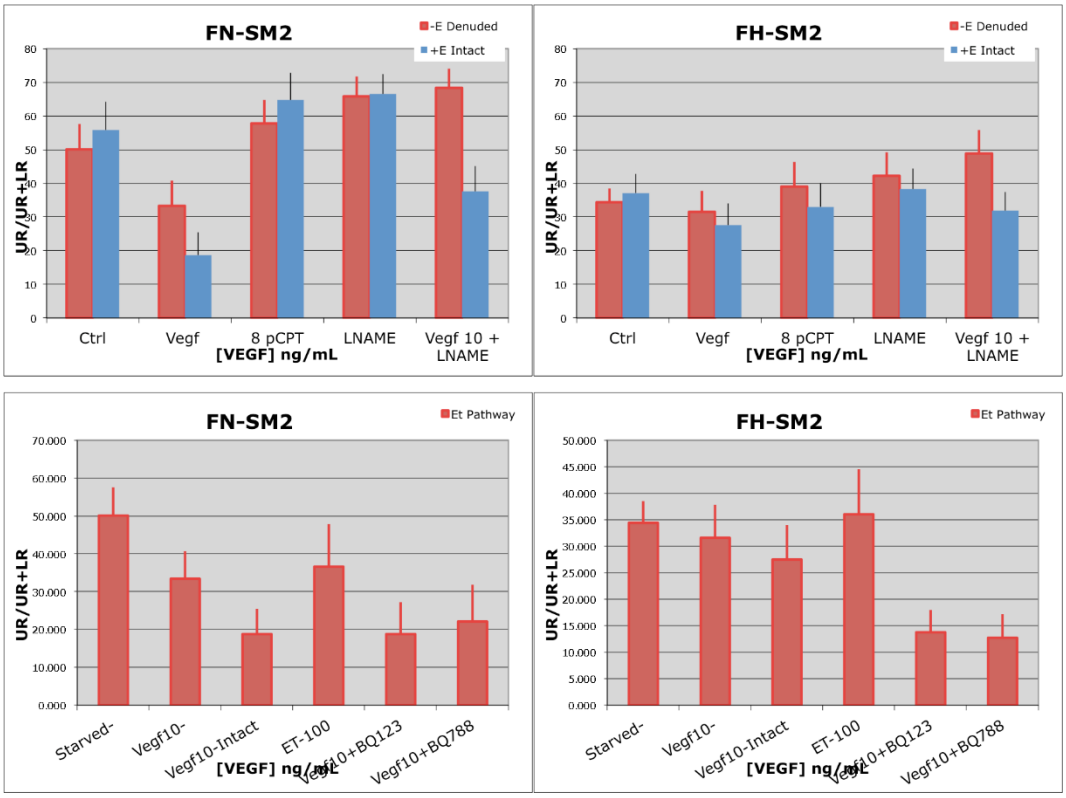

Figure 3. A separate quadrant analysis using Olympus confocal software for just UR% and threshold other than 50%. (SM-MHC also labeled as SM2).

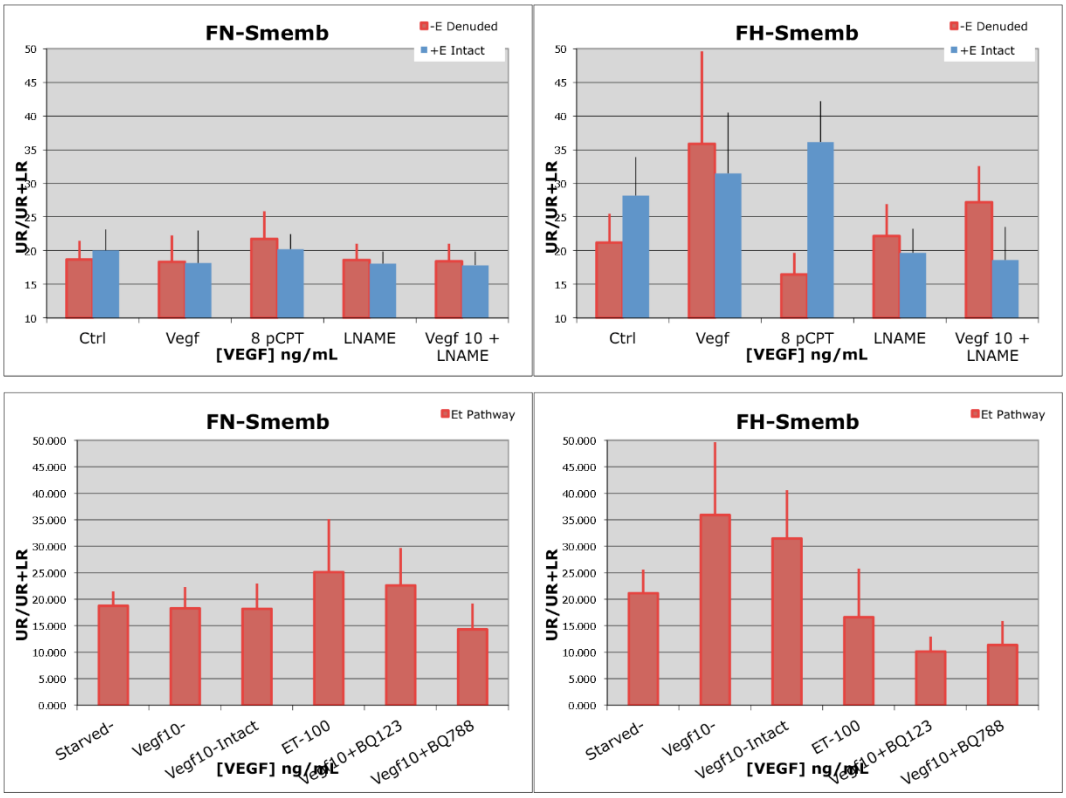

Figure 4. A separate quadrant analysis using Olympus confocal software for just UR% and threshold other than 50%. (NM-MHC also labeled as SMemb).

Fluoview- Colocalization Index 2 **Fluoview- UR/UR+UL**

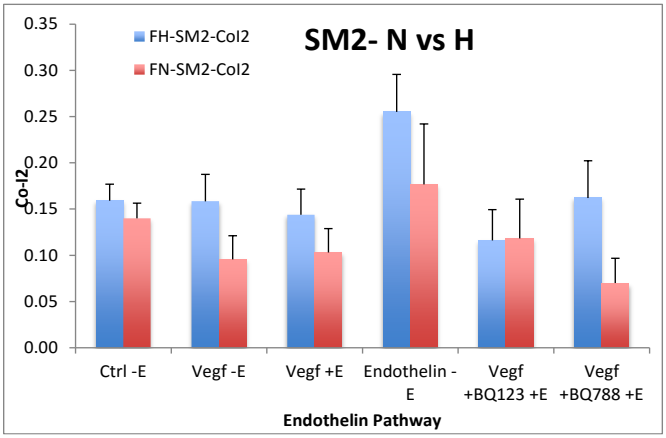

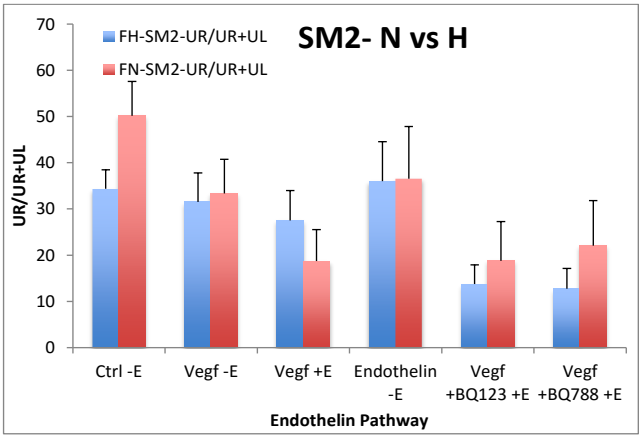

Fluoview- Colocalization Index 2 **Fluoview- UR/UR+UL**

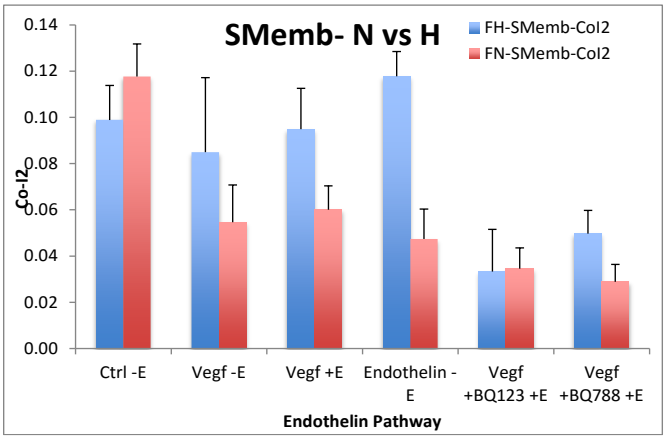

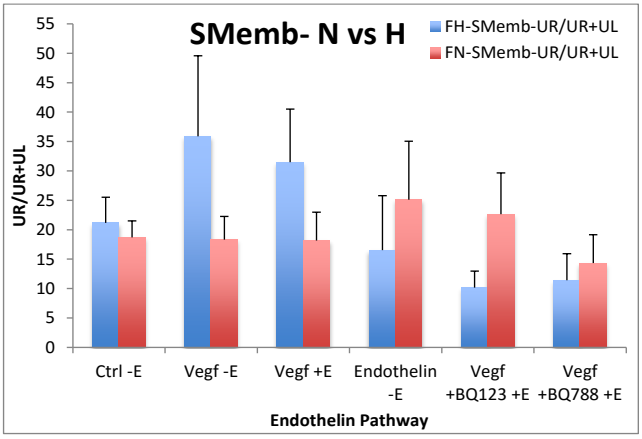

Figure 5. Fluoview Colocalization- Endothelin Pathway.

Table 2. Statistical Analysis of Fluoview Colocalization Data by Behrens–Fisher for SM-MHC, Fetal Normoxic.

SM-MHC

Normoxic:

												By Behren Fischer Mass					
												Co-I #2Sig Difference			UR/UR+UL Sig Difference		
		FN-SM2	Co-1 #2		UR/UR+LR		UR%		Thickness			N vs H	±E vs -E	Tx vs Starve	N vs H	±E vs -E	Tx vs Starved
		Tx	Avg	SE	Avg	SE	Avg	SE	Avg	SE	Count	(within tx)	(within tx)	(within Endo)	(within tx)	(within tx)	(within Endo)
		#########															
	-1	Fresh- Intact	0.086	0.029	5.983	4.669	5.983	4.669	54.232	1.208	4	-	-	-	-	X	-
	0	Starved-Intact	0.169	0.024	55.774	8.540	20.550	2.330	45.848	1.878	12	-	-	-	X	-	-
	3	Vegf3-Intact	0.105	0.042	16.789	5.562	19.080	5.853	47.573	4.835	5	-	-	X	X	-	X
	10	Vegf10-Intact	0.103	0.026	18.717	6.794	18.717	6.794	46.463	3.438	10	-	-	X	-	X	X
	30	Vegf30-Intact	0.087	0.042	40.405	21.479	40.405	21.479	41.081	4.729	2	-	-	X	-	-	-
	-1	Fresh-Denuded	0.114	0.033	16.796	3.898	20.093	2.401	41.948	5.445	5	-	-	-	-	X	-
	0	arved-Denuded	0.140	0.017	50.162	7.446	29.492	5.762	46.911	1.687	18	-	-	-	*	-	-
	3	Vegf3-Denuded	0.053	0.012	20.228	9.163	20.228	9.163	44.300	2.191	4	X	-	X	-	-	X
	10	egf10-Denuded	0.096	0.026	33.370	7.394	33.370	7.394	45.220	3.397	10	X	-	X	-	X	X
	30	egf30-Denuded	0.071	0.029	17.003	3.600	17.003	3.600	44.788	1.867	3	X	-	X	X	-	X
-E Denude	Ctrl - E	arved-Denuded	0.140	0.017	50.162	7.446	29.492	5.762	46.911	1.687	18	-	-	-	X	-	-
	Vegf - E	egf10-Denuded	0.096	0.026	33.370	7.394	33.370	7.394	45.220	3.397	10	X	-	X	-	X	X
	8 pCPT - E	pCPT-Denuded	0.119	0.022	57.855	6.831	38.735	3.253	47.787	4.249	14	X	-	-	X	-	-
	LNAME - E	NAME-Denuded	0.166	0.022	65.786	6.004	#DIV/0!	#DIV/0!	#DIV/0!	#DIV/0!	8	-	-	-	X	-	X
	Vegf 10 + LNAME - E	NAME-Denuded	0.140	0.027	68.278	5.799	#DIV/0!	#DIV/0!	#DIV/0!	#DIV/0!	10	X	-	-	X	X	X
+E Intact	Ctrl+E	Starved-Intact	0.169	0.024	55.774	8.540	20.550	2.330	45.848	1.878	12	-	-	-	X	-	-
	Vegf+E	Vegf10-Intact	0.103	0.026	18.717	6.794	18.717	6.794	46.463	3.438	10	-	-	X	-	X	X
	8 pCPT+E	8-pCPT-Intact	0.125	0.026	64.744	8.151	#DIV/0!	#DIV/0!	#DIV/0!	#DIV/0!	8	-	-	-	X	-	-
	LNAME+E	L-NAME-Intact	0.160	0.028	66.503	5.980	#DIV/0!	#DIV/0!	#DIV/0!	#DIV/0!	10	-	-	-	X	-	-
	Vegf 10 + LN	L-NAME-Intact	0.153	0.028	37.523	7.513	16.389	6.406	58.243	4.327	14	-	-	-	-	X	X
	Ctrl -E	arved-Denuded	0.140	0.017	50.162	7.446	29.492	5.762	46.911	1.687	18	-		-	X		-
	Vegf -E	egf10-Denuded	0.096	0.026	33.370	7.394	33.370	7.394	45.220	3.397	10	X		X	-		X
	Vegf +E	Vegf10-Intact	0.103	0.026	18.717	6.794	18.717	6.794	46.463	3.438	10	-		X	-		X
	Endothelin -	ET-100	0.177	0.065	36.554	11.269	36.554	11.269	53.500	7.521	5	-		-	-		-
	Vegf +BQ123	Vegf10+BQ123	0.118	0.042	18.778	8.502	18.778	8.502	53.860	4.324	6	-		-	-		X
	Vegf +BQ788	Vegf10+BQ788	0.070	0.027	22.054	9.778	22.054	9.778	57.999	5.859	6	X		X	-		X

Table 3. Statistical Analysis of Fluoview Colocalization Data by Behrens–Fisher for SM-MHC, Fetal Hypoxic.

Hypoxic:

												Co-1 #2Sig Difference			UR/UR+UL Sig Difference		
		FH-SM2	Co-1 #2		UR/UR+LR		UR%		Thickness			N vs H	+E vs -E	Tx vs Starved	N vs H	+E vs -E	Tx vs Starved
		Tx	Avg	SE	Avg	SE	Avg	SE	Avg	SE	Count	(within tx)	(within tx)	(within Endo)	(within tx)	(within tx)	(within Endo)
		##########															
	-1	Fresh- Intact	0.151	0.077	27.152	18.079	27.152	18.079	47.452	2.894	2	-	-	-	-	-	-
	0	Starved-Intact	0.179	0.026	37.128	5.707	43.937	8.141	40.506	2.054	14	-	-	-	X	-	-
	3	Vegf3-Intact	0.146	0.055	38.229	3.472	38.229	3.472	50.528	9.211	4	-	-	-	X	-	-
	10	Vegf10-Intact	0.144	0.028	27.514	6.487	29.968	6.331	47.517	3.571	11	-	-	-	-	-	-
	30	Vegf30-Intact	0.108	0.055	35.435	12.037	35.435	12.037	44.224	12.416	4	-	X	X	-	-	-
	-1	Fresh-Denuded	0.266	#DIV/0!	51.535	#DIV/0!	51.535	#DIV/0!	42.132	#DIV/0!	1	-	-	-	-	-	-
	0	tarved-Denuded	0.159	0.018	34.361	4.105	26.531	3.677	49.416	3.131	22	-	-	-	X	-	-
	3	Vegf3-Denuded	0.123	0.023	37.854	11.958	37.854	11.958	47.430	9.611	4	X	-	-	-	-	-
	10	Vegf10-Denuded	0.158	0.029	31.539	6.234	31.539	6.234	45.313	2.870	9	X	-	-	-	-	-
	30	Vegf30-Denuded	0.217	0.035	39.492	2.880	39.492	2.880	44.899	4.320	4	X	X	X	X	-	-
-E Denude	Ctrl -E	tarved-Denuded	0.159	0.018	34.361	4.105	26.531	3.677	49.416	3.131	22	-	-	-	X	-	-
	Vegf -E	Vegf10-Denuded	0.158	0.029	31.539	6.234	31.539	6.234	45.313	2.870	9	X	-	-	-	-	-
	8 pCPT -E	-pCPT-Denuded	0.162	0.019	40.727	7.707	12.220	3.525	46.125	0.982	14	X	-	-	X	-	-
	LNAME -E	NAME-Denuded	0.215	0.042	42.331	6.880	#DIV/0!	#DIV/0!	#DIV/0!	#DIV/0!	10	-	-	X	X	-	-
	Vegf 10 + LNAME -E	NAME-Denuded	0.244	0.040	48.875	7.017	#DIV/0!	#DIV/0!	#DIV/0!	#DIV/0!	10	X	X	X	X	X	X
+E Intact	Ctrl+E	Starved-Intact	0.179	0.026	37.128	5.707	43.937	8.141	40.506	2.054	14	-	-	-	X	-	-
	Vegf+E	Vegf10-Intact	0.144	0.028	27.514	6.487	29.968	6.331	47.517	3.571	11	-	-	-	-	-	-
	8 pCPT+E	8-pCPT-Intact	0.162	0.030	31.113	6.576	#DIV/0!	#DIV/0!	#DIV/0!	#DIV/0!	10	-	-	-	X	-	-
	LNAME+E	L-NAME-Intact	0.164	0.032	38.320	6.130	#DIV/0!	#DIV/0!	#DIV/0!	#DIV/0!	9	-	-	-	X	-	-
	Vegf 10 + LNAME+E	L-NAME-Intact	0.173	0.024	31.790	5.597	17.633	1.960	53.624	2.287	15	-	X	-	-	X	-
	Ctrl -E	tarved-Denuded	0.159	0.018	34.361	4.105	26.531	3.677	49.416	3.131	22	-		-	X		-
	Vegf -E	Vegf10-Denuded	0.158	0.029	31.539	6.234	31.539	6.234	45.313	2.870	9	X		-	-		-
	Vegf +E	Vegf10-Intact	0.144	0.028	27.514	6.487	29.968	6.331	47.517	3.571	11	-		-	-		-
	Endothelin -(	ET-100	0.255	0.041	36.022	8.532	36.022	8.532	72.230	2.649	4	-		X	-		-
	Vegf +BQ123	Vegf10+BQ123	0.116	0.033	13.738	4.177	13.738	4.177	47.288	1.608	5	-		X	-		*
	Vegf +BQ788	Vegf10+BQ788	0.162	0.040	12.715	4.394	12.715	4.394	50.660	3.062	5	X		-	-		X

Table 4. Statistical Analysis of Fluoview Colocalization Data by Behrens-Fisher for NM-MHC, Fetal Normoxic

NM-MHC

Normoxic:

												By Behren Fischer Mass					
												Co-I #2Sig Difference			UR/UR+UL Sig Difference		
		FN-Smemb	Co-1 #2		UR/UR+LR		UR%		Thickness			N vs H	+E vs -E	Tx vs Starve	N vs H	+E vs -E	Tx vs Starved
		Tx	Avg	SE	Avg	SE	Avg	SE	Avg	SE	Count	(within tx)	(within tx)	(within Endo)	(within tx)	(within tx)	(within Endo)
		#########															
	-1	Fresh- Intact	0.113	0.039	16.314	4.173	14.386	4.274	54.879	1.137	5	-	-	-	X	-	-
	0	Starved-Intact	0.126	0.015	20.043	3.086	17.113	5.651	45.848	1.804	13	-	-	-	X	-	-
	3	Vegf3-Intact	0.131	0.016	15.120	1.653	15.120	1.653	44.811	5.123	4	-	X	-	-	-	-
	10	Vegf10-Intact	0.060	0.010	18.150	4.823	18.150	4.823	49.191	3.558	10	X	-	X	X	-	-
	30	Vegf30-Intact	0.081	0.000	7.330	0.138	7.330	0.138	41.081	4.729	2	X	-	X	X	-	X
														-			
	-1	Fresh-Denuded	0.097	0.043	20.961	8.922	20.961	8.922	44.858	5.942	4	-	-	-	-	-	-
	0	arved-Denuded	0.118	0.014	18.701	2.808	17.927	3.276	46.911	1.687	18	-	-	-	-	-	-
	3	/egf3-Denuded	0.069	0.016	9.288	4.176	9.288	4.176	44.300	2.191	4	-	X	X	X	-	X
	10	egf10-Denuded	0.055	0.016	18.320	3.930	18.320	3.930	45.220	3.397	10	-	-	X	X	-	-
	30	egf30-Denuded	0.109	0.021	12.679	5.919	12.679	5.919	46.225	1.951	4	-	-	-	X	-	-
-E Denude	Ctrl	arved-Denuded	0.118	0.014	18.701	2.808	17.927	3.276	46.911	1.687	18	-	-	-	-	-	-
	Vegf	egf10-Denuded	0.055	0.016	18.320	3.930	18.320	3.930	45.220	3.397	10	-	-	X	X	-	-
	8 pCPT	pCPT-Denuded	0.098	0.014	21.772	4.098	26.985	6.089	48.909	4.855	13	-	-	-	-	-	-
	LNAME	NAME-Denuded	0.143	0.005	18.645	2.355	#DIV/0!	#DIV/0!	#DIV/0!	#DIV/0!	9	-	-	X	-	-	-
	Vegf 10 + LNAME	NAME-Denuded	0.145	0.018	18.470	2.530	#DIV/0!	#DIV/0!	#DIV/0!	#DIV/0!	8	-	X	-	X	-	-
+E Intact	Ctrl+E	Starved-Intact	0.126	0.015	20.043	3.086	17.113	5.651	45.848	1.804	13	-	-	-	X	-	-
	Vegf+E	Vegf10-Intact	0.060	0.010	18.150	4.823	18.150	4.823	49.191	3.558	10	X	-	X	X	-	-
	8 pCPT+E	8-pCPT-Intact	0.122	0.019	20.238	2.171	#DIV/0!	#DIV/0!	#DIV/0!	#DIV/0!	9	X	-	-	X	-	-
	LNAME+E	L-NAME-Intact	0.159	0.016	18.065	1.814	#DIV/0!	#DIV/0!	#DIV/0!	#DIV/0!	8	-	-	X	-	-	-
	Vegf 10 + LNAME+E	L-NAME-Intact	0.102	0.016	17.847	2.020	16.892	2.687	58.243	4.327	14	-	X	-	-	-	-
	Ctrl -E	arved-Denuded	0.118	0.014	18.701	2.808	17.927	3.276	46.911	1.687	18	-		-	-		-
	Vegf -E	egf10-Denuded	0.055	0.016	18.320	3.930	18.320	3.930	45.220	3.397	10	-		X	X		-
	Vegf +E	Vegf10-Intact	0.060	0.010	18.150	4.823	18.150	4.823	49.191	3.558	10	X		X	X		-
	Endothelin -	ET-100	0.047	0.013	25.104	9.942	25.104	9.942	50.358	7.293	5	X		X	-		-
	Vegf +BQ123	Vegf10+BQ123	0.035	0.009	22.625	7.044	22.625	7.044	53.860	4.324	6	-		X	X		-
	Vegf +BQ788	Vegf10+BQ788	0.029	0.008	14.320	4.838	14.320	4.838	57.999	5.859	6	X		X	-		-

Table 5. Statistical Analysis of Fluoview Colocalization Data by Behrens-Fisher for NM-MHC, Fetal Hypoxic

Hypoxic:

		FH-Smemb	Co-1 #2		UR/UR+LR		UR%		Thickness			Co-1 #2Sig Difference			UR/UR+UL Sig Difference		
		Tx	Avg	SE	Avg	SE	Avg	SE	Avg	SE	Count	N vs H (within tx)	+E vs -E (within tx)	Tx vs Starve (within Endo)	N vs H (within tx)	+E vs -E (within tx)	Tx vs Starve (within Endo)
		##########															
	-1	Fresh- Intact	0.215	0.038	84.893	1.007	84.893	1.007	47.452	2.894	2	-	-	-	X	-	-
	0	Starved-Intact	0.120	0.018	28.177	5.752	39.918	7.935	40.506	1.984	15	-	-	-	X	-	-
	3	Vegf3-Intact	0.104	0.029	21.344	5.935	21.344	5.935	50.528	9.211	4	-	-	-	-	X	-
	10	Vegf10-Intact	0.095	0.018	31.499	9.021	31.499	9.021	47.116	4.389	9	X	-	-	X	-	-
	30	Vegf30-Intact	0.040	0.014	30.062	13.892	30.062	13.892	44.324	9.618	5	X	X	X	X	-	-
	-1	Fresh-Denuded	0.033	#DIV/0!	71.490	#DIV/0!	71.490	#DIV/0!	42.132	#DIV/0!	1	-	-	-	-	-	-
	0	tarved-Denuded	0.099	0.015	21.168	4.367	21.637	5.796	48.205	3.377	21	-	-	-	-	-	-
	3	Vegf3-Denuded	0.090	0.019	43.176	12.613	43.176	12.613	47.430	9.611	4	-	-	-	X	X	X
	10	Vegf10-Denuded	0.085	0.032	35.876	13.715	43.494	14.902	44.108	2.955	8	-	-	-	X	-	X
	30	Vegf30-Denuded	0.134	0.056	43.858	11.164	43.858	11.164	40.805	3.794	6	-	X	-	X	-	X
-E Denude	Ctrl -E	tarved-Denuded	0.099	0.015	21.168	4.367	21.637	5.796	48.205	3.377	21	-	-	-	-	-	-
	Vegf -E	Vegf10-Denuded	0.085	0.032	35.876	13.715	43.494	14.902	44.108	2.955	8	-	-	-	X	-	X
	8 pCPT -E	8-pCPT-Denuded	0.118	0.028	18.445	3.445	6.284	0.415	44.395	0.422	13	-	-	-	-	X	-
	LNAME -E	L-NAME-Denuded	0.146	0.024	22.198	4.684	#DIV/0!	#DIV/0!	#DIV/0!	#DIV/0!	10	-	-	X	-	-	-
	Vegf 10 + LNAME -E	L-NAME-Denuded	0.167	0.031	27.156	5.384	#DIV/0!	#DIV/0!	#DIV/0!	#DIV/0!	10	-	X	X	X	-	-
+E Intact	Ctrl+E	Starved-Intact	0.120	0.018	28.177	5.752	39.918	7.935	40.506	1.984	15	-	-	-	X	-	-
	Vegf+E	Vegf10-Intact	0.095	0.018	31.499	9.021	31.499	9.021	47.116	4.389	9	X	-	-	X	-	-
	8 pCPT+E	8-pCPT-Intact	0.080	0.014	29.612	6.467	#DIV/0!	#DIV/0!	#DIV/0!	#DIV/0!	10	X	-	X	X	X	-
	LNAME+E	L-NAME-Intact	0.168	0.031	19.695	3.555	#DIV/0!	#DIV/0!	#DIV/0!	#DIV/0!	10	-	-	X	-	-	-
	Vegf 10 + LNAME+E	L-NAME-Intact	0.100	0.014	18.585	4.930	8.067	1.482	55.118	2.446	15	-	X	-	-	-	X
	Ctrl -E	tarved-Denuded	0.099	0.015	21.168	4.367	21.637	5.796	48.205	3.377	21	-		-	-		-
	Vegf -E	Vegf10-Denuded	0.085	0.032	35.876	13.715	43.494	14.902	44.108	2.955	8	-		-	X		X
	Vegf +E	Vegf10-Intact	0.095	0.018	31.499	9.021	31.499	9.021	47.116	4.389	9	X		-	X		-
	Endothelin -	ET-100	0.118	0.011	16.545	9.232	31.654	5.225	72.230	2.649	4	X		-	-		-
	Vegf +BQ123	Vegf10+BQ123	0.033	0.018	10.157	2.796	10.157	2.796	47.759	1.669	5	-		X	X		X
	Vegf +BQ788	Vegf10+BQ788	0.050	0.010	11.402	4.515	11.402	4.515	53.981	3.097	3	X		X	-		X